INTERACTION BETWEEN CO AND PtSn ALLOY: A THEORETICAL STUDY ON UNDERSTANDING SELECTIVE CO OXIDATION

by

Birim Duru

B. S. in Ch.E., Boğaziçi University, 2006

Submitted to the Institute for Graduate Studies in
Science and Engineering in partial fulfillment of
the requirements for the degree of
Master of Science

Graduate Program in Chemical Engineering

Boğaziçi University

2008

ACKNOWLEDGEMENTS

Firstly, I would like to thank my thesis supervisor Prof. Ahmet Erhan Aksoylu, for his support, guidance and help throughout my thesis. He supported me from the beginning and his advices helped me to improve my work.

I want to thank my friends from CATREL; Tuğba Davran Candan, Feyza Gökaliler, Burcu Selen Çağlayan. I also have special thanks to Aslıhan Sümer and Duygu Başaran for their endless help and support throughout my thesis. I would like to express my gratitude to my partner Ilgaz Soykal; working with him was a pleasure for me.

I am grateful to my friends Gökhan Kabukcu, Nurdan Özcan, and Neslihan Özcan for their moral support and great help.

This thesis is dedicated to my family, especially to my nephew. I am grateful to them for their endless love, support and encouragement throughout my life.

Financial support provided by the State Planning Organization of Turkey, DPT, through projects 03K120250 and 07K120630, and TUBITAK through project 105M282 is gratefully acknowledged.

ABSTRACT

INTERACTION BETWEEN CO AND PtSn ALLOY: A THEORETICAL STUDY ON UNDERSTANDING SELECTIVE CO OXIDATION

The adsorption properties of CO on PtSn(110) surface were investigated via quantum mechanical calculations. The adsorption energies and the geometries of CO molecule for all possible adsorption sites were calculated. The energetically most favourable CO adsorption site was found as Pt-Pt bridge site, site B. The adsorption properties of CO on PtSn(110) were compared with those on $Pt_3Sn(110)$ and Pt(110). The CO adsorption strength of bridge sites on three surfaces decreased with increasing Sn content. The adsorption properties of other PROX reactants and products, namely H_2, CO_2 and O_2, were also investigated on PtSn(110) surface. Pt-Pt bridge site B was found as the only site adsorbing H atom stably. Stable CO_2 adsorption was observed only on Pt-Sn bridge site C on PtSn(110) surface. For atomic oxygen adsorption, Sn-Sn bridge site F was the most favourable adsorption site on PtSn(110) surface. The adsorption properties of H_2, CO_2 and O_2 gases were also compared for the three surfaces, namely PtSn(110), $Pt_3Sn(110)$ and Pt(110). In order to understand electronic interactions between the surface metals and the adsorbates, local density of states (LDOS) profiles were examined for bare and adsorbed states of the metal atoms and the adsorbate involved in the adsorption process. The common behaviour observed for all adsorbates was that electronic density around surface Pt atom increased with increasing Sn content in the alloy and the electronic interactions occurred in lower energy levels as Sn concentration in the alloy was increased.

ÖZET

KARBONMONOKSİTİN PtSn ALAŞIMIYLA ETKİLEŞİMİ: KARBONMONOKSİTİN SEÇİMLİ OKSİDASYONU ÜZERİNE TEORİK ÇALIŞMA

Karbonmonoksitin PtSn(110) yüzeyindeki adsorpsiyon özellikleri kuantum mekaniksel hesaplamalar yoluyla incelendi. Karbonmonoksitin tüm olası adsorpsiyon merkezlerindeki adsorpsiyon enerjileri ve geometrileri hesaplandı. Enerji bakımından en tercih edilebilir karbonmonoksit adsorpsiyon merkezi Pt-Pt köprü merkezi olarak bulundu. Karbonmonoksitin PtSn(110) yüzeyi üzerindeki adsorpsiyon özellikleri Pt_3Sn(110) ve Pt(110) yüzeyleri üzerindeki özellikleriyle karşılaştırıldı. Köprü merkezleri üzerindeki CO adsorpsiyon kuvvetinin alaşımdaki artan Sn miktarıyla azaldığı görüldü. Seçimli karbonmonoksit oksidasyon (PROX) reaksiyonuna diğer girenler ve ürünlerin, yani H_2, CO_2 ve O_2 gazlarının, PtSn(110) yüzeyindeki adsorpsiyon özellikleri incelendi. Hidrojen atomunu kararlı olarak adsorbe eden tek merkezin Pt-Pt köprü merkezi olduğu bulundu. Kararlı CO_2 adsorpsiyonu da sadece Pt-Sn köprü merkezinde gözlemlendi. Atomik oksijen adsorpsiyonu için en tercih edilebilir merkez Sn-Sn köprü merkezi olarak bulundu. H_2, CO_2 ve O_2 gazlarının adsorpsiyon özellikleri PtSn(110), Pt_3Sn(110) ve Pt(110) yüzeyleri için karşılaştırıldı. Yüzeyde adsorbe edilen maddelerin yüzey metal atomlarıyla yaptığı etkileşimleri anlamak için adsorpsiyon öncesi ve sonrası enerji düzeyleri lokal yoğunluğu (LDOS) profilleri incelendi. Yüzeydeki Pt atomonun etrafındaki elektron yoğunluğunun, alaşımın içerdiği Sn miktarıyla arttığı ve Sn konsantrasyonun artmasıyla elektronik etkileşimlerin daha düşük enerji seviyelerinde meydana geldiği tüm adsorbe edilen maddeler için gözlemlendi.

TABLE OF CONTENTS

ACKNOWLEDGEMENTS iii
ABSTRACT iv
ÖZET v
LIST OF FIGURES viii
LIST OF TABLES xiii
1. INTRODUCTION 1
2. LITERATURE SURVEY 3
2.1. Importance of Fuel Cells and PROX 3
2.2. Investigated Catalysts for PROX 5
2.3. Effect of Alloying on CO oxidation 7
2.4. Effect of CO_2 and H_2 Presence on CO Oxidation 8
2.5. Pt and Alloyed Pt Surfaces 8
2.6. Theoretical Studies on Pt and Alloyed Pt Surfaces 12
2.7. Theory of Computational Methods 15
3. CALCULATIONS 19
3.1. Computational Details of CASTEP Calculations 19
3.2. Building the PtSn Crystal 19
3.3. Building and Optimizing the PtSn(110) Surface 20
3.4. Determination of Active Sites for CO Adsorption 23
3.5. Optimization of the Adsorption System 24
3.6. Adsorption of Other Reactants and Products of PROX 25
3.7. Plotting the LDOS Charts 27
4. RESULTS AND DISCUSSION 29
4.1. Bare PtSn(110) Surface 29
4.2. CO Molecule 29
4.3. CO Adsorption on PtSn(110) Surface 29
4.3.1. CO Adsorption on PtSn(110), Pt_3Sn(110), and Pt(110) Surfaces: The Effect of Sn Presence 33
4.4. Hydrogen Adsorption on PtSn(110), Pt_3Sn(110), Pt(110) Surfaces and Their Comparison 35

4.5. CO_2 Adsorption on PtSn(110) and Pt(110) Surfaces 39
4.5.1. Comparison of CO_2 Adsorption on PtSn(110), Pt_3Sn(110), and Pt(110) Surfaces 42
4.6. Oxygen Adsorption on PtSn(110), Pt_3Sn(110), and Pt(110) Surfaces and Their Comparison 44
4.7. Co-adsorption of CO and O on PtSn(110) Surface 49
4.8. Effect of Bonding Competition on CO Adsorption on PtSn(110) surface 53
4.9. Electronic Mechanism of CO Adsorption on PtSn(110) Surface 54
4.9.1. Comparison of Electronic Mechanism of CO Adsorption of Pt(110), PtSn(110), Pt_3Sn(110) Surfaces Using LDOS Profiles 59
4.10. Electronic Mechanism of H Adsorption on PtSn(110), Pt_3Sn(110) and Pt(110) Surfaces and Their Comparison 66
4.11. Electronic Mechanism of O Adsorption on PtSn(110), Pt_3Sn(110) and PtSn(110) Surfaces and Their Comparison 72
5. CONCLUSIONS 85
6. RECOMMENDATIONS 86
REFERENCES 87

LIST OF FIGURES

Figure 2.1. Simplified Diagram of the Proton Exchange Membrane Fuel Cell..... 3

Figure 2.2. Structure of PtSn alloy 9

Figure 2.3. Representation of low-index faces of hexagonal PtSn phase..... 10

Figure 2.4. Structure of Pt3Sn alloy 10

Figure 2.5. Representation of low-index faces of the cubic Pt_3Sn phase. 11

Figure 2.6. The X-Ray diffraction pattern for sample T and N. 12

Figure 3.1. Structure of PtSn alloy 20

Figure 3.2. The cleaved PtSn(110) surface..... 21

Figure 3.3. The (1x1) vacuum slab for the PtSn(110) surface..... 22

Figure 3.4. The (1x1) vacuum slab for the PtSn(110) surface..... 22

Figure 3.5. Schematic representation for the active sites on the PtSn(110) surface 24

Figure 3.6. Pt_2Sn bonded CO on PtSn(110)..... 25

Figure 3.7. Schematic representation for the active sites on the Pt_3Sn(110) mixed (left) and pure-Pt ending (right) surfaces..... 26

Figure 3.8. Schematic representation for the active sites on the Pt(110) surface 27

Figure 4.1. The optimized Pt_2Sn site on the PtSn(110) surface, as an illustration of an unstable adsorption site 30

Figure 4.2. Comparison of CO adsorption strengths of atop sites of PtSn(110), $Pt_3Sn(110)$ and Pt(110) surfaces (θ=0.25)..... 34

Figure 4.3. Comparison of CO adsorption strengths of bridge sites of PtSn(110), $Pt_3Sn(110)$ and Pt(110) surfaces (θ=0.25)..... 35

Figure 4.4. Comparison of hydrogen adsorption strengths of bridge sites of PtSn(110), $Pt_3Sn(110)$ and Pt(110) surfaces (θ=0.25)..... 38

Figure 4.5. Comparison of oxygen adsorption strengths of bridge sites of PtSn(110), $Pt_3Sn(110)$ and Pt(110) surfaces..... 49

Figure 4.6. The adsorption energy of CO as a function of total coverage..... 51

Figure 4.7. The adsorption energy of O as a function of total coverage. 52

Figure 4.8. CO adsorption on Pt-Pt bridge site B of PtSn(110) surface without bonding competition 53

Figure 4.9. CO adsorption on Pt-Pt bridge site B of PtSn(110) surface with bonding competition (θ=0. 25 ML)..... 54

Figure 4.10. LDOS profiles of C of adsorbed CO and Pt for atop type adsorption on PtSn(110) (a) of C atom (b) of Pt atom. 56

Figure 4.11. LDOS profiles of Pt atom at bridge site and C of adsorbed CO for Pt-Pt bridge site, adsorption on PtSn(110) (a) of C atom (b) of Pt atom..... 58

Figure 4.12. LDOS profiles of Pt for bare surfaces of PtSn(110), Pt(110) and (a) pure Pt ending termination (b) mixed atom ending termination of $Pt_3Sn(110)$ alloys. 60

Figure 4.13. LDOS profiles of C of adsorbed CO for Pt-Pt bridge type adsorption on PtSn(110), Pt(110) and (a) pure Pt ending termination (b) mixed atom ending termination of $Pt_3Sn(110)$ alloys. 61

Figure 4.14. LDOS profiles of Pt atom upon Pt-Pt bridge type CO adsorption on PtSn(110), Pt(110) and (a) pure Pt ending termination (b) mixed atom ending termination of $Pt_3Sn(110)$ alloys. 62

Figure 4.15. LDOS profiles of C of adsorbed CO for atop Pt site of PtSn(110), Pt(110) and (a) pure Pt ending termination (b) mixed atom termination of $Pt_3Sn(110)$ surfaces. 64

Figure 4.16. LDOS profiles of Pt atom of atop site on PtSn(110), Pt(110) and (a) pure Pt ending termination (b) mixed atom ending termination of $Pt_3Sn(110)$ .. 65

Figure 4.17. LDOS profiles of Pt atom at bridge site and adsorbed H atom for H adsorption on Pt-Pt bridge site B of PtSn(110). LDOS profile of bare Pt is given as comparison basis. 66

Figure 4.18. LDOS profiles of Pt atom at bridge site and adsorbed H atom for H adsorption on Pt-Pt bridge site on Pt atom, site G, on pure Pt atom ending termination of $Pt_3Sn(110)$. 67

Figure 4.19. LDOS profiles of Pt and adsorbed H atom for H adsorption on atop Pt site F on pure Pt atom ending termination of $Pt_3Sn(110)$. 68

Figure 4.20. LDOS profiles of Pt atom at bridge site and adsorbed H atom for H adsorption on Pt-Pt bridge site on Sn atom, site H, on pure Pt atom ending termination of $Pt_3Sn(110)$. LDOS profile of bare Pt is given as comparison basis. 68

Figure 4.21. LDOS profiles of adsorbed H atom and Pt for atop type H adsorption on Pt(110) surface LDOS profile of bare Pt is given as comparison basis. 69

Figure 4.22. LDOS profiles of adsorbed H atom and Pt for short bridge type O adsorption on Pt(110) surface. LDOS profile of bare Pt is given as comparison basis. 70

Figure 4.23. Comparison of LDOS profiles for Pt-Pt bridge type H adsorption on Pt(110), $Pt_3Sn(110)$ and Pt(110) surfaces (a) for adsorbed state of Pt and (b) for adsorbed H atom. 71

Figure 4.24. LDOS profiles of adsorbed O atom and Pt for Pt-Pt bridge type O adsorption on PtSn(110) surface. 72

Figure 4.25. LDOS profiles of adsorbed O atom and Sn for Sn-Sn bridge type O adsorption on PtSn(110) surface. 73

Figure 4.26. LDOS profiles for Pt2Sn type O adsorption on PtSn(110) surface (a) for adsorbed states of Pt and of O (b) for adsorbed states of Sn. 75

Figure 4.27. LDOS profiles of Pt atom at bridge site and adsorbed O atom for O adsorption on Pt-Pt bridge site on Sn atom, site H, on pure Pt atom ending termination of $Pt_3Sn(110)$. 76

Figure 4.28. LDOS profiles of Pt atom at bridge site and adsorbed O atom for O adsorption on Pt-Pt bridge site on Pt atom on pure Pt atom ending termination of $Pt_3Sn(110)$ surface. 76

Figure 4.29. LDOS profiles of adsorbed O atom and Pt for Pt-Pt long bridge type O adsorption on pure Pt ending termination of $Pt_3Sn(110)$ surface. 77

Figure 4.30. LDOS profiles for Pt-Sn bridge type O adsorption on mixed atom ending termination of $Pt_3Sn(110)$ surface (a) for adsorbed states of Pt and of O (b) for adsorbed states of Sn. 78

Figure 4.31. LDOS profiles of adsorbed O atom and Sn for Sn-Sn bridge type O adsorption on mixed atom ending termination of $Pt_3Sn(110)$ surface. 79

Figure 4.32. LDOS profiles of adsorbed O atom and Pt for Pt-Pt long bridge type O adsorption on mixed atom ending termination of $Pt_3Sn(110)$ surface..... 80

Figure 4.33. LDOS profiles of adsorbed O atom and Pt for atop type O adsorption on Pt(110) surface. LDOS profile of bare Pt is given as comparison basis..... 81

Figure 4.34. LDOS profiles of adsorbed O atom and Pt for short bridge type O adsorption on Pt(110) surface..... 81

Figure 4.35. LDOS profiles of adsorbed O atom and Pt for long bridge type O adsorption on Pt(110) surface..... 82

Figure 4.36. Comparison of LDOS profiles for Pt-Pt bridge type O adsorption on Pt(110), pure Pt atom ending termination of $Pt_3Sn(110)$ and Pt(110) surfaces (a) for adsorbed state of Pt and (b) for adsorbed O atom. 83

Figure 4.37. Comparison of LDOS profiles for Pt-Pt bridge type O adsorption on Pt(110), mixed atom ending termination of $Pt_3Sn(110)$ and Pt(110) surfaces (a) for adsorbed state of Pt and (b) for adsorbed O atom. 84

LIST OF TABLES

Table 2.1. Bond distances for different Pt-Sn alloy phases and the element Pt..... 9

Table 2.2. Surface composition for samples T and N from XPS measurements. The bulk values are given in parentheses..... 12

Table 3.1. List of active sites for PtSn(110) surface 23

Table 3.2. List of active sites for $Pt_3Sn(110)$ surface 26

Table 3.3. List of active sites for PtSn(110) surface 27

Table 4.1. Possible CO adsorption sites, corresponding adsorption energies and data on geometric 31

Table 4.2. Possible H adsorption sites, corresponding adsorption energies and data on geometric properties of H-Surface complex upon atomic H adsorption on PtSn(110), $Pt_3Sn(110)$ and Pt(110) surfaces..... 37

Table 4.3. Possible CO_2 adsorption sites, corresponding adsorption energies and data on geometric properties of CO_2-Surface complex upon CO_2 adsorption on PtSn(110), $Pt_3Sn(110)$ and Pt(110) 41

Table 4.4. Comparison of simulation results of Pt-Sn bridge site, site B, of mixed atom ending termination of $Pt_3Sn(110)$ surface in Basaran's study with current work..... 42

Table 4.5. Possible O adsorption sites, corresponding adsorption energies and data on geometric properties of CO2-Surface complex upon CO2 adsorption on PtSn(110), Pt3Sn(110) and Pt(110)..... 47

Table 4.6. CO adsorption energies on O-precovered surface 51

Table 4.7. O adsorption energies on CO-precovered surface 52

1. INTRODUCTION

Fuel cell technologies have been accepted as a key solution for the energy problems, providing clean, environmental friendly and efficient production of power and heat from a range of primary sources. Among the numerous types of fuel cells developed so far, one of the most promising one for small scale applications is the Proton Exchange Membrane Fuel Cell (PEMFC) fueled with hydrogen. PEM fuel cells use CO-free hydrogen as the fuel. Since the transportation and storing of hydrogen introduces problems, hydrogen can be produced in an onboard fuel processor [1]. Fuel processors produce hydrogen via three reaction steps, namely partial oxidation, water gas shift reaction, and preferential oxidation [2]. Preferential oxidation reaction is used to eliminate CO down below in hydrogen fuel since Pt-anode of fuel cell is posioned at CO levels above 4 ppm [3].

The PROX reaction temperature, which is improved by the energy efficiency considerations of combined fuel processor-fuel cell system and operation temperature of PEMFC, should be between 80-120 ˚C. The reaction is demanding considering the fact that the catalyst must have high activity and stability as well as CO oxidation selectivity at relatively low, reaction temperature under the presence of CO_2 and water vapor. Thus, understanding steps of CO oxidation reaction starting from adsorption of reactants on the specific active sites to determination of reaction path at atomic scale is of extreme importance.

The specific DFT codes available for simulation of surfaces, adsorbate-adsorbent interaction and surface reactions, and powerful computers enable us to scrutinize the reaction steps at atomic scale. CO oxidation is one of the most important reactions that have been studied theoretically; various research groups studied the adsorption and reaction on various metals, alloys and metal on metal oxide surfaces.

In this study, the adsorption properties of CO on PtSn(110) surface were investigated via quantum mechanical calculations. The adsorption properties of PtSn(110) surface was compared with those of Pt_3Sn(110) and Pt(110) surfaces. Additionally, the adsorption properties of other species present in a realistic hydrogen stream produced by a fuel

processor, namely H_2, CO_2, and O_2, were investigated on PtSn(110) surface and compared with those obtained from the adsorption studies conducted on Pt_3Sn(110) and Pt(110) surfaces. The procedure can be summarized in a stepwise manner:

- The structures of the stable PtSn, Pt_3Sn and Pt surfaces and their reconstructions were found from the literature.

- The possible adsorption sites for all adsorbates were determined under the light of previous QM simulation studies.

- The adsorption energies and the geometries of the adsorbates on each specific site were calculated.

- The comparison of the adsorption energies of all adsorbates for same sites present on Pt, Pt_3Sn, and PtSn surfaces were made.

- In order to understand the detailed interactions between the surfaces and the adsorbates, the local density of states (LDOS) analysis were made for all adsorbates on PtSn(110) as well as on Pt_3Sn(110), and Pt(110) surfaces and the results obtained are compared.

2. LITERATURE SURVEY

2.1. Importance of Fuel Cells and PROX

The most promising system to be used in energy production for the vehicles in future is combined fuel processor – fuel cell systems [1]. Fuel processors converts hydrocarbon fuels to hydrogen. A typical fuel processor has three catalytic reactions, namely reforming, water-gas shift and preferential oxidation, in series. Since fuel cells need pure hydrogen for producing electricity, the hydrogen produced by fuel processor must be free from CO impurity [4].

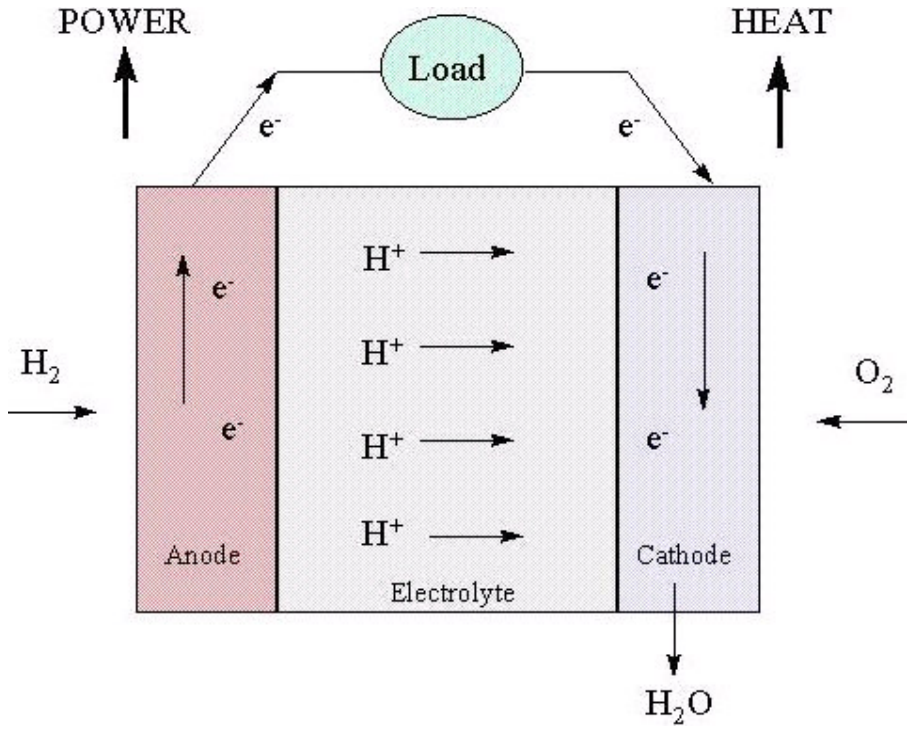

Figure 2.1. Simplified Diagram of the Proton Exchange Membrane Fuel Cell [5]

The main constituents of a fuel cell are the anode, cathode and an electrolyte. H_2 gas is carried through anode to the electrolyte where hydrogen is oxidized to protons and electrons:

$$H_2 \rightarrow 2H^+ + 2e^- \quad (2.1)$$

The free electrons move towards the cathode through the external circuit, meanwhile the H^+ protons are diffused across the electrolyte. At the cathode the following reaction takes place:

$$O_2 + 4H^+ + 4e^- \rightarrow 2H_2O \quad (2.1)$$

The overall reaction produces H_2O and electricity.

Platinum is the most widely preferred anode catalyst due to its high efficiency for electrochemical oxidation of H_2. On the other hand, it readily deactivates if H_2 feed contains even trace amounts of carbon monoxide. Presence of carbon monoxide creates two competing reaction at the anode:

Desired reaction: $2Pt + H_2 \rightarrow 2Pt\text{-}H_{ads}$ (2.2)

$$H\text{-}Pt \rightarrow H^+ + e^- + Pt \quad (2.3)$$

Undesired reaction: $Pt + CO \rightarrow Pt\text{-}CO_{ads}$ (2.4)

Irreversible CO adsorption on Pt sites leads to poisoning of the catalyst. In order to overcome this deactivation problem either the fuel should be clean enough, which is stated as less than 4 ppm carbon monoxide in it [3], or catalysts with higher CO tolerance should be prepared and used in the fuel cell anode. Preferential oxidation of CO, which is the last reaction in a fuel processor, appears as a solution for eliminating CO from the H_2-feed through selective conversion of CO to CO_2:

$$CO + \tfrac{1}{2} O_2 \rightarrow CO_2 \quad (2.5)$$

Besides CO oxidation, hydrogen in the reformate is consumed and this lowers overall efficiency. Thus, selectivity is a critical issue for PROX catalysts. In a typical fuel processor -fuel cell system PROX reactor is present between low temperature WGS

reactor, which operates ca. 200 ˚C, and fuel cell, which operates ca. 85 ˚C. Thus, considering the energy efficiency, operation temperature of the PROX reactor should be between 85 ˚C and 200 ˚C [4].

2.2. Investigated Catalysts for PROX

The catalysts studied for PROX reaction are mostly include noble metals or mixed metal oxides. Nobel metals like platinum, palladium, and ruthenium are highly active and selective for CO oxidation. The high activity and selectivity of the catalysts stems from the strong preferential binding of CO over H_2, which is the reason for its removal from the fuel cell feed stream. Considering the cost efficiency, possible reduction in the noble metal loading, through either promoting or substituting it with a transition metal, would be beneficial [6]. For instance, the activity of the Pt catalyst for the PROX reaction was reported to be improved by the addition of a transition metal like Fe, Sn, Co, and Ce [7].

Pt-based catalysts are the most commonly used catalysts for preferential oxidation of CO and Pt/Al_2O_3 is the widely tested catalsyt [8, 9, 10, 11, 12-15]. However, Pt on zeolites [16] and TiO_2 [12] were found to be more active and selective than Pt on Al_2O_3. In another study [17], $Pt\text{-}Co/Al_2O_3$ showed the best performance among many different noble metal based and base metal promoted catalysts supported on metal oxides. Pt was also promoted with Fe on metal foams with different geometries. These geometries were specified according to by the volume of solid material and catalysts with lower solid material content gave higher CO activity and selectivity [18]. In order to understand the role of alkali promoter, PdO/SnO_2 catalyst was promoted with Na; this promotion has reported to enhance the CO oxidation rate [19].

Precious metals are doped on metal oxide supports individually or as bimetallic catalysts. In a study, Pt, Rd and Ru were doped on $CuO\text{-}CeO_2$ support and highest activity was observed in the case of Pt on $CuO\text{-}CeO_2$ because of strong metal-support interaction [20]. Pt and Ru were studied on SiO_2 and it was concluded that CO adsorption was weaker on bimetallic catalyst than both on monometallic ones because of bimetallic interactions between Pt and Ru [21]. For low temperature CO oxidation one of the most active catalysts

is Pt supported on tin oxide, either in promoted form or as it is. The activity of this catalyst was higher than the individual activities of Pt and SnO_x [1].

Gold-based catalysts are of great scientific interest due to high activity of gold in CO oxidation, especially for low temperature. Another characteristic of gold catalysts is their resistance to moisture and less sensitivity to CO_2 when excess H_2 exists in the reaction mixture [1]. Gold supported on different metal oxides are investigated by different groups. TiO_2, α-Fe_2O_3, Co_3O_4, NiO, $Be(OH)_2$, and $Mg(OH)_2$ were used as supports and it was observed that the catalysts are highly active even at very low temperatures. Small gold particles provide both reversible CO adsorption and increase oxygen adsorption capacity of the catalyst [24]. In another paper investigating TiO_2 support it was found that when gold is supported on titania it is very active for room temperature CO oxidation. Since deactivation was observed after long periods of reaction time, various preparation methods have been studied in order to obtain stable catalysts. Impregnated Au/TiO_2 was found to be the most active one after a sequential pretreatment process. The applied pretreatment process consisted of high temperature reduction and calcination followed by a low temperature reduction [11]. Activity of gold is also compared with Pt for CO oxidation. When both metals are supported on titania, Au/ TiO_2 catalysts exhibited higher activity than Pt/ TiO_2 [24]. In another study, CO oxidation at atmospheric pressure was investigated by using Au catalyst supported on α-Fe_2O_3. Two different CO partial pressure values and different temperatures were applied. Reformer gas which includes CO, H_2, N_2, and O_2 was used. The selectivity was found to be increasing with decreasing temperature due to higher apparent activation energy for H_2 oxidation than for CO oxidation. Kahlich et al. also compared the activities of Au/α-Fe_2O_3 and Pt/γ-Al_2O_3 catalysts. Au supported on α -Fe_2O_3 was found to give the best results [11]. A low-Au content catalyst prepared on ceria was appeared to give high activity for both PROX and WGS [25]. In another study, a gold catalyst was doped on CoO_x (x=1.00 to 1.33) as nanoparticles to investigate the catalytic activity towards CO oxidation. Activities of the catalysts increased with increasing ratio x. Deposited Au particles both promote activity and alter the kinetic order of carbon monoxide [26]. To compare the activity of gold base catalysts with metal oxides and Pt, three catalysts were prepared and tested, namely Au/α-$Fe2O_3$, CuO-CeO_2 and Pt/γ-Al_2O_3. At low reaction temperatures the Au/α-Fe_2O_3 appears to be the most active one. At higher temperatures, CuO-CeO_2 exhibits the highest activity and selectivity [27].

2.3. Effect of Alloying on CO oxidation

Several kinds of alloys have also been investigated for CO oxidation. It was observed in a study that Au-Ag alloy supported on mesoporous Si/Al is active for CO oxidation reaction. Activity of the alloy increased with increasing Al content [28]. The alloys of Rh and Pt metals supported on silica were also examined. As Pt:Rh ratio of bulk concentrations of the metals increases, the alloy become Pt-like more than Rh-like; leading to increase in activity [29]. In another study on Rh-Pt alloy, metals were deposited on a thin film of alumina supported on a Ta foil. The results were compared with the data obtained over both of the metals individually. It was concluded that alloy catalyst is less active than Rh alone. This consequence may be an outcome of less synergistic interaction between the metals on CO oxidation [30]. Another alloy studied for CO oxidation is Pt-Fe/Mordenite. When its results were compared with the Pt/Mordenite catalyst, alloy catalyst appears to be superior to monometallic catalyst [31]. In another study, activity of Pt-Au bimetallic system supported on CeO_2 was compared with activities of Pt/ CeO_2 and Au/ CeO_2 catalysts; results have shown that bimetallic catalyst is more active than the monometallic catalysts [32].

Another alloy giving high CO conversion is Pt-Sn alloy with a stoichiometry of 3:1. In a study [33], both monometallic Pt catalysts and bimetallic Pt-Sn catalysts were prepared on activated carbon supports. Preparation methods, Sn loadings and reduction methods were found to have an effect on catalyst activity. Pt loading was kept constant and Sn loadings were changed. After reduction of the catalyst, Pt-Sn alloy structure was obtained. It was concluded that AC support pretreated by HNO_3 oxidation helps formation of Pt-Sn alloy structure. Among the catalysts that were prepared in different methods the one with 1% wt. Pt – 0.25% wt. Sn over HNO_3 reduced activated carbon showed 100% activity in H_2 free systems. In another study on Pt-Sn alloys [34], it was concluded that the characteristic of the alloy is related to surface chemistry of activated carbon support. The excess in acidic oxygen bearing groups caused more Pt_3Sn formation. The 1% wt. Pt – 0.25% wt. Sn over HNO_3 reduced activated carbon catalyst was investigated in H_2-rich system, also. The catalyst showed a high activity in this condition. However, excessive formation of Pt_3Sn alloy was observed to diminish CO oxidation activity for this catalyst. In hydrogen rich systems Pt-Sn system supported on air-oxidized activated carbon showed

the highest activity and selectivity. The XRD studies showed that PtSn alloy was formed on Pt-Sn system supported on air oxidized AC [3].

2.4. Effect of CO_2 and H_2 Presence on CO Oxidation

Landon et al. have studied Au/Fe_2O_3 catalyst prepared by coprecipitation. The catalyst was initially tested in absence of H_2 and excess CO_2. Afterwards, H_2 was added to reactant gases with 2:1 H_2:CO molar ratio, and this addition diminished the CO conversion for all reaction temperatures [35].

In another paper, α-Fe_2O_3 promoted CuO-CeO_2 catalysts were investigated for their catalytic selective CO oxidation activities. The experiments were conducted in the presence and absence of CO_2. It was found that CO_2 in the reactant stream diminishes the catalytic activity [36]. The study comparing the activities of Au/α-Fe_2O_3, CuO-CeO_2 and Pt/γ-Al_2O_3 have also examined the behaviour of the catalysts in the presence of CO_2. Three of the catalysts were impressed by presence of CO_2 in the reactant stream and exhibited relatively low activity and selectivity. The sensitivity of the catalyst depends on the nature of the catalyst; the gold catalyst was observed as the most sensitive one while Pt catalyst was found resistant [27]. Simsek et al. tested the same catalyst by adding CO_2 to H_2-rich feed stream. The CO conversion increased for all 1% Pt–0.25% SnOx and 1% Pt–1% CeOx catalysts supported on AC1, AC2 or AC3 regardless of the impregnation strategy used. This behaviour was unlike the effect of CO_2 observed with other types of catalysts prepared for selective CO oxidation [37].

2.5. Pt and Alloyed Pt Surfaces

PtSn alloy has the hexagonal $P6_3/mmc$ structure with an enthalpy of formation -58.6 kJ/mol and a melting point of 1549 K [38]. PtSn is the chemical formula for the mineral niggliite.

The Pt-Pt, Pt-Sn and Sn-Sn distances and coordination numbers for pure Pt, PtSn and Pt_3Sn are given in Table 2.1.

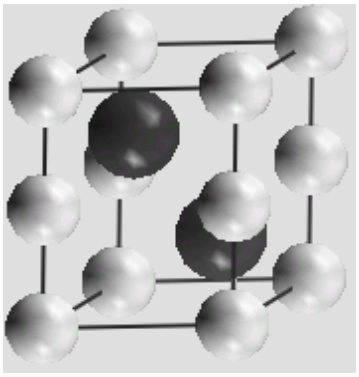

Figure 2.2. Structure of PtSn alloy (Pt: ○ Sn:●)

Table 2.1. Bond distances for different Pt-Sn alloy phases and the element Pt.[39]

Compound	Bond	Number	Distance (Å)
Pt metal	Pt-Pt	12	2.77
		6	3.92
Pt_3Sn	Pt-Pt	8	2.83
	Pt-Pt	6	4.00
	Pt-Sn	4	2.83
	Sn-Sn	6	4.00
PtSn	Pt-Pt	2	2.72
	Pt-Sn	6	2.73
	Sn-Sn	6	3.60

The structures of the low index faces of PtSn allow are shown in Figure 2.3. For the (001) face of the alloy, the shortest contacts correspond to Pt-Sn bindings of 2.73 Å (Table 2.1) between the top and the underlying layers; value is lower than the expected nuclear distance between the elements which is 2.90 Å. The Pt-Pt distances in one layer are large for orbital overlapping and prevent continuous metallic character on this face.

The (100) face is constructed by a layer of parallel platinum chains between isolated tin layers. Short Pt-Pt distance, which is 2.72 Å, appears as the main characteristic of the chains since it is shorter than the one in pure platinum metal (2.77 Å). The third low index face is the (110) face, which exhibits the bulk stoichiometry and includes platinum rows parallel to the c axis. This geometry is the most promising face for surface interactions,

with platinum atoms holding a metallic character; isolated tin atoms are bonded only to platinum chains, leading to the electronic transfer. This structure disfavours the interchange between tin and platinum due to the different functions of both elements [39].

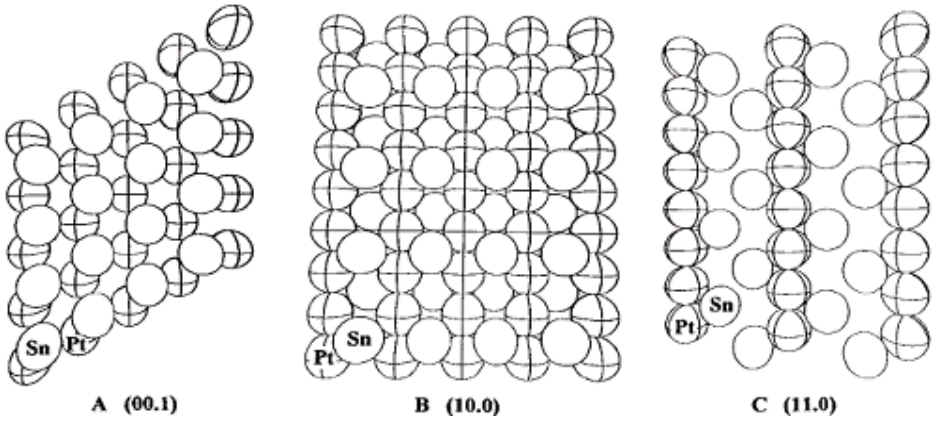

Figure 2.3. Representation of low-index faces of hexagonal PtSn phase [39]

The Pt_3Sn alloy has the $L1_2$ structure including tin atoms on the corners of the cubic unit cell and platinum atoms on the center of faces. Pt_3Sn has an enthalpy of formation of -50.2 KJ/mol and a melting point of 1675 K.

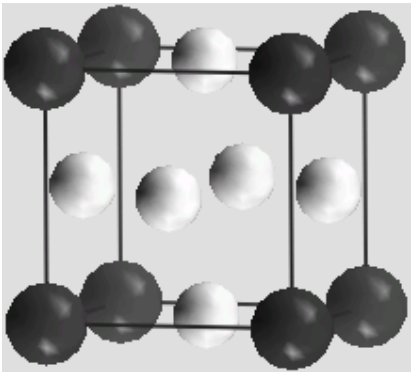

Figure 2.4. Structure of Pt3Sn alloy (Pt: ○ Sn:●)

The structures of Pt_3Sn low index surfaces are given in Figure 2.3.

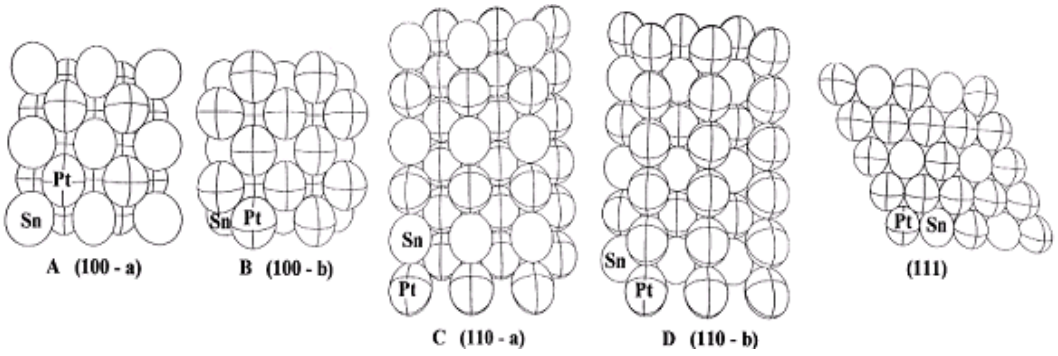

Figure 2.5. Representation of low-index faces of the cubic Pt_3Sn phase.

The (110) planes consist of rows of alternating atoms for (110-a) and of rows of platinum atoms for (100-b). The distance between the rows is 4.00Å. The (111) face exhibits the bulk stoichiometry including Pt-Pt contacts and isolated tin atoms. This face shows an ordered 2D alloy with possible interchanges between platinum and tin atoms which leads to surface enrichment in tin.

Two Pt-Sn/Al_2O_3 catalysts were prepared by different procedures. They were investigated through several characterisation methods to observe the types of alloys. One of the methods was conventional coimpregnation with H_2PtCl_6 and $SnCl_4$ (Sample T). The other catalysts was prepared by using a bimetallic precursor $[Pt(NH_3)_4]SnCl_6$ (Sample N). In the latter sample, the phases PtSn and Pt_3Sn were observed as the most predominant alloy phases besides the minor existence of Pt. The X-Ray diffraction pattern that supports the above conclusion is given in Figure 2.6.

Another characterisation method, X-Ray photoelectron spectroscopy, showed results supporting the XRD data. For both samples, tin was observed to be oxidized. For sample T, the atomic Sn:Al ratio was higher than the bulk value, in agreement with a lower part of tin engaged in alloys as displayed by XRD data. On the other hand, for sample N, with a higher alloy percentage, revealed a lower Sn:Al ratio is observed than the bulk value, which is related to low dispersion of the tin atoms exist in alloy phases with high crystallite sizes [39].

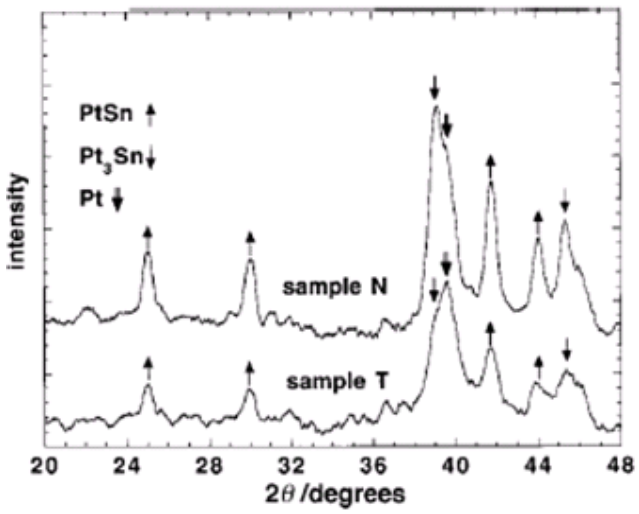

Figure 2.6. The X-Ray diffraction pattern for sample T and N.

Table 2.2. Surface composition for samples T and N from XPS measurements. The bulk values are given in parentheses

Species	Sample T	Sample N
	Atomic ratio (relative deviation 14%)	
O/Al	1.8 (1.5)	1.7 (1.5)
Sn/Al	0.0055 (0.0039)	0.0035 (0.0039)
Cl/Al	0.025 (0.049)	0.025 (0.035)

2.6. Theoretical Studies on Pt and Alloyed Pt Surfaces

Theoretical studies have been conducted to understand the experimental results at atomic scale. The simulations were carried out with the experimentally investigated surfaces of the catalysts. In a study, adsorption of CO on Pt(111) was investigated by using density functional theory method with full geometry optimization. To obtain the full geometry optimization, calculation parameters such as core treatment, number of slab layer, k-points, and size of unit cell were changed. The main aim was to determine the site preference of the adsorption of CO on Pt(111). Atop site is followed by bridge and then hollow sites [40]. In another study, adsorption of CO and atomic O on Pt(111) was investigated by utilizing again density functional theory. It was found that on this surface

the high symmetry sites are energetically similar [41]. In the study of CO adsorption on O-precovered surface, Pt-atop site was the most favoured one [42]. Another study on CO adsorption on defect sites, it was found that CO adsorption was highly sensitive to electronic structure, which was modelled as the d-band center of Pt [42]. In some studies, [42-49], CO adsorption on Pt(111) surfaces were observed to show clear evidence of new step-induces adsorption properties with larger binding energies than CO on flat terraces.

In a study investigating the site preference of CO on Pt(111), different results were obtained from experimental and computational works. Experiments showed the atop site as the preferred one but computational studies found the hollow site as the strongest CO adsorption site [47].

In a theoretical study of CO oxidation on metal and metal oxides, the metal surfaces Ru(0001), Rh(111), Pd(111), Os(0001), Ir(111), Pt(111), and their corresponding metal oxide surfaces (RuO_2(110), RhO_2(110), PdO_2(110), OsO_2(110), IrO_2(110), and PtO_2(110)) were examined. It was observed that barriers on metal oxide surfaces were lower than those on corresponding metal surfaces for CO oxidation. Surface geometry was found as the main parameter leading to higher activity of metal oxide surfaces [49].

The experimentally investigated alloy surfaces were also studied theoretically. In a study investigating alloying effects on the bonding sites of Cu_3Pt(111), it was found that CO is preferentially adsorbed on an atop-Pt site and atomic oxygen is adsorbed on a fcc-hollow site of three Pt atoms. The results for the alloy were compared with those of Pt(111) and Cu(111). It was concluded that adsorption energies of CO and atomic oxygen are less on the alloy surface than the pure metal surfaces [50]. Different metals such as Ru, Mo, and Sn were alloyed with Pt and DFT calculations were used to study CO and OH adsorption on these surfaces. OH was used as oxygen precursor. Results showed that CO is adsorbed on Pt only and not on Sn included sites. OH preferred Sn sites of Pt_3Sn(111) surface [51].

Pt_3Sn, one of the most promising catalysts of CO oxidation, is examined through series of theoretical studies. In the study of low index Pt_3Sn surfaces, adsorption properties of CO were investigated by using quantum mechanical calculations. The studied low index

surfaces were (111), (110), (001). All possible active sites were determined on all possible bulk terminations. The adsorption energies and geometries of CO were determined for all active sites. The results obtained over the alloy surface were compared with those obtained over pure Pt surface for the same geometries. It was found that CO adsorption is weaker on Pt_3Sn surfaces than pure Pt surfaces and this result supports the experimental findings where Pt_3Sn was found to be resistant to CO poisoning. The effect of alloying with Sn was studied through comparing the local density of states profiles for atop-Pt adsorption, both for the carbon end of CO, for its adsorbed and free states, and the Pt atom of the binding site for bare and CO adsorbed surface. To elucidate the electronic changes occurred on CO and Pt upon adsorption, the local density of states profiles of the C end of CO in its free and atop adsorbed states on Pt_3Sn and local density of states of Pt on bare and CO adsorbed Pt_3Sn surface were compared. It was concluded that adding a Sn atom to surface decreases CO adsorption stability of the surface since CO is not adsorbed on Sn sites. Additionally, number of possible CO adsorption sites on alloy surface is limited. It was also found that presence of Sn beneath the adsorption site strengthens the adsorption of CO but the neighbouring Sn on the surface weakens CO adsorption. In case of the site preference of CO for adsorption, the atop-Pt site of the mixed atom termination of $Pt_3Sn(110)$ was found to be the most favourable [52].

In another study, stepped $Pt_3Sn(102)$ surface was examined by quantum mechanical calculations. All possible active sites were determined on two possible bulk terminations. The adsorption energies and geometries of CO were determined for all active sites. The results showed the most favorable adsorption sites as the short bridge site on the terrace of pure-Pt row of the mixed-atom-ending termination, atop site at the step-edge of the pure row of pure-Pt-ending termination and atop site at the step-edge of the pure-Pt row of the mixed-atom-ending termination. Comparisons with $Pt_3Sn(110)$ were considered due to (110) orientation of $Pt_3Sn(102)$ terraces. The local density of states analysis was utilized to understand the changes in electronic structure of surface atoms as well as adsorbed CO molecule. The electronic properties of Pt atoms at stepped $Pt_3Sn(102)$ surface were found different from those at (110) surface. CO adsorption on $Pt_3Sn(102)$ sites was found to be stronger than those on $Pt_3Sn(110)$. The local density of states of Pt and C of adsorbed CO was generated. The effect of CO chemisorption on the electron density distribution of the corresponding Pt atom was investigated by performing the local density of states

calculations; the LDOS profiles of the surface metal atoms with CO-adsorbed atop and of their bare state were compared. The results showed that presence of Sn beneath the adsorption site was again found strengthening the adsorption of CO but the neighboring Sn on the surface weakens CO adsorption as in low index Pt_3Sn surfaces [53].

2.7. Theory of Computational Methods

Ab inito quantum mechanical techniques optimize the geometries of molecules by minimizing energy either partially or fully. Quantum mechanical models are different solutions to Schrödinger equation with different approximations. Schrödinger equation considers molecules as collections of nuclei and electrons without taking chemical bonds into account. The general approach to find the energy of a system is to make Born-Oppenheimer approximation, and than Hartree-Fock assumption in which electrons move essentially as independent particles and do not interact each other. The most difficult issue in any electronic structure calculation is handling the electron-electron interaction. Due to Coulomb forces between electron charges, they interact with each other. The energy between electrons can be diminished by separating the electrons spatially, but the deformation of electronic wave functions to increase the distance needs kinetic energy. The energy between electrons and the kinetic energy should be balanced. The wave function of a many-electron system must be antisymmetric under exchange of any two electrons since the electrons comply with the Fermi-Dirac statistics and are subject to the Pauli Exclusion Principle. This antisymmetric property produces a spatial distance between electrons which have the same spin and decreases the Coulomb energy of the electronic system. The energy stems from the antisymmetry is called as the exchange energy. This energy is added to total energy calculation and it is stated as Hartree-Fock approximation. If the electrons which have opposite spins are spatially separated, the Coulomb energy can be reduced below the Hartree-Fock energy of the system. If this is the case, the Coulomb energy of the system is reduced at the cost of increasing the kinetic energy of the electrons. The difference between the energy of the system calculated using the Hartree-Fock approximation and the many-body energy is called as the correlation energy.

To describe the effects of exchange and correlation in an electron gas Hohenberg and Kohn and Kohn and Sham developed Density Functional Theory. Hohenberg and Kohn

stated that the total energy together with exchange and correlation of an electron gas is a unique functional of the electron density. The minimum value of this functional is the ground state energy of the electronic system and the density that corresponds to this minimum value is the exact single-particle ground-state density. Kohn and Sham showed how it can be managed to replace the many-electron equations. Kohn-Sham energy functional is written as:

$$[\rho] = T[\rho] + \int V_{ext}(r)\rho(r)dr + V_H[\rho] + E_{xc}[\rho] \tag{2.6}$$

where ρ is the charge density, T is the kinetic energy of the system, V_{ext} is an external potential acting on the system, E_{xc} is the exchange correlation energy, and

$$V_H = \frac{e^2}{2}\int \frac{\rho(r)\rho(r')}{|r-r'|}drdr' \tag{2.7}$$

is the Hartree energy. As proposed Kohn and Sham the charge density can be written as the sum of squares of a set of orthonormal wave functions $\psi_i(r,s)$:

$$\rho(r) = \sum_i^N \sum_s |\psi_i(r,s)|^2 \tag{2.8}$$

which are the solutions to the Schrödinger equation for N noninteracting electrons moving in an effective potential $v_{eff}(r)$

$$-\frac{\hbar}{2m}\nabla^2\psi_i(r,s) + v_{eff}(r)\psi_i(r,s) = \varepsilon_i\psi_i(r,s) \tag{2.9}$$

where the effective potential is defined to be

$$v_{eff}(r) = V_{ext}(r) + e^2 \int \frac{\rho(r')}{|r - r'|} dr' + \frac{\delta E_{xc}[\rho]}{\delta \rho} \tag{2.10}$$

These three equations form the Kohn-Sham equations in their canonical form [54]. If the exchange-correlation energy functional were known exactly, then taking the functional derivative with respect to the density would produce an exchange-correlation potential that included the effects of exchange and correlation exactly. Two problems arise while handling an infinite number of noninteracting electrons moving in the static potential of an infinite number of nuclei or ions. Firstly, a wave function must be calculated for each of the infinite number of electrons in the system. In the second place, since each electronic wave function extends over the whole solid, the basis set required to expand each wave function is infinite. These problems can be overcome by applying supercell approach to calculations and using Bloch's theorem which states that in a periodic solid each electronic wave function can be written as the product of a cell-periodic part and a wavelike part.

$$\psi_i(\mathbf{r}) = \exp[\mathrm{i}\,\mathbf{k}\cdot\mathbf{r}]\mathrm{f}_i(\mathbf{r}) \tag{2.11}$$

The cell-periodic part of the wave function can be extended using a basis set including a discrete set of plane waves whose wave vectors are reciprocal lattice vectors of the crystal.

$$\mathrm{f}_i(\mathbf{r}) = \sum_{\mathbf{G}} \mathrm{c}_{i,\mathbf{G}} \exp\,[\mathrm{i}\mathbf{G}\cdot\mathbf{r}] \tag{2.12}$$

where the reciprocal lattice vectors G are defined by $\mathbf{G}\cdot l = 2\pi m$ for all l where l is a lattice vector of the crystal and m is an integer. So, each electronic wave function can be written as a sum of plane waves,

$$\psi_i(\mathbf{r}) = \sum_{\mathbf{G}} \mathrm{c}_{i,\mathbf{k}+\mathbf{G}} \exp\,[\mathrm{i}(\mathbf{k}+\mathbf{G})\cdot\mathbf{r}] \tag{2.13}$$

Electronic states are allowed only at a set of k points determined by the boundary conditions that apply to the bulk solid. The density of the allowed k points is proportional to the volume of the solid. The infinite number of electrons in the solid is elucidated by an infinite number of k points and only a finite number of electronic states are occupied at each k point. The Bloch theorem converts the problem of calculating an infinite number of electronic wave functions to one of calculating a finite number of k points. The occupied states at each k point contribute to the electronic potential in the bulk solid so that an infinite number of calculations are needed to compute this potential. However, the electronic wave functions at k points that are very close together will be almost identical. So, it is possible to represent the electronic wave functions over a region of k space by the wave functions at a single k point. In this case the electronic states at only a finite number of k points are required to calculate the electronic potential and hence determine the total energy of the solid.

3. CALCULATIONS

3.1. Computational Details of CASTEP Calculations

Density functional theory calculations were performed in a repeated slab geometry, using the program package CASTEP in Material Studio of Accelrys Inc. (version 4.0). The slabs were constructed using the core product of Material Studio Visualizer. It is used to construct and manipulate graphical models. The PtSn surfaces were modelled as five-layer slabs, with the upper two layers relaxed with the adsorbate and the bottom two layers are fixed in their bulk positions. The vacuum thickness between the slabs was 10 Å. The electron-ion interaction was included through the use of ultrasoft pseudopotentials and the electronic wave functions were expanded in a basis set of plane waves, up to a kinetic energy cutoff of 340 eV. Sampling of the (1x1) and (2x1) Brillouin zones were achieved by summation over Monkhorst-Pack meshes of dimensions 3x6x1 and 3x3x1, respectively.

Exchange and correlation were included through the use of generalized gradient approximation (GGA) with the Perdew-Burke-Ernzerhof (PBE) functional. No spin polarization effects were included in the exchange-correlation functional, thus the calculations use the same orbitals for alpha and beta spins. Pulay's density mixing scheme was used for the SCF electronic minimization. A smearing range of 0.1 eV was applied at the Fermi level and 12 empty bands were introduced in order to speed up the convergence. The energy was corrected by extrapolation to zero temperature.

3.2. Building the PtSn Crystal

The PtSn alloy has the hexagonal $P6_3/mmc$ structure with an enthalpy of formation -58.6 kJ/mol and a melting point of 1549 K [38] and is the chemical formula for the mineral niggliite. The unit cell was constructed using MS Visualizer with the information above. The bulk structure of the alloy was optimized using CASTEP with the parameters given in Section 3.1.

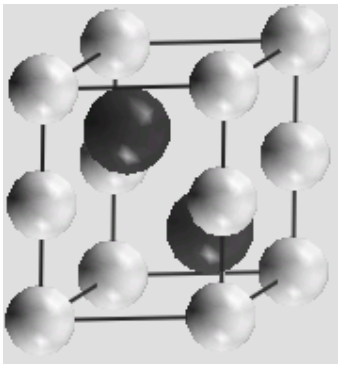

Figure 3.1. Structure of PtSn alloy (Pt: ○ Sn:●)

3.3. Building and Optimizing the PtSn(110) Surface

The surface was created in two steps. Firstly, the surface was cleaved with the specified Miller indices. Then a vacuum slab was constructed containing the cleaved surface.

When cleaving the surface, the Miller indices of the desired plane were written to "Cleave Surface" dialog box. The "depth" on the same dialog box specifies the atomic layers of the slab. For this study number of layers of the 3D slab was chosen as 5 layers since it provides accurate results for a reasonable computational time. The "top" option provides to choose different surface characteristics if there exists any. For the PtSn(110) surface there is one possible termination.

The five – layer PtSn(110) surface is given in Figure 3.2. Cleaving crystals creates 2D periodic surface whereas CASTEP take 3D systems as input. Therefore, this surface was used to form the vacuum slab.

To construct the vacuum slab the surface was repeated in a given direction using a repeat distance. Since the repeat distance is greater than the surface thickness, it introduces a region of vacuum or a vacuum slab between the surface units. It must be noted that the cell should be wide enough to prevent the interactions of adsorbent with the molecules in neighbouring cells. The attractions from the top and bottom cells were tried to be diminished by introducing the thick enough vacuum layer. On the other hand, the wider the

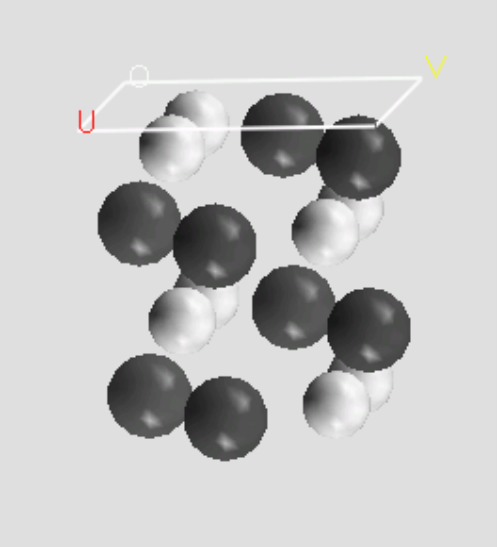

Figure 3.2.The cleaved PtSn(110) surface (Pt: ○ Sn:●)

the vacuum layer is, the slower the calculations are. Therefore, an optimized vacuum layer should be constructed. For this work, 10 Å of vacuum thickness was observed as to be sufficient for accurate results.

The repeat distance was achieved by adding the vacuum thickness value to the surface thickness and this gives the thickness of the vacuum slab. The (1x1) slab of PtSn(110) surface is given in Figure 3.3. The standard orientation was chosen from the software while visualizing the structure.

The 20 atom slab of PtSn(110) surface in Figure 3.3 displays the model for the 2D-infinite surface which is given in Figure 3.4 in CPK style display. The CPK style represents the atoms as spheres with radii related to the van der Waals radii scaled by the CPK scale factor.

After constructing the vacuum slab, it was optimized with the parameters given in Section 3.1. When optimizing the surface, the top two layers were relaxed and the lower three layers were fixed at their positions. The number of layers to be relaxed was determined by a set of optimization simulations.

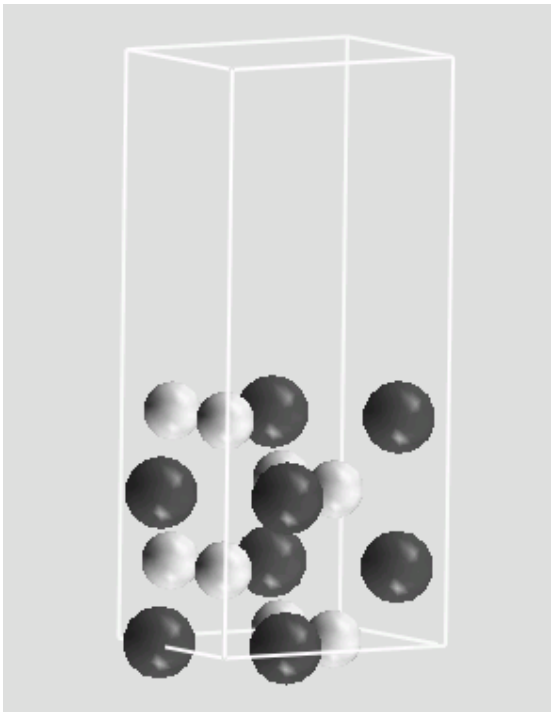

Figure 3.3. The (1x1) vacuum slab for the PtSn(110) surface (Pt: ○ Sn:●)

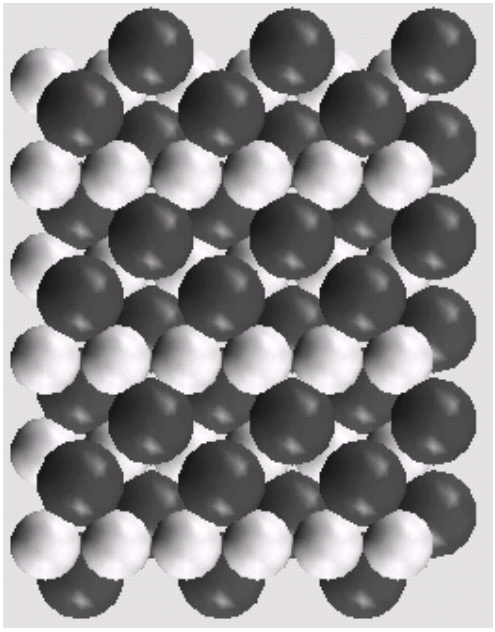

Figure 3.4. The (1x1) vacuum slab for the PtSn(110) surface (Pt: ○ Sn:●)

3.4. Determination of Active Sites for CO Adsorption

For CO adsorption in this study, the determination of active sites was carried out by considering the sites found to be suitable in the study of Gülmen et al. [52]. CO is known to be adsorbed on or move toward Pt sites, therefore sole Sn sites were not investigated for CO adsorption in this study. Figure 3.5 shows all of the sites for PtSn(110) surface. The names of the sites, the coverage of the surface, and the width of the supercell involved in the simulation are given in the Table 3.1.

Table 3.1. List of active sites for PtSn(110) surface

Site	Name	Supercell	Coverage
A	Atop Pt	(1×1)	0.25
B	Pt-Pt Bridge	(1×1)	0.25
C	Pt-Sn Bridge	(1×1)	0.25
D	Pt_2Sn	(1×1)	0.25
E	Atop Sn	(1×1)	0.25
F	Sn-Sn Bridge	(1×1)	0.25

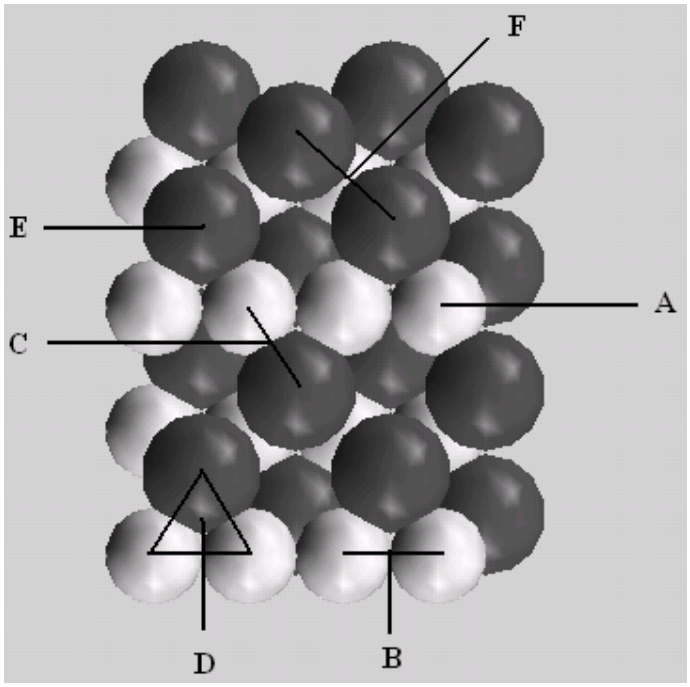

Figure 3.5. Schematic representation for the active sites on the PtSn(110) surface (Pt: ○ Sn:●)

3.5. Optimization of the Adsorption System

The CO molecule was bound to the site by its carbon end, and then the oxygen atom was bound to carbon by a bond distance of free CO. The bond length of CO molecule was calculated by geometry optimization using CASTEP. The resultant values of the study involving CO adsorption on $Pt_3Sn(110)$ [52] were used as the initial values of the site-carbon bonds for the current study, since there is no data reported for PtSn surfaces. The geometry and adsorption energy of all sites was calculated by optimizing the system using CASTEP. Optimization processes were conducted by relaxing the top two layers of the adsorbate.

The illustration of bonded CO molecule prior to optimization is given in Figure 3.6 for Pt_2Sn site.

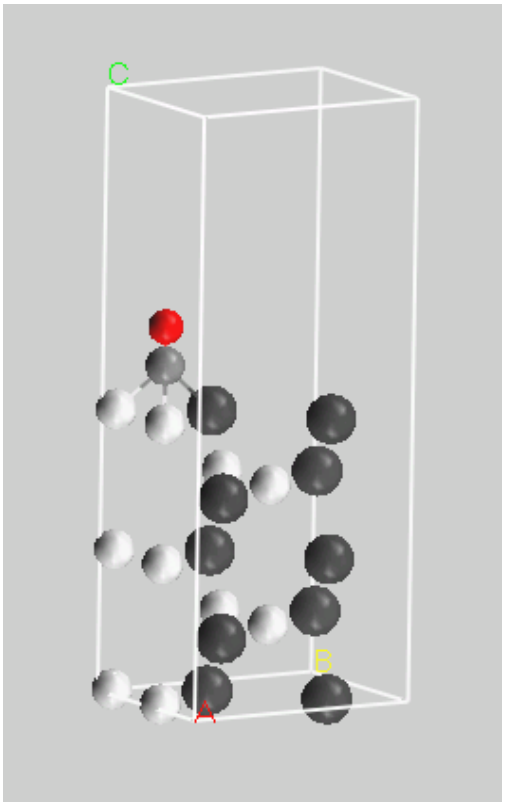

Figure 3.6. Pt_2Sn bonded CO on PtSn(110)

The adsorption energies per CO molecule was calculated as:

$$E_{ads} = E_{CO + slab} - (E_{CO} + E_{slab}) \quad (3.1)$$

where E_{ads} is the adsorption energy of CO at that site, $E_{CO + slab}$ is the total energy of the slab with the adsorbed CO on the surface, E_{CO} is the total energy of the optimized free CO molecule which was found as -592.216 eV and E_{slab} is the energy of the optimized bare slab.

3.6. Adsorption of Other Reactants and Products of PROX

A realistic PROX system includes CO_2, O_2, and H_2 gases besides CO. In order to investigate the behaviours of these gases on Pt and Pt-Sn alloys, a comparative study was

carried out. The adsorption strengths and adsorbate-adsorbent interactions for these gases were studied on monometallic Pt(110) and on the alloys of Pt-Sn, namely Pt-Sn(110) and Pt3Sn(110). The adsorption studies were carried out on the active sites of those surfaces; the adsorption energies obtained and the extent of electronic interactions between the adsorbate and the site were analyzed through a comparative study. The active sites for surfaces Pt_3Sn surfaces are given in Figure 3.7 and Table 3.2.

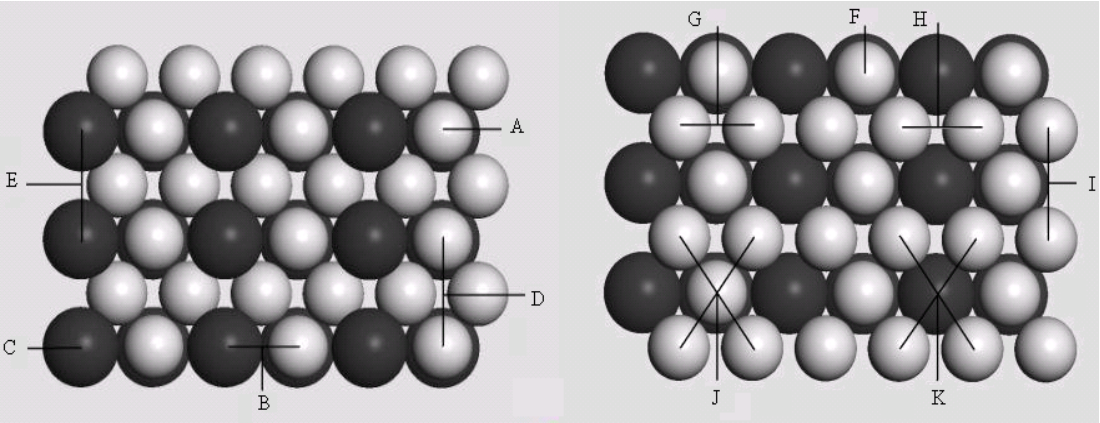

Figure 3.7. Schematic representation for the active sites on the $Pt_3Sn(110)$ mixed (left) and pure-Pt ending (right) surfaces (Pt: ○ Sn:●)

Table 3.2. List of active sites for $Pt_3Sn(110)$ surface

Surface	Site	Name	Supercell	Coverage
Mixed atom ending	A	Atop Pt	(1×1)	0.5
	B	Pt-Sn Bridge	(1×1)	0.5
	C	Atop Sn	(1×1)	0.5
	D	Pt-Pt Long Bridge	(2×1)	0.25
	E	Sn-Sn Long Bridge	(2×1)	0.25
Pure-Pt ending	F	Atop Pt	(1×1)	0.5
	G	Pt-Pt Bridge on Pt	(1×1)	0.5
	H	Pt-Pt Bridge on Sn	(1×1)	0.5
	I	Pt-Pt Long Bridge	(2×1)	0.25
	J	ffh, Pt at bottom	(2×1)	0.25
	K	ffh, Pt at bottom	(2×1)	0.25

The active sites for surfaces Pt_3Sn surfaces are given in Figure 3.8 and Table 3.3.

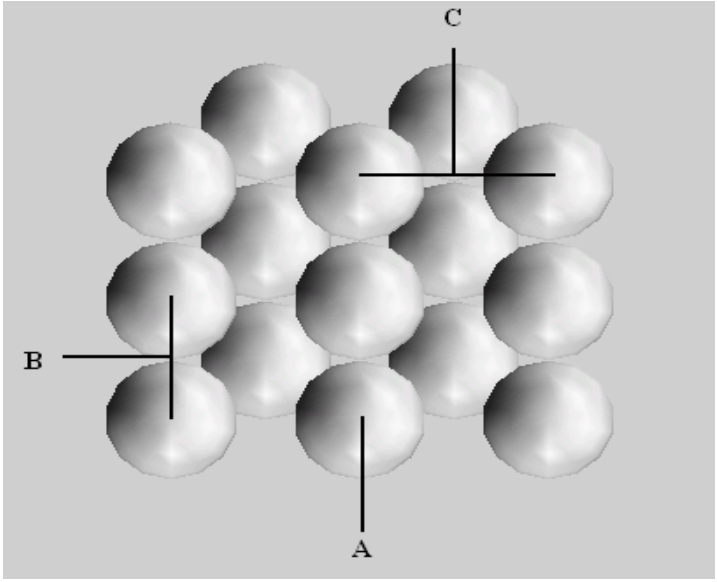

Figure 3.8. Schematic representation for the active sites on the Pt(110) surface

Table 3.3. List of active sites for PtSn(110) surface

Site	Name	Supercell	Coverage
A	Atop	(1×2)	0.5
B	Short Bridge	(1×2)	0.5
C	Long Bridge	(2×2)	0.25

3.7. Plotting the LDOS Charts

Local density of states is a semi-qualitative tool to analyze electronic mechanism of adsorption process. LDOS exhibits the contribution of the atoms to electronic states of the system in various parts of the energy spectrum without resolving the contributions according to the angular momenta of the states (i.e. identifying the s, p, d, and f characters).

Material Studio produces several types of DOS plots using the optimization results generated by CASTEP. CASTEP uses a simplified linear interpolation scheme developed by Ackland (1998). This method is based on linear interpolation in paralelopipeds formed

by the points of the Monkhorst set, followed by the histogram sampling of the resultant set of band energies. Smearing method is applied with a width of 0.1 eV. Charts are produced by plotting the LDOS data (electrons/eV) vs. energy (eV) [55].

LDOS analysis was conducted for Pt and Sn atoms on the surface as well as the adsorbate species. The LDOS charts were used to elucidate the electronic modification of the adsorption sites when the surface geometry changes by comparing the bare states of the adsorbates and surface atoms.

The LDOS of adsorbent atom was determined for both bare surface and for adsorbed state at the binding surface atom. The LDOS profiles were presented in same figure in order to examine the modifications occurred on the profile upon adsorption. The isolated state of adsorbent species was created by approximating it to an empty slab of the same size as the adsorption system, and placing the species in that slab. A Single-Point-Energy (SPE) calculation was carried out by CASTEP to obtain the LDOS data.

4. RESULTS AND DISCUSSION

4.1. Bare PtSn(110) Surface

The PtSn(110) surface has one type of ending, which includes Pt and Sn atoms at its surface. The (1x1) slab of 5-layer thick PtSn(110) consists of 20 atoms; 10 Pt atoms and 10 Sn atoms are in the slab unit. During the simulations, the top two layers are relaxed and the bottom three layers are kept fixed in their positions. The energy of relaxed surface was calculated as -8209.402 eV.

The number of layers to be relaxed was decided based on the comparison of the results obtained from the two and three layers relaxed cases. For that comparison, first, two layers of the slab were relaxed and the remaining layers were kept fixed. Later, the number of relaxed layers was increased to three. The CO adsorption energies were then calculated for atop Pt site for both cases; -1.086 eV was obtained when two layers relaxed and -1.080 eV was obtained three layers relaxed cases. Since the difference in CO adsorption energies obtained was as small as 0.006 eV, the simulations were carried out with five layers slab having top two layers relaxed for the rest of this study considering the shorter computational time necessary for this option.

4.2. CO Molecule

The bond length of the optimized free CO molecule was calculated as 1.134 Å which is in good agreement with its experimental (1.123 Å [55]) and theoretical (1.138 Å [56], 1.128 Å [57]) values. The energy of CO molecule was determined as -592.217 eV.

4.3. CO Adsorption on PtSn(110) Surface

CO adsorption studies in literature verified that CO interacts preferentially with Pt, but does not bind to the Sn atoms or Sn included sites on a Pt-Sn cluster. Starting from this point, CO binding preferences of each site were investigated for all possible adsorption sites on PtSn(110) surface. The calculations were conducted with the parameters

mentioned in Section 3.1. For each of the sites, the calculated adsorption energies, and Pt-C, C-O, Sn-C bond lengths are given in Table 4.1. The newly formed and broken bonds are underlined. The CO binding energy for all sites was obtained from Equation 3.1.

Geometry optimization gives the relaxed metal surface and adsorbate molecule with a minimum energy configuration. For some sites, surface position of CO molecule was observed to deviate from its original geometry significantly and diffuse to the neighbouring site. For instance, for site D, which is comprised from two Pt atoms and one Sn atom, the adsorbed CO molecule moves away from the adsorption site. (Figure 4.1) As observed from the optimized geometry, the adsorbed CO molecule has moved towards the Pt atoms and, at the same time, away from the Sn atoms; resultantly it approached to the nearest stable adsorption position, which is found as Pt-Pt bridge site, site B. Thus, the Pt_2Sn site, site D, clearly does not adsorb CO stably. The other sites present on PtSn surface which can not adsorb CO stably are marked with (*) in Table 4.1. As indicated in the literature, the sites including Sn were found not able to adsorb CO stably [58-60].

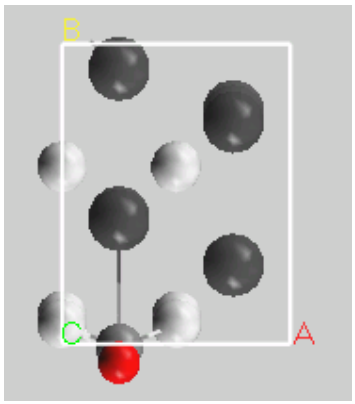

Figure 4.1. The optimized Pt_2Sn site on the PtSn(110) surface, as an illustration of an unstable adsorption site (Pt: ○ Sn:●)

The order of CO binding preferences of the stable sites was investigated using calculated adsorption energies for PtSn, Pt_3Sn, and Pt surfaces.

Table 4.1. Possible CO adsorption sites, corresponding adsorption energiesand data on geometric properties of CO-Surface complex upon CO adsorption on PtSn(110), Pt_3Sn(110) and Pt(110) surfaces

Surface		Site	Name	Size	Coverage	E_{ads} (eV)	Bond Lengths (Å)			
							Pt-C		Sn-C	C-O
PtSn		A	Atop Pt	1x1	0.25	-1.006	1.924			1.157
		B	Pt-Pt Bridge	1x1	0.25	-1.258	2.025	2.027		1.178
		C*	Pt-Sn Bridge	1x1	0.25	-1.032	1.917		3.168	1.158
		D*	Pt_2Sn	1x1	0.25	-1.279	2.029	2.029	3.296	1.177
Pt_3Sn	Mixed	A	Atop Pt	1x1	0.5	-1.544	1.891			1.161
				2x1	0.25	-1.607	1.884			1.161
		D	Pt-Pt Long Bridge	2x1	0.25	-1.631	2.048	2.039		1.191
	Pure	F	Atop Pt	1x1	0.5	-2.464	1.865			1.158
				2x1	0.25	-2.255	1.873			1.159
		G	Pt-Pt Bridge on Pt	1x1	0.5	-2.160	2.019	2.071		1.176
				2x1	0.25	-2.472	2.020	2.036		1.176
		H	Pt-Pt Bridge on Sn	1x1	0.5	-2.309	2.016	2.048		1.176
				2x1	0.25	-2.402	2.015	2.049		1.178
		I	Pt-Pt Long Bridge	2x1	0.25	-2.666	2.019	2.021		1.180
Pt		A	Atop	1x2	0.5	-2.458	1.856			1.158
				2x2	0.25	-2.4004	1.852			1.159
		B	Short Bridge	1x2	0.5	-2.328	2.005	2.014		1.176
				2x2	0.25	-2.585	1.997	1.994		1.800
		C	Long Bridge	2x2	0.25	-2.190	2.038	2.047		1.187

Firstly, CO adsorption on atop Pt site, site A, was investigated. The adsorption energy for this site was calculated as -1.006 eV. At the end of the optimization process, the Pt-C bond length was found as 1.93 Å. The C-O bond length prior to optimization was 1.148 Å and this bond elongated to 1.157 Å at the end of the optimization. This indicates that the structure of the CO molecule has changed due to the adsorption since the interaction between the C-end and the surface weakens the C-O bond. The orientation of the CO molecule was perpendicular to the surface before optimization and it remained the same during the optimization. It is clearly observed that the CO adsorption is stable for this site.

Another site on which CO adsorption was examined is Pt-Pt bridge site (B). Site B was found as the most favourable CO adsorption site with the lowest adsorption energy of -2.025 eV among the stable sites on PtSn(110) surface adsorbing CO stably. The O end of the CO molecule slightly tilted towards Sn atom on the surface at the end of the optimization process. The bond length of the CO molecule was elongated to 1.178 Å. The Pt-C bonds were measured as 2.025 Å and 2.027 Å.

CO adsorption was not fount stable on the other two possible sites. One of those sites is Pt-Sn bridge site, site C. The CO molecule move towards to nearest stable site, site A. In the final structure, only Pt atom was bonded to C end of the CO molecule, while the Sn-C bond was broken with a distance of 3.168 Å from the surface Sn. The Pt-C bond length was 1.917 Å, which is a value very close to the Pt-C bond length obtained upon atop adsorption. The C-O bond length is also almost the same with atop value, being 1.158 Å.

Other site on which CO adsorption was found unstable is Pt_2Sn site, D. The adsorbed CO molecule have moved and stabilized at site B, the Pt-Pt bridge site. The Pt-C bond lengths were 2.029 Å, and the Sn-C bond was broken with a distance of 3.296 Å from the surface Sn. The C-O bond length was 1.177 Å, as in the case of Pt-Pt bridge site B. The adsorption energy for this site was calculated as -1.032 eV.

4.3.1. CO Adsorption on PtSn(110), Pt_3Sn(110), and Pt(110) Surfaces: The Effect of Sn Presence

In order to examine the effect of Sn content of the alloy on CO adsorption, the CO adsorption energies on similar adsorption sites belong to three different alloy surfaces, namely Pt(110), Pt_3Sn(110) and PtSn(110), were compared. Gülmen et al. investigated all possible faces of the Pt_3Sn and Pt surfaces for CO adsorption. For an appropriate comparison, the CO adsorption on the sites of (110) surfaces, which have been reported as adsorbing CO stably, were again studied with the parameters that were mentioned in Section 3.1.

First of all, atop sites were previously reported as the most energetically favoured sites in experimental works for both Pt_3Sn(110) and Pt(110) surfaces. After optimizing the possible sites with the new parameters, it was observed that atop CO adsorption was the strongest for Pt(110) surface, however, for pure-Pt ending termination of Pt_3Sn(110) surface, long Pt-Pt bridge site, site I, was favoured by CO molecule more than the atop site, site F. On the other hand, among the possible adsorption sites that exist for θ=0.5, atop Pt site appears as the most energetically preferred site of Pt_3Sn(110) surface, with CO adsorption energy of -2.4644 eV. The C-O bond elongated to 1.158 Å and Pt-C bond length was 1.865 Å. For lower surface coverage (θ=0.25), atop Pt site, F, of Pt_3Sn(110) was not the strongest site adsorbing CO stably. The adsorption energy was calculated as -2.255 eV. The elongation in C-O bond length and increase in Pt-C distance were observed for atop adsorption on Pt and PtSn surfaces; for PtSn surface for 0.25 ML coverage, Pt-C was 1.924 Å with C-O as 1.157; while the same parameters were calculated as 1.852 Å and 1.159 Å, respectively, for monometallic Pt surface. The relation between the Sn content and strength of CO adsorption is given in Figure 4.2. The surface coverage is taken 0.25 ML for all surfaces. Presence of Sn metal on the surface is known to be weakening CO adsorption. The comparison of adsorption energies of atop sites revealed that as Sn content of the surface increases, strength of CO adsorption diminishes. In order to determine the effect of Sn on top layer of the alloy surface, the comparison is conducted using atop site, site A, of mixed atop ending configuration of Pt_3Sn(110) surface. The decrease in CO adsorption strength with increasing Sn content on the surface is observed more clearly from Figure 4.1. Surface coverage of CO is taken as 0.25 for this comparison.

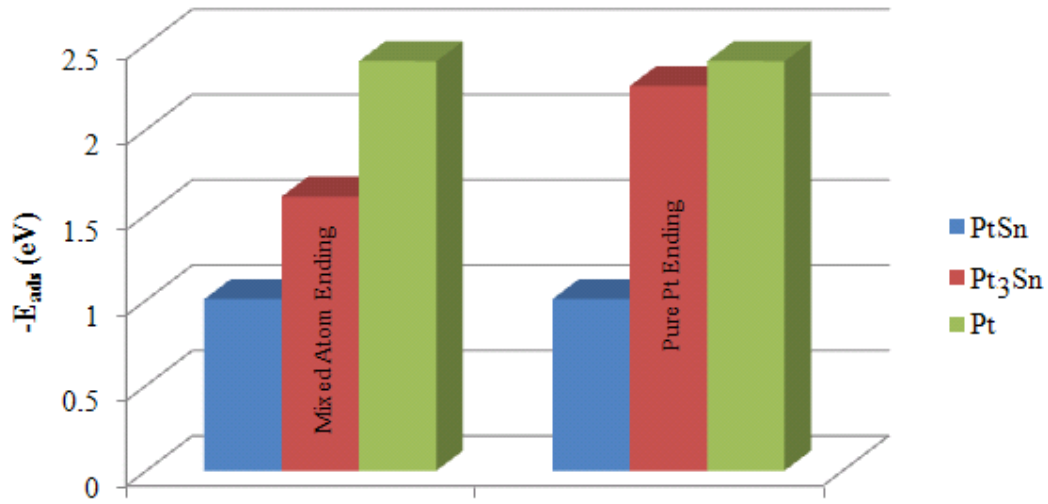

Figure 4.2. Comparison of CO adsorption strengths of atop sites of PtSn(110), Pt_3Sn(110) and Pt(110) surfaces (θ=0.25)

Pt-Pt bridge site B of PtSn(110) surface is favored most. For pure Pt ending configuration of Pt_3Sn(110) surface, there are two different bridge sites. The difference between them is the type atom beneath the adsorption site. There is a Pt atom beneath site G, and an Sn atom under site H. The adsorption strength of CO on these sites was found depend on coverage. At low coverage (θ=0.25), the site on Pt atom was found more favored than the site on Sn atom, with adsorption energies -2.472 eV and -2.402 eV, respectively. However, at high coverage (θ=0.5), site H was found energetically more favoured then site G, with adsorption energies of -2.309 eV and -2.160 eV, respectively. Since the adsorption strenghts are compared at θ=0.25, the Pt-Pt bridge site on Pt, site G, found as the more preferred site at this coverage. The C-O bond lengths and Pt-C bond lengths are consistent with the adsorption energies for the three surface. C-O bond lengths are 1.176 Å for both Pt_3Sn(110) and Pt(110) surfaces. Pt-C bond lengths are 2.020 Å and 2.036 Å for Pt_3Sn(110), and 2.005 Å and 2.014 Å for Pt(110) surface. The relation between Sn content and CO adsorption energy for the bridge sites is given in Figure 4.3. The adsorption energies for 0.25 surface coverage are used for comparison. Increase in Sn content seems to decrease the adsorption energy for bridge sites as well. Another comparison is conducted using the values of mixed atom ending configuration of Pt_3Sn(110) surface. The dependence of adsorption energy on Sn content on top layer of the alloy can be clearly observed from Figure 4.3.

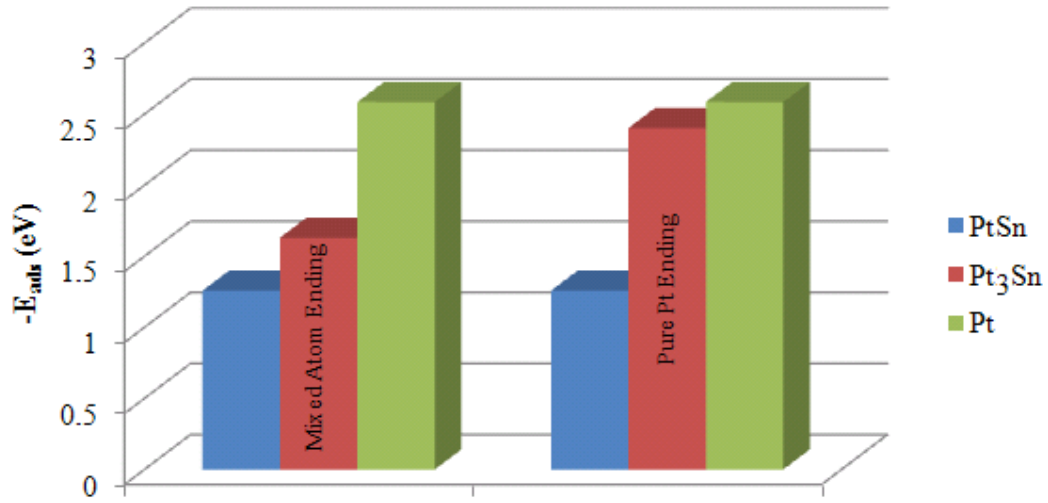

Figure 4.3.Comparison of CO adsorption strengths of bridge sites of PtSn(110), $Pt_3Sn(110)$ and Pt(110) surfaces (θ=0.25)

4.4. Hydrogen Adsorption on PtSn(110), $Pt_3Sn(110)$, Pt(110) Surfaces and Their Comparison

Atomic hydrogen adsorption was investigated for (110) surfaces of pure Pt and PtSn and Pt_3Sn alloys. Although H_2 is certainly the most common and simple molecule involved in catalytic processes, its surface behaviour has not yet been cleared. On the other hand, it is known that hydrogen is adsorbed dissociatively on Pt surfaces [61]. Based on reported findings, atomic adsorption of hydrogen was analyzed in this study. The results for all sites that have been optimized are given in the Table 4.2. The energy of free H atom was calculated as -12.5279 eV.

It is very well known that hydrogen adsorption properties of the active metal/alloy crystals play a crucial role in PROX, for which nearly 60% of the feed is hydrogen. A surface with high hydrogen capacity (i.e. large number of sites for hydrogen adsorption) and ability to adsorb hydrogen strongly may suffer from both low CO oxidation activity and low CO selectivity.

Hydrogen adsorption on PtSn(110) surface was investigated for all possible sites. The only stable site for hydrogen adsorption was the Pt-Pt bridge site, the site B. Altough it

seems to be tilted towards empty area of the unit cell, when CO adsorption on other sites was examined, it was observed that bonded hydrogen move towards to bridge position from its initial state for all sites. Therefore, Pt-Pt bridge site B is designated as the sole stable site for hyrogen adsorption on PtSn(110) surface. The length of Pt-H bonds were 1.755 Å and 1.753 Å for this site and the adsorption energy was calculated as -3.804 eV.

The other H adsorption sites that were investigated are namely atop Pt, Pt_2Sn, and sites. At the end of the calculations of all sites, the geometry of hydrogen atom present on those sites was found assume the position of H atom adsorbed on the Pt-Pt bridge site B with slightly different Pt-H bond lengths. (Table 4.2)

There exists two possible sites for atomic hydrogen adsorption on Pt(110) surface. Both of them were found suitable for stable H adsorption. First one is atop site A, on which H was adsorbed with adsorption energy of -3.91 eV. The Pt-H bond length was 1.57 Å.

Another stable site for H adsorption is short bridge site B on Pt(110) surface. Adsorption energy for this site was evaluated as -3.99 eV, which exhibits that the site is the most energetically preferred for atomic hydrogen adsorption. That supports the conclusion of a study investigating H adsorption on Pt(110) surface [62]. Zhang et al. stated the short bridge site B on Pt(110) surface as the most favored one for atomic hydrogen adsorption.

For $Pt_3Sn(110)$ surface, the possible adsorption sites for hydrogen atom are atop Pt site F, Pt-Pt bridge on Sn site H, and Pt-Pt bridge on Pt site G for pure-Pt ending termination; and atop Pt site A and Pt-Sn bridge site B for mixed atom ending termination. The three sites on pure-Pt ending termination of $Pt_3Sn(110)$ surface adorbed H atom stably. Adsorption energy for atop site was calculated as -3.91 eV. The Pt-H bond length was 1.59 Å for this site.

Table 4.2. Possible H adsorption sites, corresponding adsorption energies and data on geometric properties of H-Surface complex upon atomic H adsorption on PtSn(110), Pt_3Sn(110) and Pt(110) surfaces

Surface		Site	Name	Size	Coverage	E_{ads} (eV)	E_{ads}-E_{diss} (eV)†	Bond Lengths (Å)		
								Pt-H		Sn-H
PtSn		A*	Atop Pt	1x1	0.25	-3.773	-1.5135	1.756	1.755	
		B	Pt-Pt Bridge	1x1	0.25	-3.804	-1.5437	1.755	1.753	
		D*	Pt_2Sn	1x1	0.25	-3.795	-1.5349	1.753	1.754	3.047
Pt_3Sn	Mixed	A	Atop Pt	1x1	0.5	-3.18	-0.92	1.585		
		B*	Pt-Sn Bridge	1x1	0.5	-3.502	-1.2421	1.593		3.326
	Pure	F	Atop Pt	1x1	0.5	-3.908	-1.6477	1.591		
		G	Pt-Pt Bridge on Pt	2x1	0.25	-4.190	-1.9296	1.777	1.731	
		H	Pt-Pt Bridge on Sn	1x1	0.5	-3.963	-1.7028	1.784	1.785	
				2x1	0.25	-4.042	-1.7825	1.791	1.777	
Pt		A	Atop	1x2	0.5	-3.939	-1.679	1.574		
		B	Short Bridge	1x2	0.5	-3.989	-1.7295	1.748	1.751	
				2x2	0.25	-4.019	-1.7592	1.752	1.752	

† The hydrogen adsorption energies including H-H bond dissociation energy

Another stable site on pure-Pt ending termination is Pt-Pt bridge on Sn atom site H. The binding energy of hydrogen was evaluated as -3.96 eV. The distances between Pt and H atom were 1.784 Å and 1.785 Å. The other bridge site of pure-Pt ending termination of $Pt_3Sn(110)$ is site G. This site was found as the most energetically preferred site among all possible sites on $Pt_3Sn(110)$ surface, having binding energy of -4.19 eV.

For mixed atom ending configuration of $Pt_3Sn(110)$ surface, atop site adsorbed H atom stably, whereas H atom on Pt-Sn bridge site B was shifted away from the Sn atom. The Pt-H bond length was 1.59 Å where Sn-H bond was elongated to 3.33 Å at the end of the optimization process.

The only common stable site for the three surfaces is the Pt-Pt bridge site. Figure 4.4 illustrates the relation between Pt:Sn ratio of the surface with adsorption energy. The coverage was taken 0.25 for all surfaces.

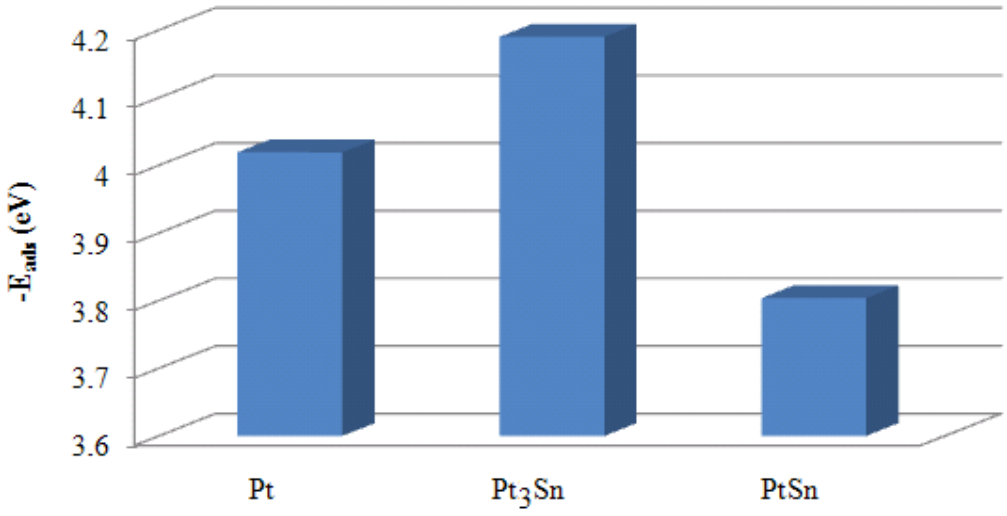

Figure 4.4. Comparison of hydrogen adsorption strengths of bridge sites of PtSn(110), $Pt_3Sn(110)$ and Pt(110) surfaces (θ=0.25)

This figure explains why catalysts having PtSn alloy, like Pt-Sn/AC on air oxidized AC, was not suffered from activity loss when CO oxidation with hydrogen rich feed was tested on it. On the other hand, experimental works indicated that Pt_3Sn suffers from

activity loss with H_2 rich streams; the activity loss disappears when CO_2 and H_2O vapor were added to H_2-rich reactant stream.

The results of H-adsorption on possible sites of Pt, Pt_3Sn and PtSn surfaces indicated that number of H adsorption sites are very limited and can not decrease CO oxidation rate and CO selectivity in oxidation reaction.

4.5. CO_2 Adsorption on PtSn(110) and Pt(110) Surfaces

The C-O bond lengths of the optimized CO_2 molecule was found as 1.171 Å, which is in agreement with the results from experimental (1.168 Å [63]) and theoretical (1.171 Å [64]) studies. Its energy is recorded as -1031.822 eV. The optimization results of CO_2 adsorption on all possible sites of the three surfaces are given in Table 4.3.

Atop CO_2 adsorption at site A was studied first. At the end of the optimization process, the resulting structure laid at a distance of 3.36 Å from the surface. CO_2 molecule was parallel to the surface before the optimization, and this orientation did not changed during the optimization. Both of the C-O bond lengths of CO_2 molecule were 1.172 Å, and O-C-O bond angle was 179.6˚. These values indicate that the geometry of the molecule did not changed during the optimization process; therefore, the geometry indicated that there was negligible interaction between the site and CO_2 molecule, and adsorption did not occur though small but an exothermic adsorption energy, -0.0734 eV, was calculated.

There are two more possible sites on which no CO_2 adsorption was observed, namely Pt-Pt bridge site B and Pt_2Sn site D. For site B, the final structure of the CO_2 molecule had O-C-O bond angle of 178.0˚. The Pt-C bonds were broken with distances of 3.757 Å and 3.776 Å from the platinum atoms on the surface. The adsorption energy of this site was calculated as 0.020 eV, showing that the adsorption was not thermodynamically favoured.

The other possible adsorption site was Pt_2Sn site, site D. At the end of the optimization, three bonds are shown broken; those are two Pt-C bonds with equal distances from the surface 3.751 Å both, and Sn-C bond with distance from the surface 3.813 Å. The

geometric configuration of CO_2 molecule remained the same with O-C-O bond angle of 179.5˚. This site had also endothermic adsorption energy of 0.014 eV.

The only site for stable CO_2 adsorption on the PtSn(110) surface is Pt-Sn bridge site, C. The binding energy calculated for this structure expressed that energy of the CO_2-Pt_3Sn system lies at a slightly higher energy level than the sum of the energies of free CO_2 molecule and the slab; the adsorption energy was indicating and endothermic process with 0.02 eV energy. The position of the molecule was assumed an equilibrium structure such that C attached to Pt atom and one O atom attached to Sn. The bond length between Pt-C was 2.136 Å and the newly formed Sn-O bond length was 2.106 Å. The bond length between Pt-bonded C and Sn-bonded O was 1.299 Å, whereas the bond length was 1.203 Å between Pt-bonded C and nonbonded O. These values differ significantly from those of free CO_2 molecule. Additionally, the molecule bent with O-C-O angle of 129.9˚. It was obviously observed that the final structure of the molecule was significantly different from its initial state indicating there has been a strong interaction between the site and the molecule, which proves stable adsorption.

Table 4.3. Possible CO_2 adsorption sites, corresponding adsorption energies and data on geometric properties of CO_2-Surface complex upon CO_2 adsorption on PtSn(110), Pt_3Sn(110) and Pt(110)

Surface		Site	Name	Size	Coverage	E_{ads} (eV)	Bond Lengths (Å)					O-C-O Bond Angle (°)
							Pt-C		Sn-O	Sn-C	C-O	
PtSn		A*	Atop Pt	1x1	0.25	-0.073	3.357				1.172 1.172	179.6
		B*	Pt-Pt Bridge	1x1	0.25	0.020	3.757	3.776			1.179 1.174	178.0
		C	Pt-Sn Bridge	1x1	0.25	0.483	2.136		2.106	2.698	1.299 1.203	129.9
		D*	Pt_2Sn	1x1	0.25	0.014	3.751	3.751		3.813	1.171 1.171	179.5
Pt_3Sn	Mixed	B	Pt-Sn Bridge	1x1	0.5	0.027	2.065		2.092		1.29 1.205	130.4
	Pure	F	Atop Pt	1x1	0.5	0.196	2.167				1.209 1.217	148.01
		G	Pt-Pt Bridge on Pt	1x1	0.5	0.086	2.382	2.382			1.219 1.219	148.9
Pt		A*	Atop	2x1	0.5	-0.302	2.072		2.093		1.274 1.206	134.9
		B	Short Bridge	2x1	0.5	-0.296	2.070	2.762	2.090		1.274 1.205	134.491
		C	Long Bridge	2x2	0.25	-0.305	2.033	3.018	2.099		1.274 1.220	129.739

4.5.1. Comparison of CO_2 Adsorption on PtSn(110), Pt_3Sn(110), and Pt(110) Surfaces

CO_2 adsorption on Pt_3Sn surfaces has been investigated by Duygu Başaran with slightly different calculation parameters. The only difference between the currently used parameters and those used in the previous work was the number of alloy layers to be relaxed. Three layers were relaxed in the mentioned study whereas it was taken as two for this study. In order to check whether it is safe to use the results of Basaran's study, one of the simulations was run relaxing top two layers only. The Pt-Sn bridge site B of mixed ending Pt_3Sn(110) surface configuration was chosen for comparison since it is found to be stable for CO_2 adsorption by Basaran. The adsorption energy was calculated as 0.03 eV in the previous study. When top two layers were relaxed, the adsorption energy is found as 0.07 eV. The slight difference of 0.04 eV was accepted as a reasonable difference to continue with the results obtained by Basaran for comparison basis, since the geometries of the optimized systems were also almost the same. Table 4.4 gives the results of the previous work and the current one.

Table 4.4. Comparison of simulation results of Pt-Sn bridge site, site B, of mixed atom ending termination of Pt_3Sn(110) surface in Basaran's study with current work

	E_{ads} (eV)	Bond Lengths (Å)				O-C-O Bond Angle (°)
		Pt-C	Sn-O	C-O	C-O	
Basaran's work	0.03	2.065	2.092	1.205	1.290	130.4
Current work	0.07	2.065	2.822	1.204	1.290	130.8

According to the Basaran's work, the sole site of mixed atom ending configuration of Pt_3Sn(110) surface on which CO_2 is adsorbed stably is Pt-Sn bridge site, B. There are two stable sites for pure-Pt ending configuration of Pt_3Sn(110) surface, namely atop Pt site and Pt-Pt bridge site. The results obtained for site B are given in Table 4.4.

For atop site F of pure termination, the binding energy was 0.20 eV. The CO_2 molecule was bonded to the Pt atom of the surface at a distance of 2.17 Å. After the optimization process, CO_2 molecule highly bent with "V" shape for which both O atoms pointing away from the surface. The O-C-O angle was 148.1°, and the C-O bond lengths

were 1.21 Å and 1.22 Å. The bond angle and the bond lengths of the optimized molecule are different from those of free CO_2. The O-C-O angle and O-C lengths obtained upon optimization are close to those in CO_2^- anion.

The other CO_2 adsorption site on the $Pt_3Sn(110)$ surface with pure termination is the Pt-Pt bridge site, G. This site had endothermic adsorption energy, which was calculated as 0.09 eV. The final structure of CO_2 molecule took a bent geometry with O-C-O angle 143.9˚. The C-O bond lengths of the CO_2 molecule at the end of the optimization process were both 1.22 Å. The final structure of the CO_2 molecule laid at a distance of 1.91 Å from the surface.

Lastly, CO_2 adsorption was examined for Pt(110) surface. There are three possible sites for CO_2 adsorption on Pt(110) surface. On short bridge site B and long bridge site C, CO_2 was adsorbed stably; whereas on atop Pt site A, CO_2 molecule moved towards the bridge site. The CO_2 molecule on short bridge site B assumes an equilibrium structure such that CO_2 molecule takes a bent geometry; the O-C-O angle is 134.5 Å. This site had exothermic adsorption energy of -0.296 eV. C atom of CO_2 was attached to one Pt atom and one of its O atom attached to another Pt at the end of the optimization process. The Pt-C bond length was 2.070 Å and the newly formed Pt-O bond length was 2.090 Å. The bond length between Pt-bonded O and C was 1.274 Å and 1.205 Å between nonbonded O and C.

The long bridge site C on Pt(110) surface also adsorbed CO_2 stably. The final structure assumes a highly bent CO_2 molecule with angle of 129.7˚. The binding energy of the site was found as -0.306 eV which indicates that it is thermodynamically favoured. The Pt-C bond length was 2.033 Å and Pt-O length was 2.099 Å. This site also appears as the most energetically favoured site for CO_2 adsorption on Pt(110) surface.

CO_2 molecule on atop site A moved through the nearest stable short bridge site at the end of the optimization. The bond lengths and the O-C-O angle slightly differ from the short bridge site, as given in Table 4.3.

After all, the behaviour of the stability of CO_2 adsorption seems to differ according to the characteristic of the surface. If the surface has Sn atoms on top layer, only the bridge site consisting of one Sn and one Pt adsorbs the molecule stably. The other sites either not adsorb CO_2 or the molecule move towards the stable site. This argument is valid both PtSn(110) surface and mixed atom ending of $Pt_3Sn(110)$ surface. On the other hand, if the top layer of the surface does not contain Sn atom, i.e. the Pt ending termination case, the Pt-Pt bridge sites are more favoured adsorption sites for CO_2 molecule than the rest of the sites. Although CO_2 adsorption on the long Pt-Pt bridge site I of pure-Pt ending termination of $Pt_3Sn(110)$ surface does not support this statement, CO_2 on other Sn free adsorption sites agrees with it.

4.6. Oxygen Adsorption on PtSn(110), $Pt_3Sn(110)$, and Pt(110) Surfaces and Their Comparison

Oxygen adsorption on Pt surfaces has been stated as dissociative adsorption in literature, therefore, adsorption of oxygen atom was investigated for this study. The optimization results are presented in Table 4.5. The energy of oxygen atom is recorded as -433.234 eV.

One of the possible oxygen adsorption sites on PtSn(110) was Pt-Pt bridge site, site B. Oxygen atom was adsorbed stably on this site. Site B was observed as the least favoured site for O adsorption with adsorption energy of -3.06 eV. The Pt-O bond lengths were both found equal to 2.022 Å.

Oxygen adsorption on Pt-Sn bridge site, site C, was found stable although O atom has slightly diffused to the other Sn atom on the surface. The Pt-O bond length was 2.226 Å and the Sn-O bond length was 1.939 Å. The adsorption energy of this site was found as -3.582 eV.

Oxygen adsorption on atop Pt site A of PtSn(110) surface was also studied. At the end of the optimization process, O atom moved toward Sn atom and formed a new bond having 1.951 Å length. The bridge structure also tilted to another Sn atom on the surface and stabilized at this position. The Pt-O bond length was 2.179 Å at the end of the

optimization process. These values are very close to those of the O adsorption on Pt-Sn bridge site C. The binding energy of the site was calculated as -3.574 eV.

The other site for stable O adsorption on PtSn(110) surface is Pt_2Sn site, D. At the end of the optimization the initial structure of O on the site remained unchanged. The bond length of Pt-O bonds were both 2.130 Å and the Sn-O bond length was 2.014 Å. The adsorption energy was -3.591 eV for this site.

Since O atom was attracted by Sn atoms on the surface of all four sites (atop Pt, Pt-Pt bridge, Pt-Sn bridge, Pt_2Sn sites) that were investigated earlier, Sn-Sn bridge site, site F, was also examined to understand the behaviour of O atom on Sn-including sites. O atom was adsorbed stably on this site. The Sn-O bonds were 2.003 Å and 2.004 Å. The adsorption energy for this site was -4.839 Å and this amount of energy reveals that this site is the most energetically favoured one among the all possible O adsorption sites on PtSn(110) surface.

The last possible O adsorption site on PtSn(110) was atop Sn site, site E. After the optimization, O atom moved towards Sn-Sn bridge position. The bond length between initially O bonded Sn and O was 1.995 Å, and the newly formed Sn-O bond length was 2.008 Å. The adsorption energy calculated for this site was -4.802 eV.

In a previous study investigating atomic O adsorption on Pt(110) surface, it is found that O atom occupies bridge site on the surface. The Pt-O bond length is reported as 1.93 Å and the binding energy for atomic oxygen on bridge site is stated as 4.00 eV [65].

Short Pt-Pt bridge site, site B, was found as the most energetically favoured site in this study as mentioned above. The adsorption energy was calculated as -3.92 eV for this site. The Pt-O bonds were 1.965 Å and 1.963 Å.

Besides short bridge site B, the long bridge site, site C, was also found suitable for stable oxygen adsorption on Pt(110) surface. The Pt-O bond lengths were 2.004 Å and 2.003Å. However, the binding energy for this site, -3.74 eV, was not as low as the adsorption energy on the short bridge site.

Another site that was investigated for atomic oxygen adsorption on Pt(110) surface is atop site, A. On this site O atom was adsorbed stably. Adsorption energy of this site was higher than the bridge sites, being -2.95 eV. The Pt-O bond length for atop site was 1.84.

Considering the fact that the most energetically favoured O-adsorption site on PtSn(110) was found as Sn-Sn bridge site F with the energy of -4.84 eV, O adsorption on Sn-Sn bridge of mixed atom ending configuration of $Pt_3Sn(110)$ surface was also investigated. O atom was adsorbed stably on this site also. The Sn-O bonds are very close to values those obtained for O adsorption on Sn-Sn bridge site F of PtSn(110) surface, being equal to 2.004 Å and 2.005 Å. The adsorption energy for Sn-Sn bridge site F was calculated as -3.51 eV, which indicates that atomic O was not adsorbed on $Pt_3Sn(110)$ surface as strongly as on PtSn(110) surface.

Another site adsorbing O atom stably was Pt-Sn bridge site B on mixed atom ending configuration of $Pt_3Sn(110)$ surface. Binding energy was calculated as -3.72 eV, indicating that the Pt-Sn bridge site B is the energetically most favoured site for O adsorption on $Pt_3Sn(110)$. The Pt-O bond length was 2.034 Å and Sn-O bond length was 1.943 Å.

Oxygen was not adsorbed stably on either of atop sites, namely atop Sn site C and atop Pt site A, on mixed atom ending configuration of $Pt_3Sn(110)$ surface. Oxygen diffused and eventually stabilized on Pt-Sn bridge position for both sites. The adsorption energies of atop Sn site C and atop Pt site A were calculated as -3.72 eV and -3.73 eV, respectively. The bond lengths were also found almost same with those of Pt-Sn site B.

Table 4.5. Possible O adsorption sites, corresponding adsorption energies and data on geometric properties of O-Surface complex upon atomic O adsorption on PtSn(110), Pt3Sn(110) and Pt(110) surfaces

Surface		Site	Name	Size	Coverage	E_{ads} (eV)	E_{ads}-E_{diss} (eV)†	Bond Lengths (Å)	
								Pt-O	Sn-O
PtSn		A*	Atop Pt	1x1	0.25	-3.575	-1.054	2.179	1.951
		B	Pt-Pt Bridge	1x1	0.25	-3.063	-0.543	2.022 2.022	
		C*	Pt-Sn Bridge	1x1	0.25	-3.582	-1.0619	2.226	1.939
		D	Pt_2Sn	1x1	0.25	-3.591	-1.0714	2.130 2.130	2.014
		E*	Atop Sn	1x1	0.25	-4.803	-2.2827		1.995 2.008
		F	Sn-Sn Bridge	1x1	0.25	-4.839	-2.3194		2.003 2.004
Pt_3Sn	Mixed	A*	Atop Pt	1x1	0.5	-3.73451	1.214	2.026	1.946
		B	Pt-Sn Bridge	1x1	0.5	-3.72491	1.205	2.034	1.943
		C*	Atop Sn	1x1	0.5	-3.7200	1.2000	2.034	1.947
		D	Pt-Pt Long Bridge	2x1	0.25	-3.4233	-0.903	2.030 2.030	
		E	Sn-Sn Long Bridge	2x1	0.25	-3.512	-0.992		2.031 2.033
	Pure	F*	Atop Pt	1x1	0.5	-3.625	-1.105	2.000 2.004	
		G	Pt-Pt Bridge on Pt	1x1	0.5	-3.962	-1.442	1.983 1.981	
				2x1	0.25	-4.262	-1.742	1.991 1.983	
		H	Pt-Pt Bridge on Sn	1x1	0.5	-3.625	-1.101	1.999 2.025	
				2x1	0.25	-3.988	-1.468	2.006 2.017	
		I	Pt-Pt Long Bridge	2x1	0.25	-4.027	-1.506	2.005 2.005	
Pt		A	Atop	2x1	0.5	-2.949	-0.429	1.840	
		B	Short Bridge	2x1	0.5	-3.918	-1.398	1.965 1.963	
				2x2	0.25	-4.038	-1.518	1.955 1.957	
		C	Long Bridge	2x2	0.25	-3.738	-1.218	2.004 2.003	

†The oxygen adsorption energies including O-O bond dissociation energy

Another possible oxygen adsorption site on mixed ending configuration of $Pt_3Sn(110)$ surface was Pt-Pt long bridge site, site D. Oxygen was adsorbed stably on this bridge site. The adsorption of the site was calculated as -3.42 eV and the Pt-O bond lengths were both equal to 2.030 Å.

For pure Pt ending configuration of $Pt_3Sn(110)$ surface Pt-Pt bridge site, site H, was investigated first. Stable adsorption of oxygen was observed on Pt-Pt bridge site. The binding energy of oxygen atom was calculated as -3.62 eV. The Pt-O bond lengths were 1.999 Å and 2.025 Å.

Another stable site for oxygen adsorption is long Pt-Pt bridge site I on pure-Pt ending termination of $Pt_3Sn(110)$ surface. The energy was calculated as -4.03 eV for this site. The lengths of Pt-O bonds were both 2.005 Å for this site.

Atop Pt site F on pure-Pt ending termination of $Pt_3Sn(110)$ surface was analyzed lastly. At the end of the optimization process, O atom diffused to Pt-Pt bridge position which was found adsorbing O atom stably. The Pt-O distance was 2.00 Å, and the newly bonded Pt-O bond length was 2.004 Å. The binding energy for this site was evaluated as -3.62 eV.

The only common site adsorbing oxygen atom stably is Pt-Pt bridge sites of the three surfaces. In Figure 4.5, comparisons using values of Pt-Pt bridge sites both mixed atom ending and pure Pt ending configurations of $Pt_3Sn(110)$ surface are given. For pure Pt atom ending termination, oxygen adsorption strength of $Pt_3Sn(110)$ surface was found higher than Pt(110), whereas for mixed atom ending termination increasing Sn content of the alloy decreases the O adsorption strength.

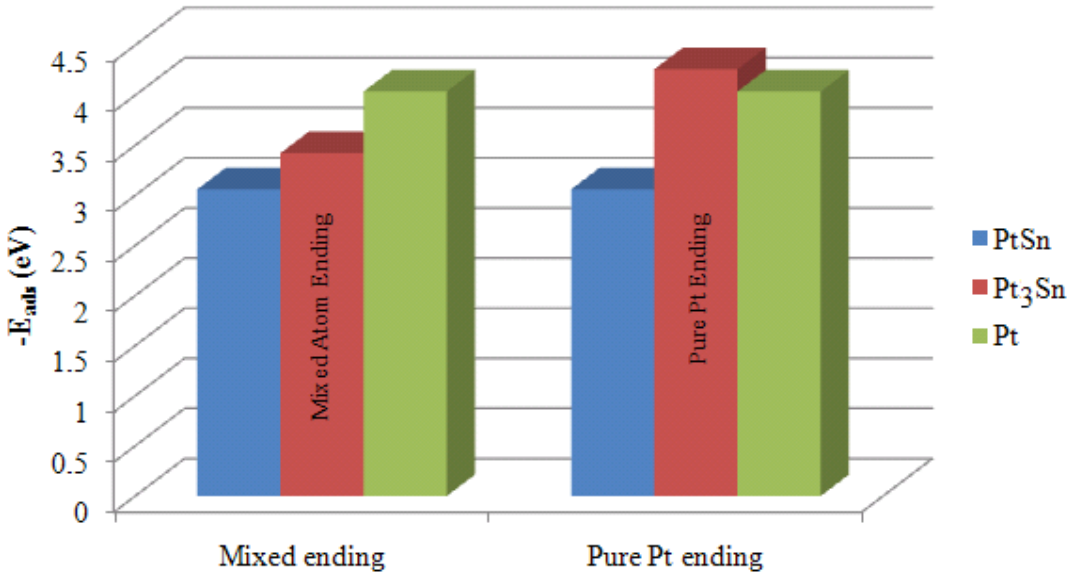

Figure 4.5.Comparison of oxygen adsorption strengths of bridge sites of PtSn(110), Pt_3Sn(110) and Pt(110) surfaces

4.7. Co-adsorption of CO and O on PtSn(110) Surface

Bimetallic alloys are reported as having higher CO oxidation activity than monometallic sites because of the combination of two factors, namely bifunctional and electronic effects. Bifunctionality of the alloys stems from the presence of a second metal atom which provides favourable sites for oxygen thus lowers the competition between CO and O. The electronic modification of the initial metal structure leads to a decrease in CO adsorption strength which makes surface more active for oxidation reaction. Since the adsorption of CO and O on active sites of the surface is the initial step of the reaction, these effects are related to adsorption properties of metal surface.

On PtSn(110) surface, Pt-Pt bridge site B was found as the energetically most favoured site for CO adsorption and the Sn-Sn bridge site F had the lowest oxygen adsorption energy. Therefore, co-adsorption of CO and O was investigated on Pt-Pt bridge site B and Sn-Sn bridge site F, respectively. The parameters in Section 3.1 were used for optimization.

The binding energy of CO on O covered surface was calculated by

$$E_{CO/O+Surface} = E^{total}_{CO+O/Surface} - (E^{total}_{O/Surface} + E^{free}_{CO}) \quad (4.1)$$

where $E^{total}_{CO+O/Surface}$ is total energy of the surface with coadsorbed O and CO, $E^{total}_{O/Surface}$ the is total energy of the surface with adsorbed O individually, and E^{free}_{CO} is free energy of CO molecule. The binding energy of CO individually was calculated by

$$E_{CO/Surface} = E^{total}_{CO/Surface} - (E^{total}_{Surface} + E^{free}_{CO}) \quad (4.2)$$

where $E^{total}_{CO/Surface}$ is total energy of the surface with adsorbed CO and $E^{total}_{Surface}$ is the energy of clean surface. The binding energy of oxygen was calculated by inserting O instead of CO in Equation 2, and the binding energy of O on CO covered surface was calculated by switching the O and CO terms in Equation 4.1.

Simulations are conducted to analyze the effect of coverage on CO and O adsorption strengths. The simulation results are given in Table 4.6 and the adsorption energy of CO as a function of coverage is given in Figure 4.6. At surface coverage of 0.125 ML, CO adsorption energy on bare and O-covered surface was -1.286 eV and -1.352 eV, respectively. For oxygen surface coverage of 0.25 ML, CO adsorption energy became -1.357 eV, indicating that second adsorbed O has no significant effect on CO adsorption energy. For higher surface coverage, i.e. 0.5 ML of CO, adsorption energy on clean and O adsorbed surface was calculated as -1.258 eV and -1.298 eV. An additional O on the surface caused enhancing CO adsorption energy.

In order to examine the behaviour of O on CO-covered surface, $-E_{O/(CO+)surface}$ values were calculated and given in Table 4.7 and the adsorption energy of O as a function of coverage is given in Figure 4.7. At surface coverage of 0.125 ML, O adsorption energy on clean and CO-covered surface was -4.964 eV and -5.031 eV. By increasing CO

coverage to 0.25 ML, O adsorption energy of -4.829 eV was obtained, indicating that second CO on the surface diminished the adsorption strength of O.

Table 4.6. CO adsorption energies on O-precovered surface

	θco	θtotal	$-E_{co(+O)/surf}$ (eV)	$-E_{co/(O+)surf}$ (eV)	-ΔE (eV)
CO	0.125	0.125	1.2860	1.2860	-
CO+O	0.125	0.25	6.3168	1.3529	-0.0669
CO+2O	0.125	0.375	11.2503	1.3577	-0.0717
2CO+2O	0.25	0.5	6.21763	1.37819	-0.1201
2CO	0.25	0.25	1.25805	1.25805	-
2CO+O	0.25	0.375	7.5593	1.2977	-0.0397

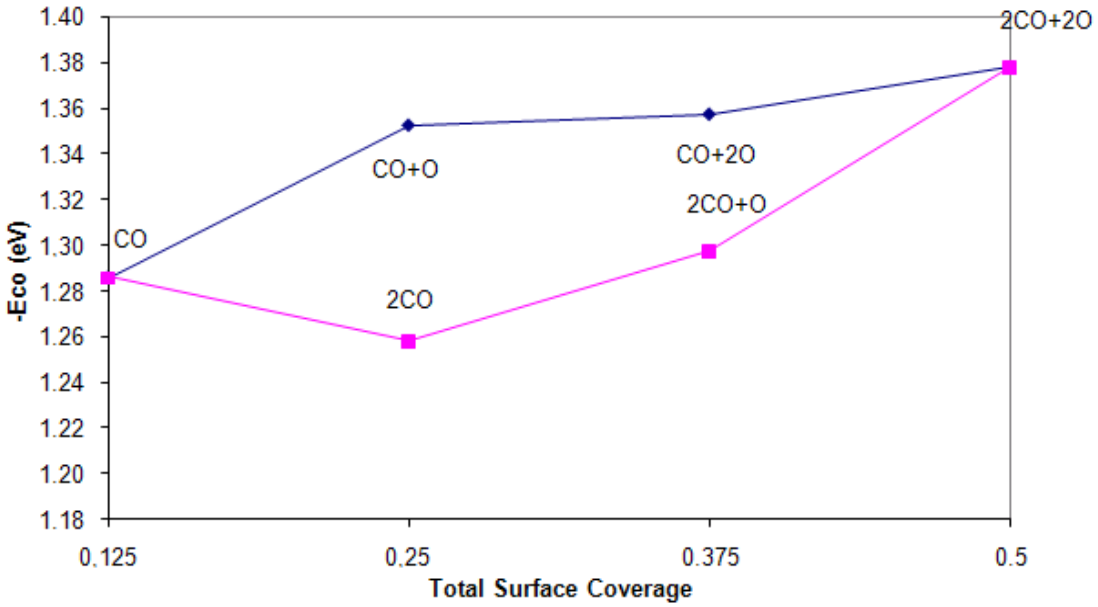

Figure 4.6. The adsorption energy of CO as a function of total coverage

At surface coverage of 0.25 ML of oxygen one CO adsorbed on the surface increased the adsorption strength of oxygen. Increasing CO coverage to 0.25 ML did not affect the O adsorption strength significantly. Another observation was the effect of hydrogen on CO adsorption energy. At total coverage of 0.25 ML, including 0.125 ML O and 0.125 ML

CO, hydrogen increased adsorption energy of CO from -1.357 eV to 1.300 eV. Presence of hydrogen seems to diminish the adsorption strength of CO.

Table 4.7. O adsorption energies on CO-precovered surface

	θo	θtotal	$-E_{o(+CO)/surf}$ (eV)	$-E_{o/(CO+)surf}$ (eV)	-ΔE (eV)
O	0.125	0.125	4.9639	4.9639	-
O+CO	0.125	0.25	6.3168	5.0308	-0.0669
O+2CO	0.125	0.375	7.5593	4.82952	0.1344
2O+2CO	0.250	0.5	6.21763	4.95958	-0.12014
2O	0.250	0.25	4.83944	4.83944	-
2O+CO	0.250	0.375	6.21763	4.98215	-0.14271

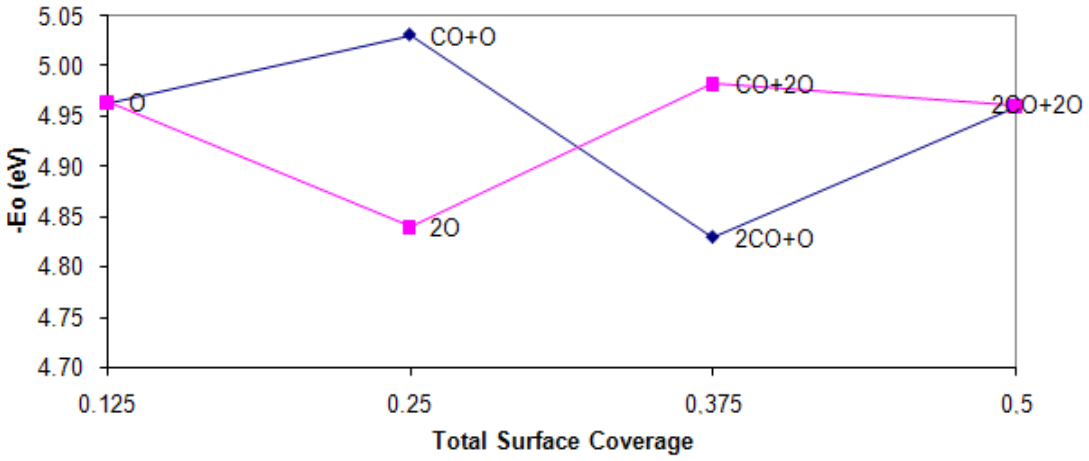

Figure 4.7. The adsorption energy of O as a function of total coverage.

On PtSn(110) surface, both of the species are adsorbed on the surface on different sites, then they react with each other, following Langmuir – Hinshelwood mechanism. For CO oxidation reaction, the reactants should be activated from coadsorption state to transition state. The stability and strength of adsorption of species prevents activation of reactants. Kinetic studies on CO oxidation reaction revealed that rate determining step of CO oxidation changed depending on CO surface coverage [41]. Changing adsorption

energy of the coadsorbed structures with different coverages may affect the activation barrier of CO oxidation reaction by changing rate determining step of the reaction pathway.

4.8. Effect of Bonding Competition on CO Adsorption on PtSn(110) surface

In order to understand the effect of the bonding competition, which exists when two adsorption sites shares the same surface atom, on adsorption properties of CO molecule, two different simulations were carried out on PtSn(110) surface. Firstly, adsorption energy of Pt-Pt bridge site B on PtSn(110) site was calculated for surface coverage of 0.125 ML. The geometry of the optimized complex is given in Figure 4.8. The adsorption energy was found as -1.286 eV.

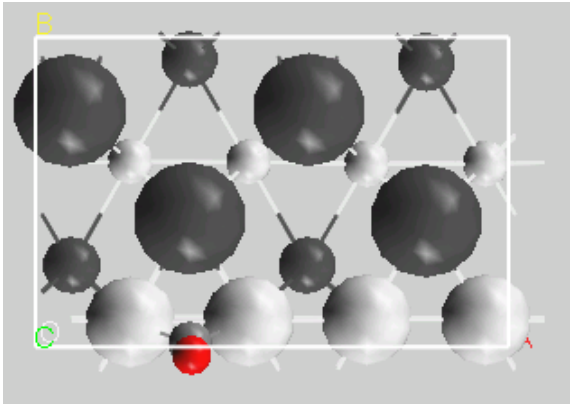

Figure 4.8. CO adsorption on Pt-Pt bridge site B of PtSn(110) surface without bonding competition (θ=0.125 ML). (Bigger atoms indicate the top layer of the surface, Pt: ○ Sn:●)

Afterwards, adsorption energy of CO was calculated when two CO molecules were adsorbed on two adjacent bridge sites on PtSn(110) surface with surface coverage of 0.25 ML (Figure 4.9). The adsorption energy was calculated as -2.303 eV.

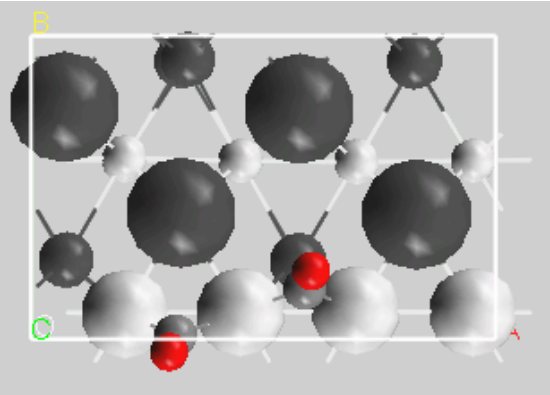

Figure 4.9. CO adsorption on Pt-Pt bridge site B of PtSn(110) surface with bonding competition (θ=0. 25 ML) (Bigger atoms indicate the top layer of the surface, Pt: ○ Sn:●)

4.9. Electronic Mechanism of CO Adsorption on PtSn(110) Surface

The mostly accepted model for CO-metal bonding was proposed by Blyholder in 1964. In later works, Blyholder's proposal was taken as a good description of the primary electronic interaction between to CO and surface for bond formation excluding the contribution of 4σ orbital. Hu et al. showed that there was significant mixing between metal d states and the CO 4σ, 1π, 5σ, and 2π orbitals and they proposed an 'orbital mixing' model. The model conceives that the overall quantum states of chemisorption system are formed by mixing of discrete CO molecular orbitals with the continuum of d states. As a consequence of orbital mixing, some bands hold predominantly metallic character, some hold predominantly molecular character, and some hold a mixture of both [41].

The LDOS profiles of C of CO and of Pt are given in Figure 4.10(a) and Figure 4.10 (b), respectively for CO adsorption atop Pt site, A. The gray curves represent the corresponding local densities in free CO, and have been superimposed for reference purposes. The Fermi level of the adsorption system lies at 0 eV. To identify the peaks in the LDOS profile of C and Pt, the LDOS profiles from a recent study on CO/Pt(111) are used [41]. Considering CO adsorption on atop Pt site A, the electron density peak corresponds to the lowest energy belongs to 3σ-derived states (Figure 4.10). This peak coincided with the energetics of 3σ molecular orbital peak with little increase in amplitude and no change in the energy, suggesting that the 3σ molecular orbital does not become

involved in bonding with the surface. The next peak at -10.3 eV represents 4σ-derived states and shifted downwards in energy relative to the 4σmolecular orbital peak at -9.1 eV. The change in energy implies that the 4σ CO orbital is involved in some mixing with the metal d states. Additionally, the intensity of the peak for adsorbed CO is larger than the corresponding molecular orbital peak, which suggests more electron density exists around carbon in 4σ-derived states after chemisorption than there is around carbon in the 4σ orbital of free CO. The shoulder at -7.8 eV and the peak at -7.2 eV represent the 5σ- and 1π-like states, respectively. Two orbitals have almost overlapped. Both orbitals of CO are involved in bonding with the metal as denoted by the downward shifts and broadening of their peaks relative to the corresponding peaks in the free CO curve. Since the most significant shifting in energy is observed at 5σ orbital, it is safe to say that most of the contribution to bonding of CO and surface comes from this molecular orbital. The peak intensity of the 1π-like states in the carbon LDOS is higher than the 1π molecular orbital peak in CO, implying that there is more electron density around carbon in 1π-derived states in the adsorption system than in its free states. The region from -6 eV up to the Fermi level includes quantum states which possess strong metal character and relatively weaker 5σ or 2π character. The low intensity in this region indicates that quantum states in this energy range have little electron density close to carbon. Thus, the electron density is located mostly within the metal atoms. Above the Fermi level at 2.5 eV, 2π-like state is observed with a peak intensity lower than the 2π molecular orbital of free CO. The significant decrease in intensity and broadening suggest strong contribution to bonding of CO and the surface.

Figure 4.10(b) shows the LDOS profiles of Pt atom at the atop site for its bare and CO adsorbed states. The electron density around the metal was slightly reduced in the region from the Fermi level to ~ -3 eV. The region from Fermi level to -6 eV contains strong metal character as expected, since most of the electron density is near Pt atom as stated before. The lowest energy peak in the curve represents density in 4σ-like states. Decrease in intensity below E_f and then increase at lower energies indicates orbital mixing between CO 4σ, 1π, and 5σ orbitals and Pt d states.

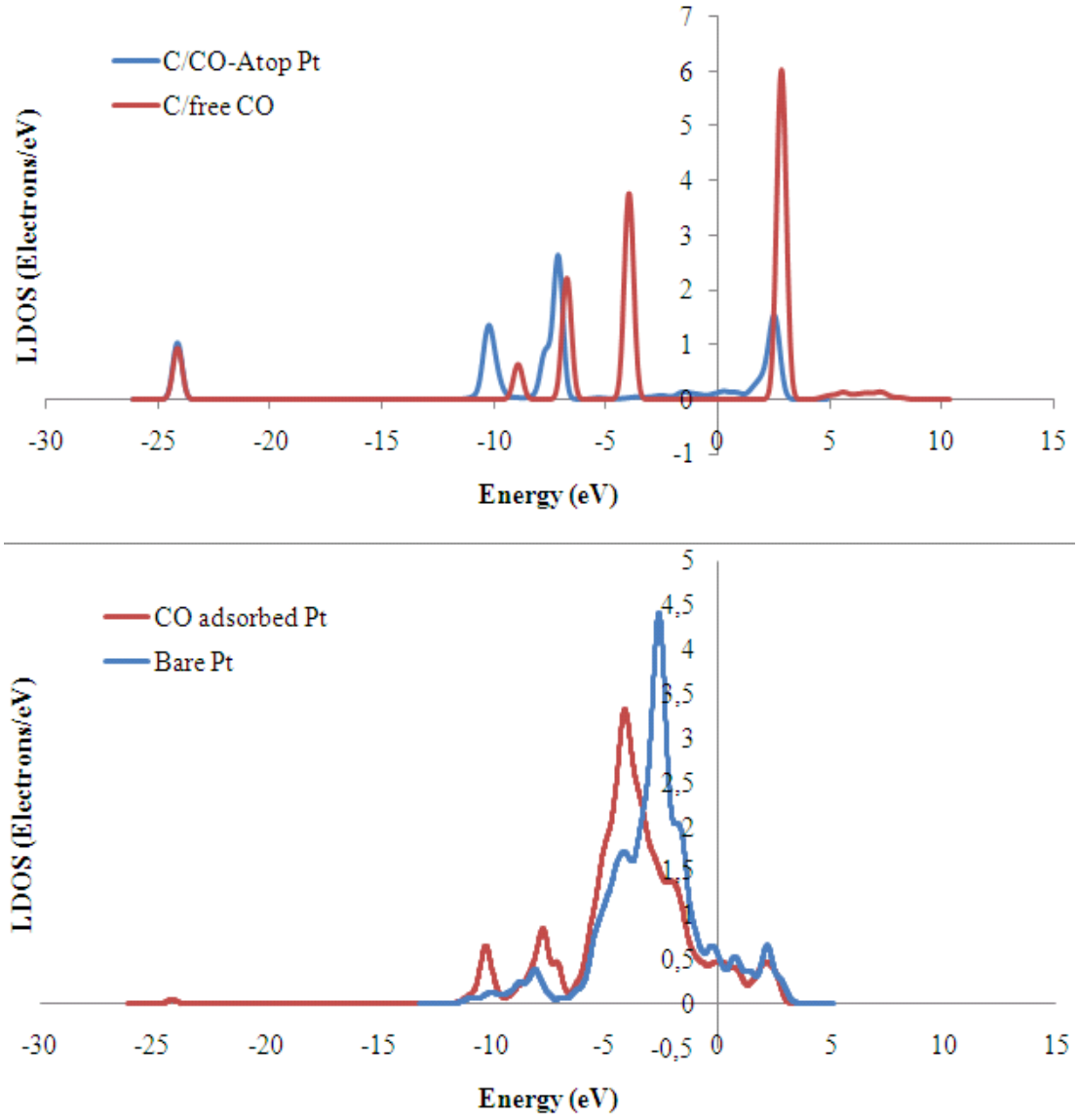

Figure 4.10. LDOS profiles of C of adsorbed CO and Pt for atop type adsorption on PtSn(110) (a) of C atom (b) of Pt atom. LDOS of C of free CO in Figure 4.10(a) and LDOS of bare Pt in Figure 4.10(b) are given as comparison basis.

The LDOS of carbon for free and adsorbed CO and one of the platinum atoms present in Pt-Pt bridge site B are given in Figure 4.11(a) and Figure 4.11(b) The 3σ-derived states is at -23.2 eV, overlapping with 3σ molecular orbital peak, indicating 3σ molecular orbital has no contribution to bonding with the surface. The peak at -10.7 eV represents 4σ-derived states. The energy of the states is significantly more negative than the 4σ molecular orbital of CO, suggesting that 4σ molecular orbital contributed to some

mixing with the metal d-states. The larger intensity of 4σ-derived states peak relative to the 4σ molecular orbital peak implies that there is more electron density around carbon in 4σ-derived states after adsorption of CO than electron density existing around carbon in the 4σ orbital of free CO.

The 1π-like states are at -7.1 eV, overlapping 5σ-like states. The electron density around 1π- and 5σ-like states after adsorption is slightly lower than the 1π molecular orbital of free CO. The quantum states in the region from -5 eV up to Fermi level have very strong metal character and relatively weaker 5σ and 2π character, indicating that electron density located within the surface Pt atoms mostly. The considerable difference in intensity between 2π molecular orbital of free CO and 2π-like states suggests strong contribution to bonding.

Figure 4.11(b) presents the LDOS profile of one of the Pt atoms included in the bridge site for its bare and CO adsorbed states. The profiles are exactly same for both Pt atoms present in the bridge site, thus one of them is investigated. The region below Fermi level shows a strong metal character with high intensity around Pt atom. The peak at -2.5 eV shifted downwards in energy, to -3 eV, after adsorption, having lower intensity, indicating contribution of Pt d states to bonding with CO molecule. Increase in intensity at lower energy states, between -6 eV and -12 eV suggests mixing of orbitals of C 4σ-like states with Pt d states. It should be noted that the decrease in intensity and the extent of downward shift for Pt metallic states between 0 eV to -5 eV is limited for bridge bond compared to the case of atop bonding suggesting that the amount of electron transfer from metal to CO necessary to for a bond was shared between two Pt atom of the bridge site.

For PtSn(110) surface sites on which CO adsorption is unstable, the LDOS profiles assumes the profiles of the sites towards which unstable CO diffuses: CO at Pt-Sn bridge site C was found diffused towards atop Pt position, and LDOS profiles of Pt-Sn bridge site is same with site A. For Pt_2Sn site D, on the other hand, Pt-Pt bridge position has observed after optimization and the LDOS of both C and Pt atoms results with the same profile.

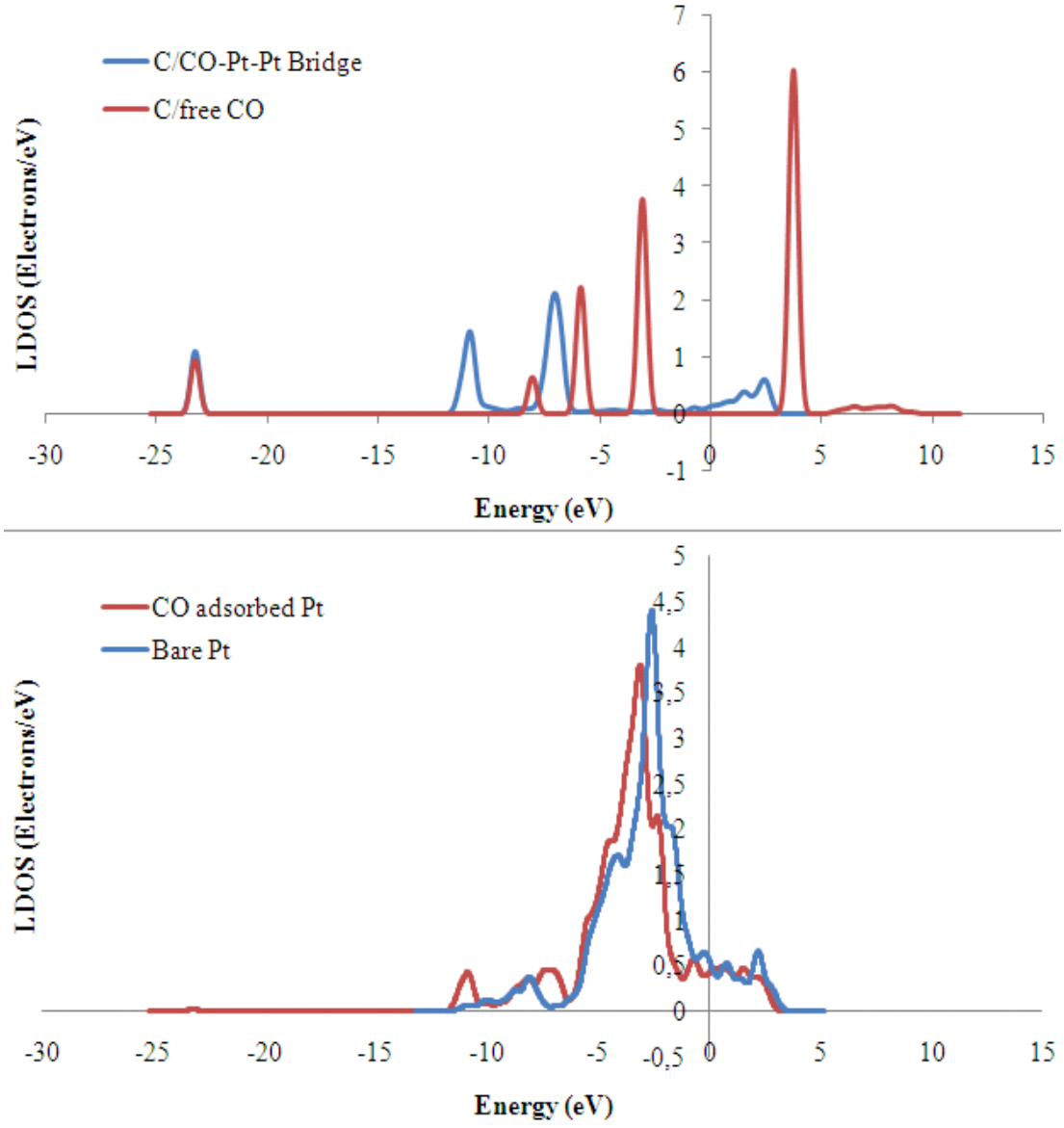

Figure 4.11. LDOS profiles of Pt atom at bridge site and C of adsorbed CO for Pt-Pt bridge site, site B, adsorption on PtSn(110) (a) of C atom (b) of Pt atom. LDOS profiles of C of free CO in Figure 4.11(a) and LDOS profiles of bare Pt in Figure 4.11(b) are given as comparison basis.

4.9.1. Comparison of Electronic Mechanism of CO Adsorption of Pt(110), PtSn(110), Pt_3Sn(110) Surfaces Using LDOS Profiles

LDOS profiles of Pt atoms present on the bare of Pt(110), PtSn(110), and Pt_3Sn(110) surfaces are given Figure 4.12(a) and Figure 4.12(b). Two different LDOS profiles are given for Pt_3Sn(110) surface; Figure 4.12(a) is for Pt atom on pure Pt ending termination and Figure 4.12(b) is for Pt atom on mixed atom ending termination. The peak at -1.73 eV is broader for pure Pt ending termination than mixed atom ending termination. At lower energies, peaks are at the same energies for both terminations; however electron density is higher for mixed atom ending termination. Both of the figures indicate that highest electron density region of the alloys shifts from Fermi level to $5\sigma/1\pi$ region as Sn concentration increases, suggesting electron density shift to lower energy levels with sharpening of the peak in 0 eV to -5 eV region as Sn content increases.

LDOS profiles of C atom of CO molecule that adsorbed on the Pt-Pt bridge sites of the (110) surfaces of PtSn, Pt_3Sn and Pt are given in Figure 4.13(a) and b; Figure 4.13(a) compares electronics of CO adsorption on pure Pt atom ending termination of Pt_3Sn(110) surface and 4.b compares electronics of CO adsorption on the mixed atom ending configuration. Figure 4.13(a) indicates that, the first peaks at -23.2 eV have not contributed to adsorption and all surfaces have the same amount of electron density at 3σ-derived states. The region between -12 eV and -8 eV is the 4σ-derived states region. The intensity of the peaks are significantly lower for Sn including surfaces, indicating that electron density around carbon decreased by presence of Sn. Addition of Sn causes a downward shift in energy at 4σ and 5σ derived peaks. As Sn content increases the overlapping of 5σ- and 1π-like derived states is more significant. Above Fermi level, electron density around C end of CO molecule increased with increasing Sn concentration on the surface. The only difference between mixed ending atom termination and pure atom ending termination was observed around 5σ- and 1π-like derived states region; the intensity of the lower one of the double peaks in -5 eV to -10 eV region enhanced for mixed termination case. In general, Sn present on the Pt_3Sn surface created similar effects as the Sn present on PtSn surface in this region.

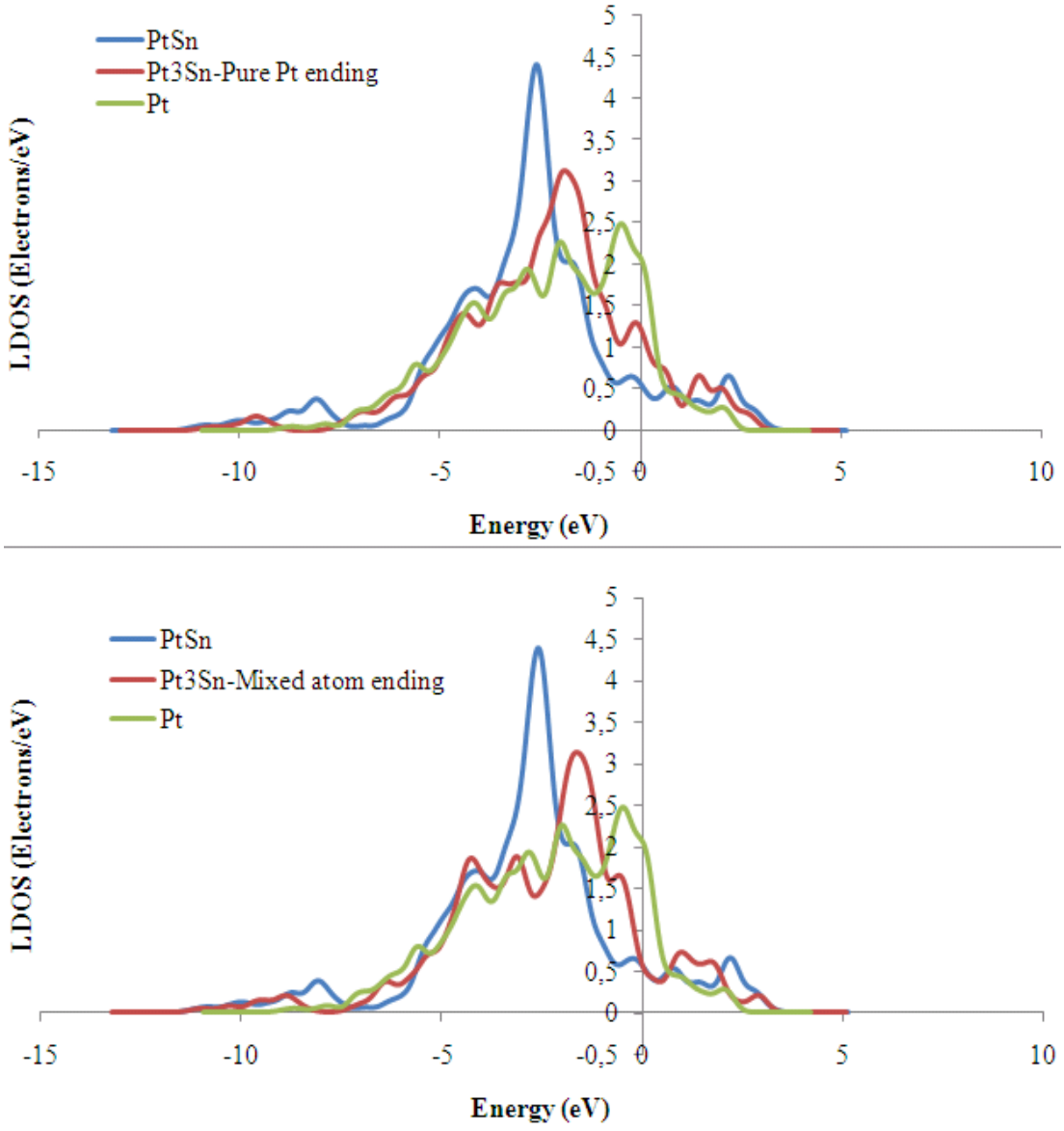

Figure 4.12. LDOS profiles of Pt for bare surfaces of PtSn(110), Pt(110) and (a) pure Pt ending termination (b) mixed atom ending termination of $Pt_3Sn(110)$ alloys.

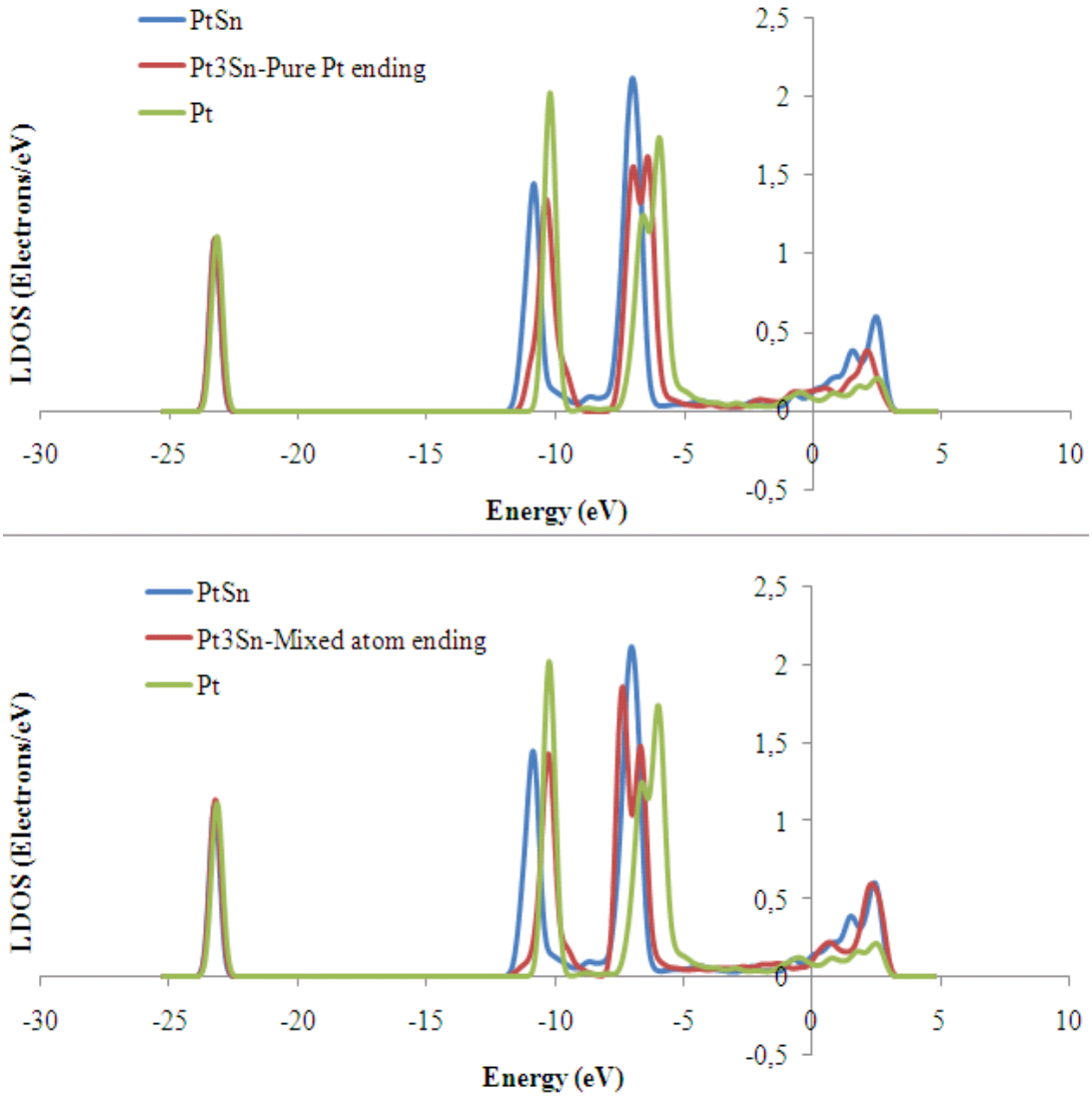

Figure 4.13. LDOS profiles of C of adsorbed CO for Pt-Pt bridge type adsorption on PtSn(110), Pt(110) and (a) pure Pt ending termination (b) mixed atom ending termination of $Pt_3Sn(110)$ alloys.

The LDOS profiles of Pt atoms present in the of the bridge sites of three surfaces upon CO adsorption are given in Figure 4.14(a) and Figure 4.14(b). Note that Figure 4.14(a) is for pure Pt ending termination of $Pt_3Sn(110)$ surface and Figure 4.14(b) for mixed atom ending termination of $Pt_3Sn(110)$ surface. Figures illustrate the comparison of LDOS profiles of one of the Pt atoms of the bridge structure since both of the Pt atoms give the same profile. The peak positions are the same with those of the bare surfaces but

the energy densities lowered for CO adsorbed case. Electron density between -6 eV to 1 eV is higher for PtSn(110) surface and decreasing with increasing Sn content.

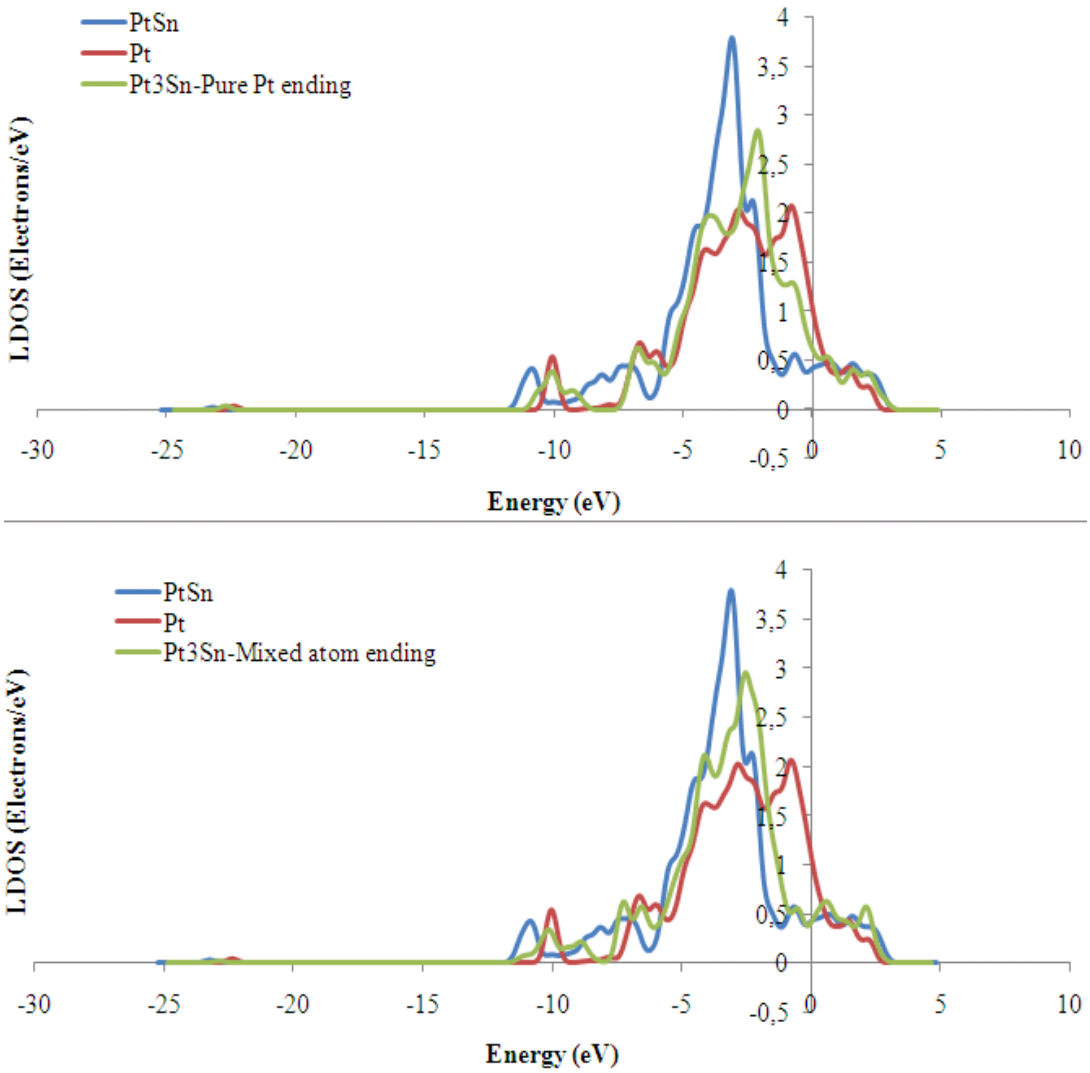

Figure 4.14. LDOS profiles of Pt atom upon Pt-Pt bridge type CO adsorption on PtSn(110), Pt(110) and (a) pure Pt ending termination (b) mixed atom ending termination of $Pt_3Sn(110)$ alloys.

The LDOS profiles of C atom of adsorbed CO on atop Pt sites of Pt(110), PtSn(110), and $Pt_3Sn(110)$ are given in Figure 4.15(a) and Figure 4.15(b) for pure Pt atom ending termination and for mixed atom ending termination of $Pt_3Sn(110)$ surface, respectively. 3σ derived states had no contribution to adsorption and the electronic density around carbon

atom was equal for all surfaces. In the 4σ-derived states region, between -12 eV to -8 eV, electron density around C atom was lower for alloy surfaces. The electron density around 5σ/1π derived states region was slightly different for Pt_3Sn and Pt surfaces. On the other hand, the overlapping of 5σ and 1π orbitals was significant for PtSn surface. The mixing of C orbitals with metal d states occurred of lower energy levels as Sn concentration of the alloy increased.

The LDOS profiles of Pt atom of atop Pt sites present on PtSn(110), Pt(110), and Pt_3Sn(110) surfaces are given in Figure 4.16(a) and Figure 4.16(b); Figure 4.16(a) for pure Pt ending termination and Figure 4.16(b) for mixed atom ending termination of Pt_3Sn(110) surface. As Sn concentration of the surface increased, the electron density around Pt atom increased as well. The significant difference between pure Pt ending termination and mixed atom ending termination of Pt_3Sn(110) surface was that the electron density around Pt atom was higher for pure Pt ending termination.

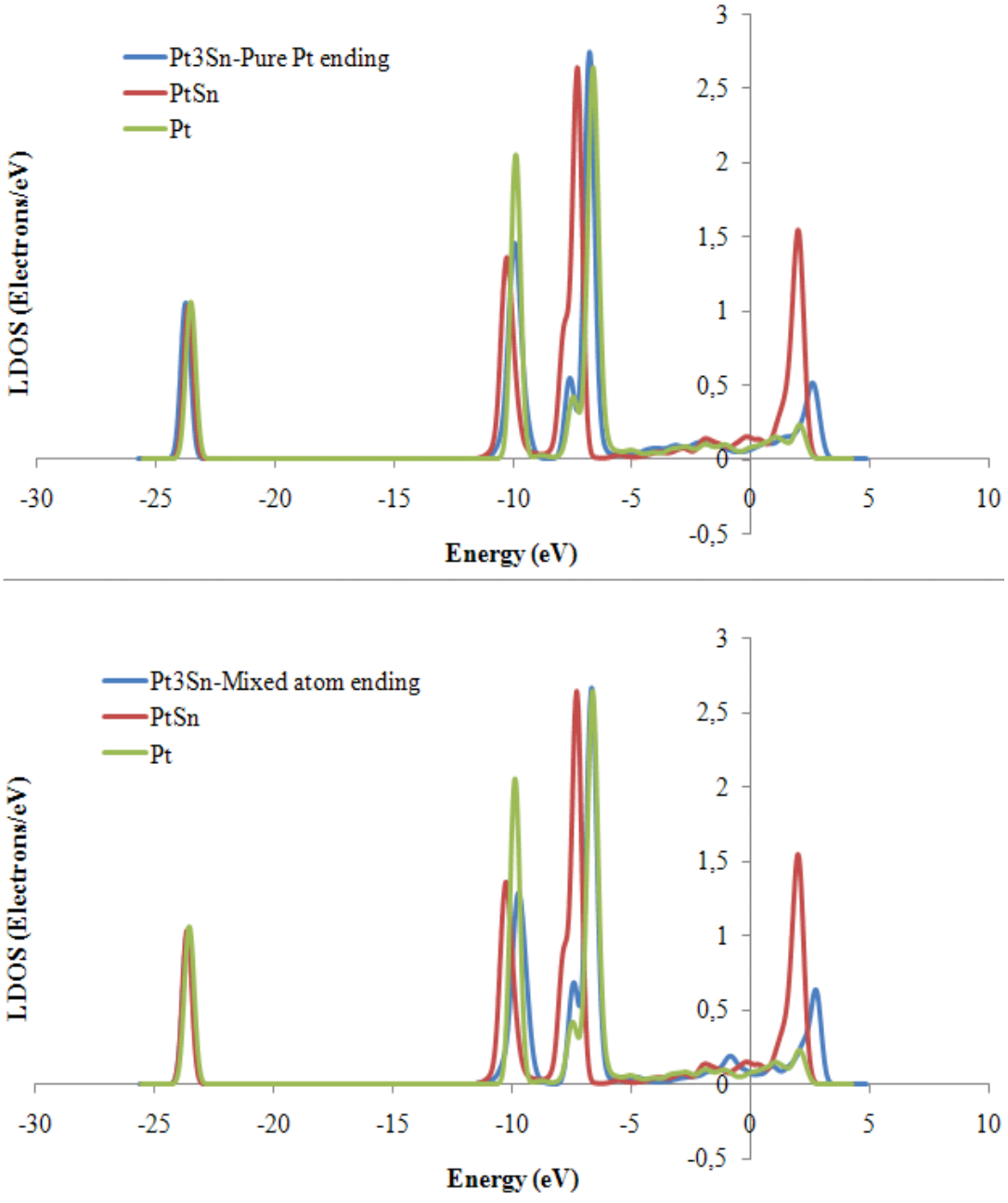

Figure 4.15. LDOS profiles of C of adsorbed CO for atop Pt site of PtSn(110), Pt(110) and (a) pure Pt ending termination (b) mixed atom termination of $Pt_3Sn(110)$ surfaces.

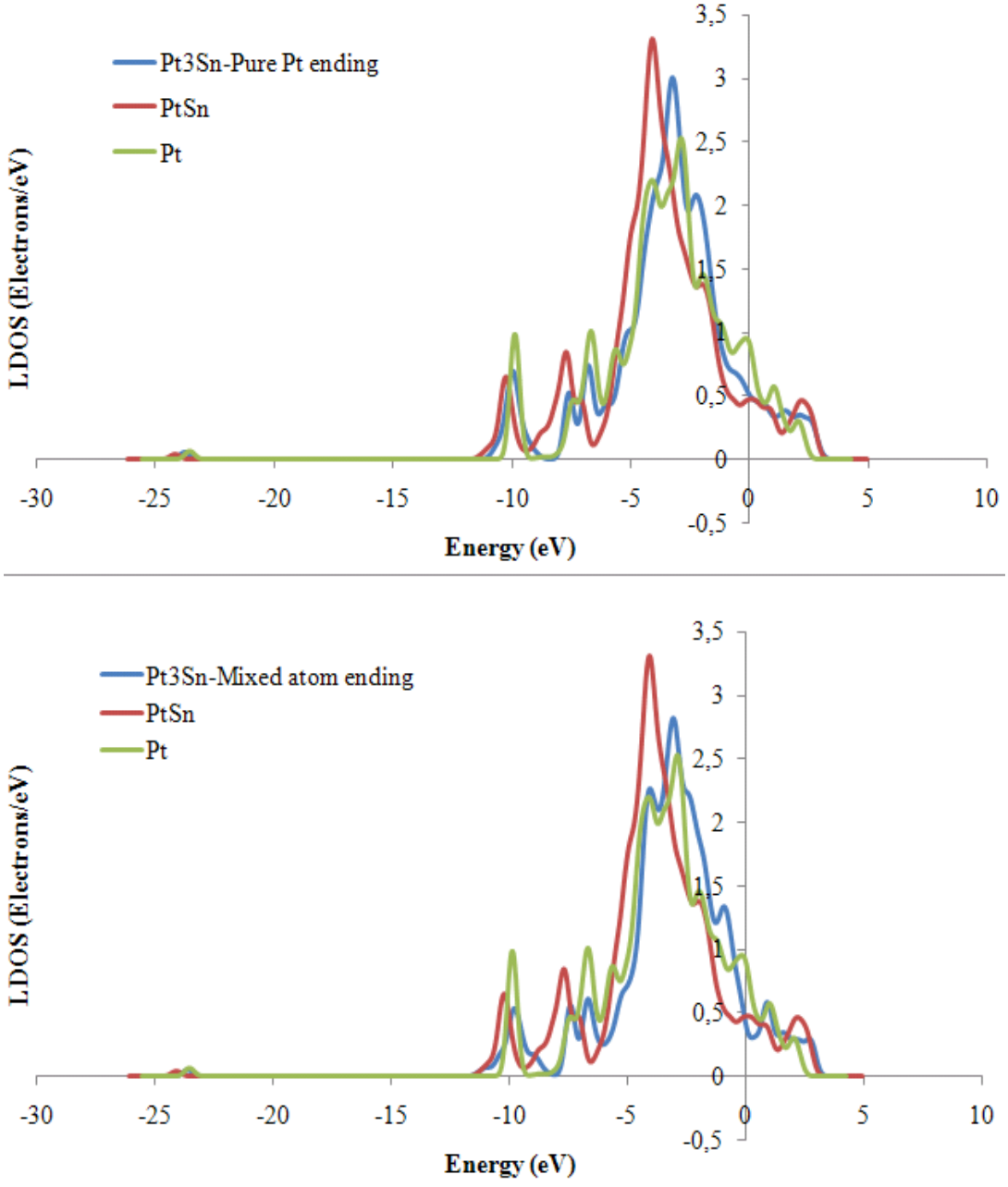

Figure 4.16. LDOS profiles of Pt atom of atop site on PtSn(110), Pt(110) and (a) pure Pt ending termination (b) mixed atom ending termination of $Pt_3Sn(110)$

4.10. Electronic Mechanism of H Adsorption on PtSn(110), Pt_3Sn(110) and Pt(110) Surfaces and Their Comparison

For atomic H adsorption, the only site adsorbing hydrogen stably is found as Pt-Pt bridge site B. H atom moved towards and stabilized at bridge position for other possible sites on PtSn(110) surface. Hence, LDOS profiles of hydrogen and Pt are exactly same for all sites. LDOS profile for Pt-Pt bridge site B is given in Figure 4.17.

Figure 4.17. represents the LDOS profiles of Pt and H upon bridge type H adsorption case as well as the bare LDOS of Pt atom present in the of Pt-Pt bridge site B of PtSn(110). The peak at -6.9 eV indicates mixing of metal d states with 1s orbital of H atom. After adsorption of H atom on the surface, electron density around Pt atom decreased slightly, but strong metal character is still observed in the region from -6 eV to 4 eV.

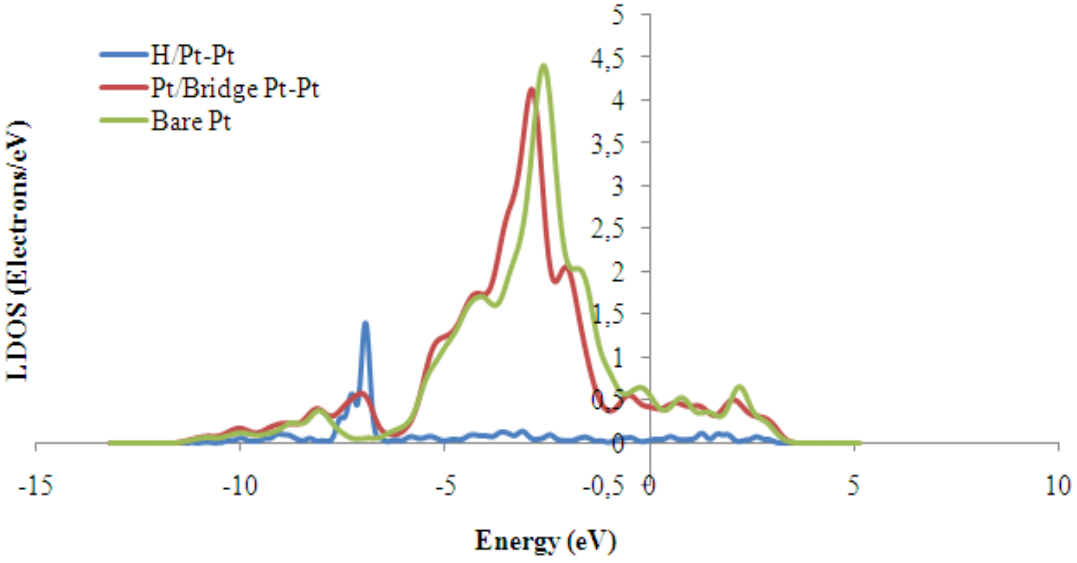

Figure 4.17. LDOS profiles of Pt atom at bridge site and adsorbed H atom for H adsorption on Pt-Pt bridge site B of PtSn(110). LDOS profile of bare Pt is given as comparison basis.

For the Pt-Pt bridge site on Pt atom of second layer present in pure Pt ending termination of Pt_3Sn(110) surface, site G, LDOS profiles of H and Pt in its bare and hydrogen adsorbed states are given in Figure 4.18. Around -7 eV electron density around Pt seems to decrease after adsorption. At the same energy level, the peak of H LDOS

indicates contribution of H 1s orbital to adsorption. At -4 eV and -0.5 eV energy levels, electronic interaction between Pt and H is observed. Electron density around Pt decreased after adsorption at those energy levels.

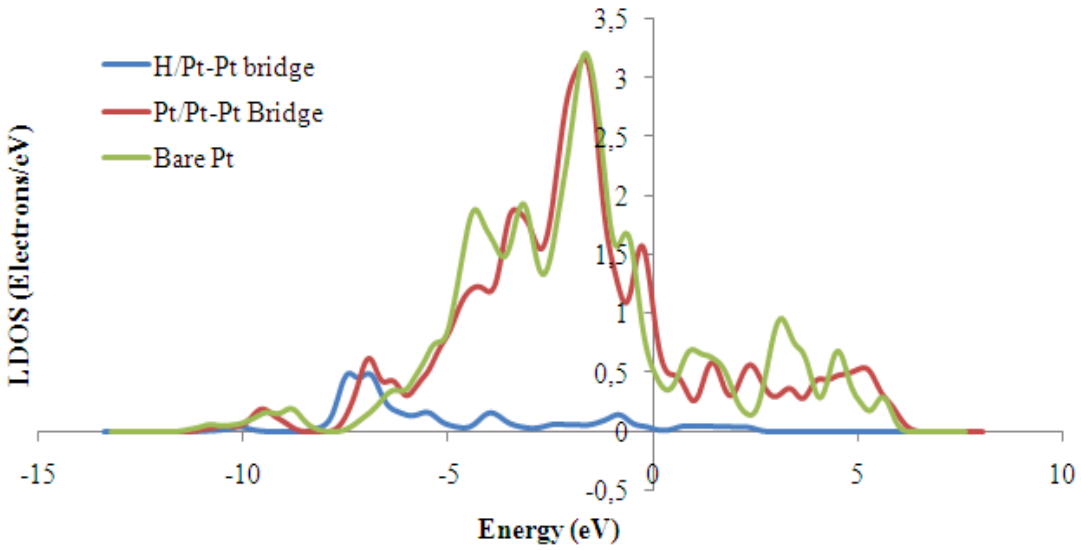

Figure 4.18. LDOS profiles of Pt atom at bridge site and adsorbed H atom for H adsorption on Pt-Pt bridge site on Pt atom, site G, on pure Pt atom ending termination of $Pt_3Sn(110)$. LDOS profile of bare Pt is given as comparison basis.

For atop Pt site F on pure Pt ending termination of $Pt_3Sn(110)$ surface, LDOS profiles of Pt for bare and H adsorbed states and H in adsorbed state are given in Figure 4.19. Electron density at around -2 eV decreased and shifted downwards after hydrogen adsorption indicating contribution of d states of Pt atom to adsorption. Interaction between H atom and surface Pt atom can be observed clearly at -1 eV and between -7 eV and -4 eV energy levels.

For Pt-Pt bridge site of $Pt_3Sn(110)$ surface present on Sn atom of the second layer, site H, the LDOS profiles of Pt atom for its bare and H-adsorbed states and of H atom upon adsorption are given in Figure 4.20. Electron density around Pt atom decreased after H chemisorption at -2 eV of energy level. The contribution of 1s H orbital is observed around -7 eV. At this energy level, electron density around Pt atom increased, suggesting mixing of Pt d states with H 1s orbital.

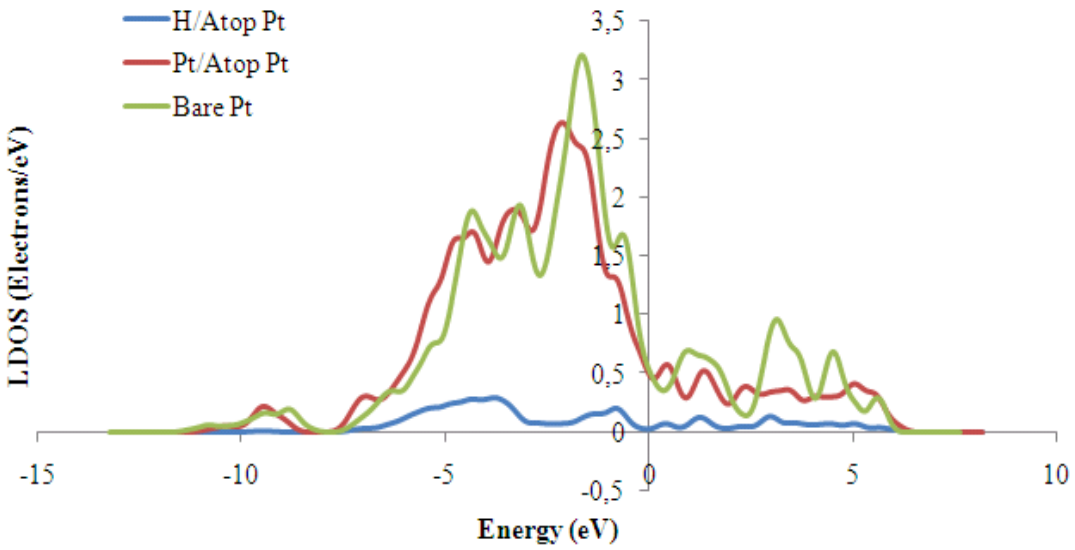

Figure 4.19. LDOS profiles of Pt and adsorbed H atom for H adsorption on atop Pt site F on pure Pt atom ending termination of $Pt_3Sn(110)$. LDOS profile of bare Pt is given as comparison basis.

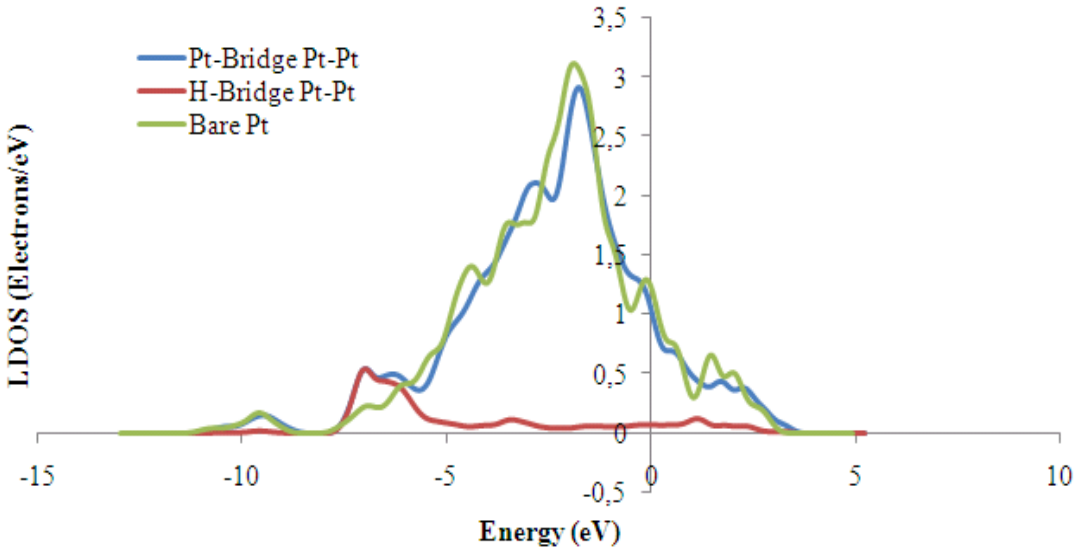

Figure 4.20. LDOS profiles of Pt atom at bridge site and adsorbed H atom for H adsorption on Pt-Pt bridge site on Sn atom, site H, on pure Pt atom ending termination of $Pt_3Sn(110)$. LDOS profile of bare Pt is given as comparison basis.

For atop site A on Pt(110) surface, the LDOS profiles of Pt for its bare and H-adsorbed states and of H atom upon adsorption are given in Figure 4.21. The downwards shift of the peaks at -3.7 eV, -2.1 eV, and -0.6 eV implies contribution of d states to adsorption. Electron density around Pt atom decreased after chemisorption around Fermi level, whereas at lower energies electron density increases around surface metal. Between the region -7 eV and -4 eV, contribution of 1s H orbital is clearly observed. Electron density around Pt increased at the energy levels correspond to mixing H orbitals with metal d states, such as -4.5 eV, -2.5 eV, and 2 eV.

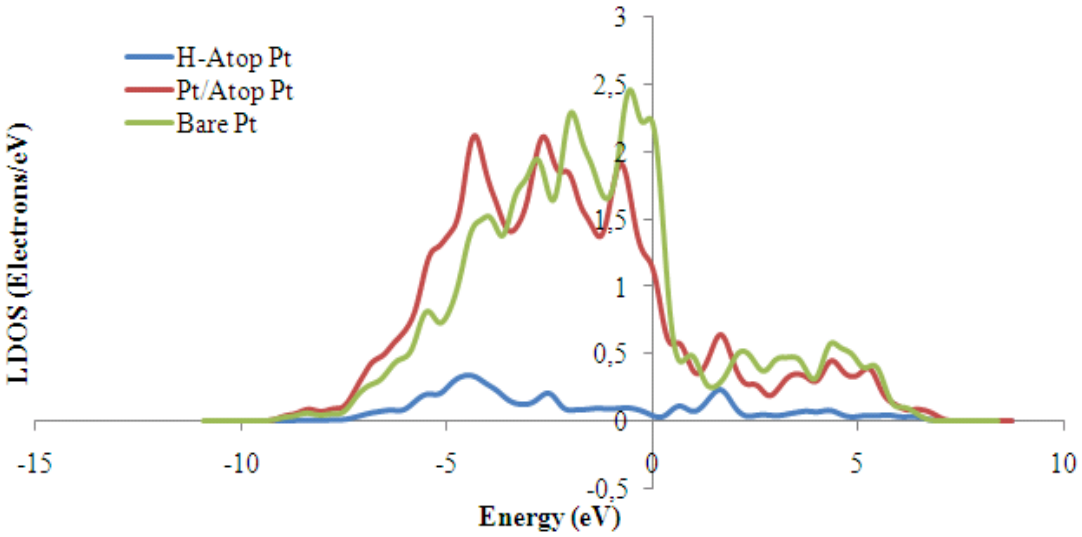

Figure 4.21. LDOS profiles of adsorbed H atom and Pt for atop type H adsorption on Pt(110) surface LDOS profile of bare Pt is given as comparison basis.

Figure 4.22 represent the LDOS profiles of atoms involved in hydrogen adsorption on short bridge site B on Pt(110) surface. LDOS of bare Pt and Pt upon adsorption as well as LDOS of H upon adsorption are given. Electron density around Pt atom slightly increased in the region between -7.5 eV and -5.5 eV, which coincides with the 1s orbital of H atom. Electron density at ca. -2.2 eV decreased, implying Pt contribution to H adsorption.

Figure 4.23(a) and Figure 4.23(b) represents the comparisons of LDOS profiles of Pt of three alloys having (110) geometry and of H for bridge type adsorption, respectively. As

Sn content increases, highest electron density region shifts downwards in energy, and the peak intensities increase around Pt; those changes indicate increased electron density, as in the bare states of the surfaces, for lower energy levels as the Sn concentration increases in the alloy. Figure 4.23(b) shows that 1s H orbital contributed least to adsorption on PtSn surface. Intensity of the LDOS peaks at -7.5eV for $Pt_3Sn(110)$ and PtSn(110) surfaces are relatively lower compared to that on PtSn(110) surface, suggesting larger contribution of H 1s orbital to adsorption on $Pt_3Sn(110)$ and Pt(110) surfaces.

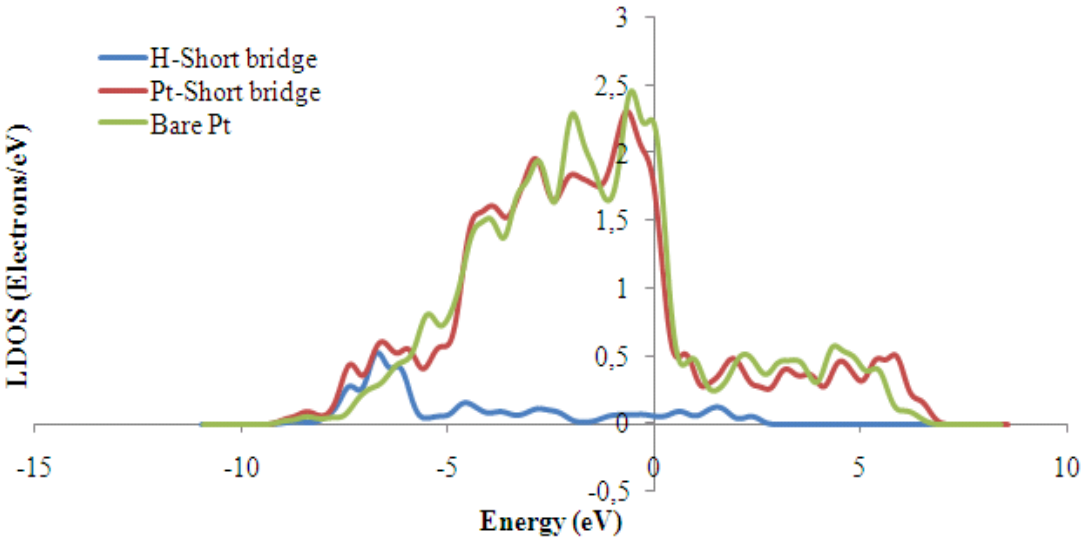

Figure 4.22. LDOS profiles of adsorbed H atom and Pt for short bridge type O adsorption on Pt(110) surface. LDOS profile of bare Pt is given as comparison basis.

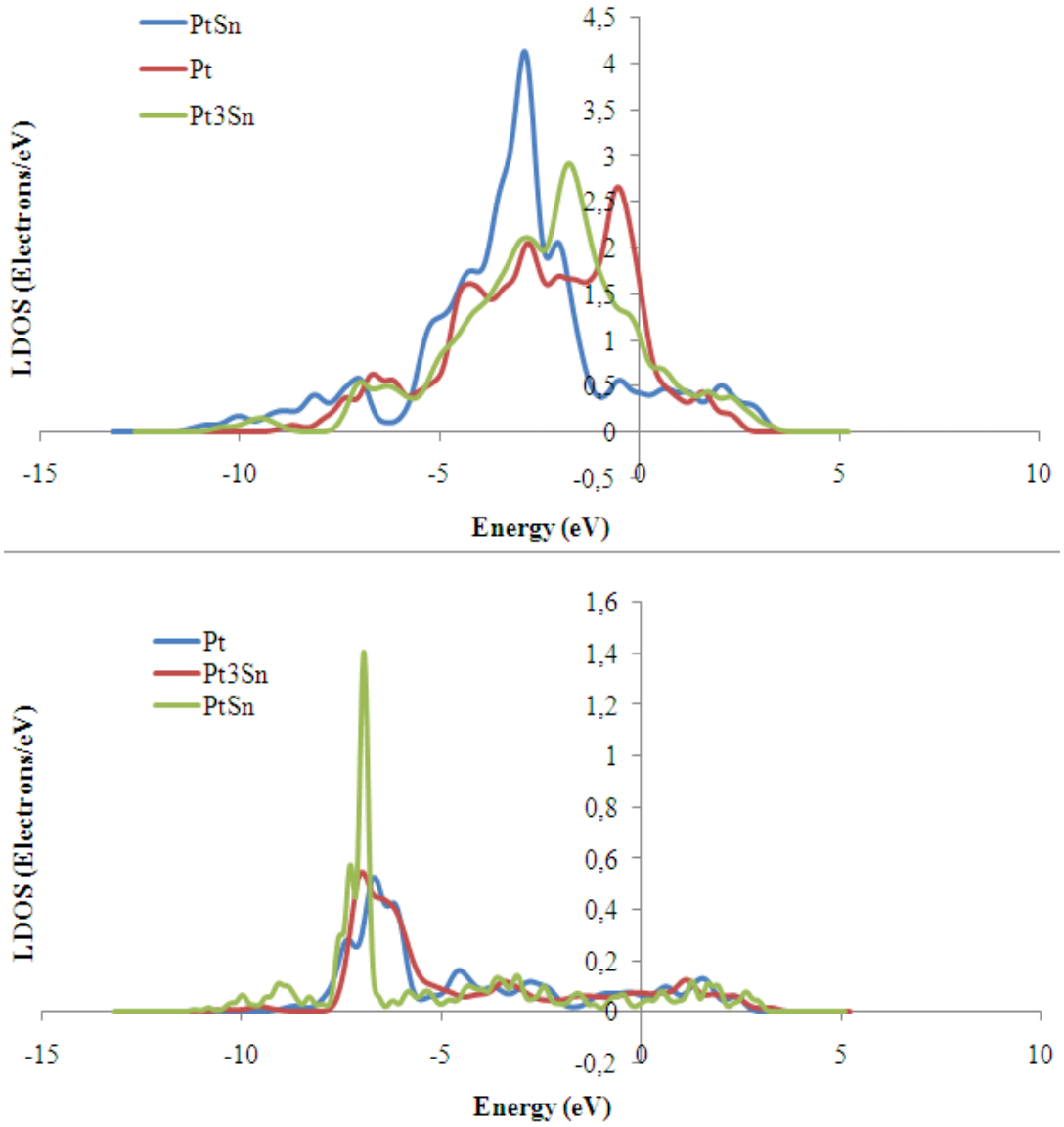

Figure 4.23. Comparison of LDOS profiles for Pt-Pt bridge type H adsorption on Pt(110), $Pt_3Sn(110)$ and Pt(110) surfaces (a) for adsorbed state of Pt and (b) for adsorbed H atom.

4.11. Electronic Mechanism of O Adsorption on PtSn(110), Pt_3Sn(110) and PtSn(110) Surfaces and Their Comparison

One of the sites adsorbing oxygen stably on PtSn(110) surface is Pt-Pt bridge site B and LDOS profiles of the atoms involved in oxygen adsorption for this site are given in Figure 4.24. The first peak of adsorbed oxygen LDOS at -17 eV is attributed to O-2s derived orbital and it slightly contributes to adsorption by mixing with Pt d states in a small extent. The peak of adsorbed oxygen LDOS in the region between -7 eV and -3 eV represents 2p orbital of free O atom; in this region, 2p orbital of O atom mixed with metal d states and it is reflected to the LDOS profile as an increase in electron density around O bonded Pt atom (at ca. -5.5 eV). The peak at -3.7 eV shifted downwards in energy after O chemisorption, indicating electronic interaction between O and Pt in Pt-O bond formation. Additionally, the intensity of the peak decreased because of electron transfer from metal d states to O 2p orbital.

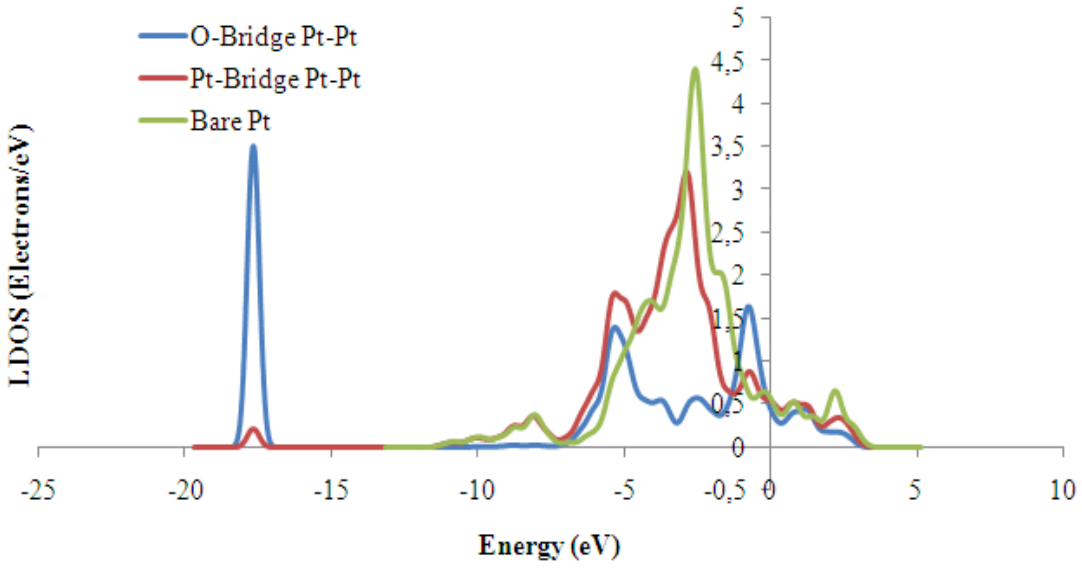

Figure 4.24. LDOS profiles of adsorbed O atom and Pt for Pt-Pt bridge type O adsorption on PtSn(110) surface. LDOS profile of bare Pt is given as comparison basis.

Sn-Sn bridge site F also adsorbed oxygen stably, and LDOS profiles of Sn in its bare and oxygen adsorbed states and O for this site are given in Figure 4.25. The region between -11 eV to -6.5 eV represents the 5s orbitals of Sn atom, and the decrease in

intensity of the electron density in this region stems from the electron transfer from Sn atom to O atom. The broadening of the LDOS peak in this region may also imply formation of Sn-O bond after adsorption. Above -5 eV, 5p Sn states contributes to adsorption strongly. High intensity of the LDOS peak of adsorbed O at -2.5 eV indicates the electron transfer from Sn atom to O atom in this region.

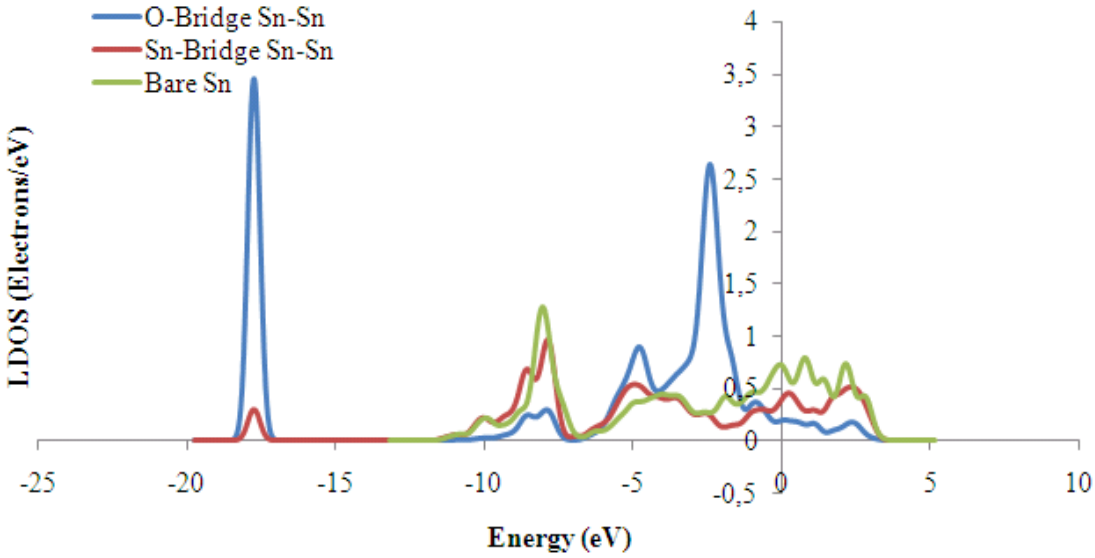

Figure 4.25. LDOS profiles of adsorbed O atom and Sn for Sn-Sn bridge type O adsorption on PtSn(110) surface. LDOS profile of bare Sn is given as comparison basis.

The LDOS profiles of the atoms involved in O adsorption on Pt_2Sn site D of PtSn(110) surface are given in Figure 4.26(a) and Figure 4.26(b). The intensity of 5s orbital of Sn atom decreased after O chemisorption, suggesting electron transfer from Sn to O atom. In this region Pt orbitals have not changed either in intensity or in energy, thus the adsorption on this multicoordinated site mostly involves Sn-O interaction rather than Pt-O. Above -6.5 eV, the peaks at Sn LDOS shifted towards lower energies indicating strong S-O bond formation. The intensity of the peaks decreased as a consequence of electron transfer from Sn to O. Intensity of the LDOS peak of Pt at -2.5 eV decreased after O chemisorption due to electron transfer between metal d states and 2p O orbital. The bond lengths suggested stronger Sn-O bond with shorter length, and analysis of LDOS profiles verifies it in terms of electronic interaction.

Pt-Pt bridge site present on Sn atom of the sublayer, site H, for pure Pt ending termination of $Pt_3Sn(110)$ surface adsorbed O stably. The LDOS profiles of the atom involved in O adsorption are given for the site in Figure 4.27. The contribution of Pt d states can be observed from the figure clearly, especially around the peak at -2 eV. The decrease in intensity of the peak indicates electron transfer from Pt to O atom.

Another site, which adsorbed O atom stably, is Pt-Pt bridge site present on Pt atom of the sublayer, site G, of pure Pt ending termination of $Pt_3Sn(110)$ surface. The LDOS profiles of Pt atom and O atom in their adsorbed state as well as LDOS of bare Pt are given in Figure 4.28. The LDOS profile of Pt is mostly the same as that of Pt at the bridge site present on Sn atom, site H, which was mentioned before. One remarkable difference is at the LDOS peak of Pt around -2 eV; which is lower in energy and intensity compared to that of Pt the bridge site on Sn atom, site H. Tthis difference indicates stronger Pt-O interaction for the site on Pt; stronger adsorption energy is reflected by Table 4.5.

Another site adsorbing O stably is Pt-Pt long bridge site I on pure Pt ending termination of $Pt_3Sn(110)$ surface. The LDOS profiles of the atoms involving O adsorption on the site are given in Figure 4.29. The peaks of the Pt and O atoms involved in adsorption are at same energy levels as with the LDOS profiles of the atoms aforementioned for bridge type O adsorption for pure Pt ending configuration of Pt_3Sn surface. However, the peak around -2 eV is broader and lower in intensity, which suggests strong Pt-O interaction. Through LDOS analysis the reason of strong oxygen adsorption of long bridge site previously found (Table 4.5) has been explained.

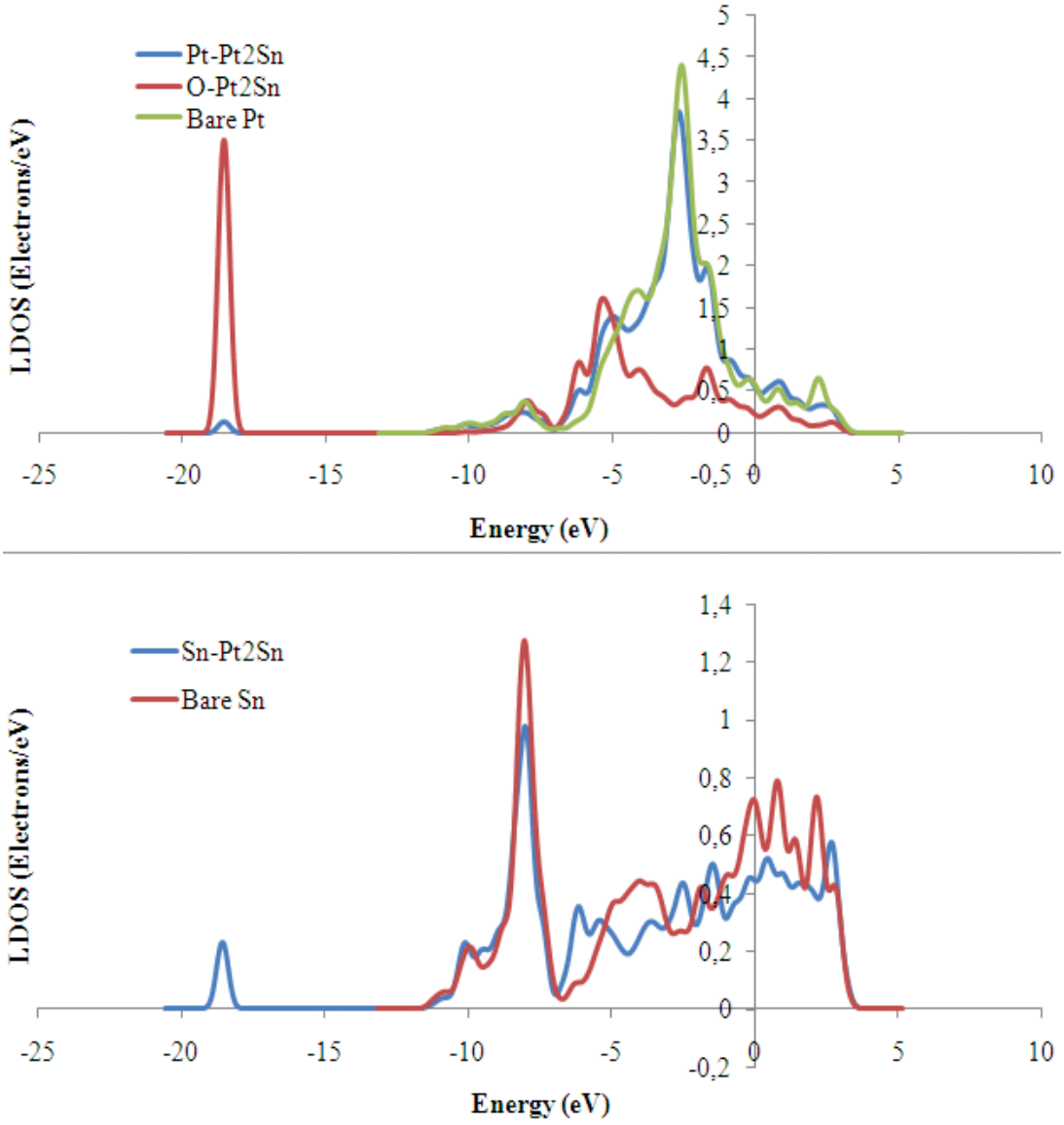

Figure 4.26. LDOS profiles for Pt2Sn type O adsorption on PtSn(110) surface (a) for adsorbed states of Pt and of O (b) for adsorbed states of Sn. LDOS of bare Pt in Figure 4.26(a) and LDOS of bare Sn in Figure 4.26(b) are given as comparison basis.

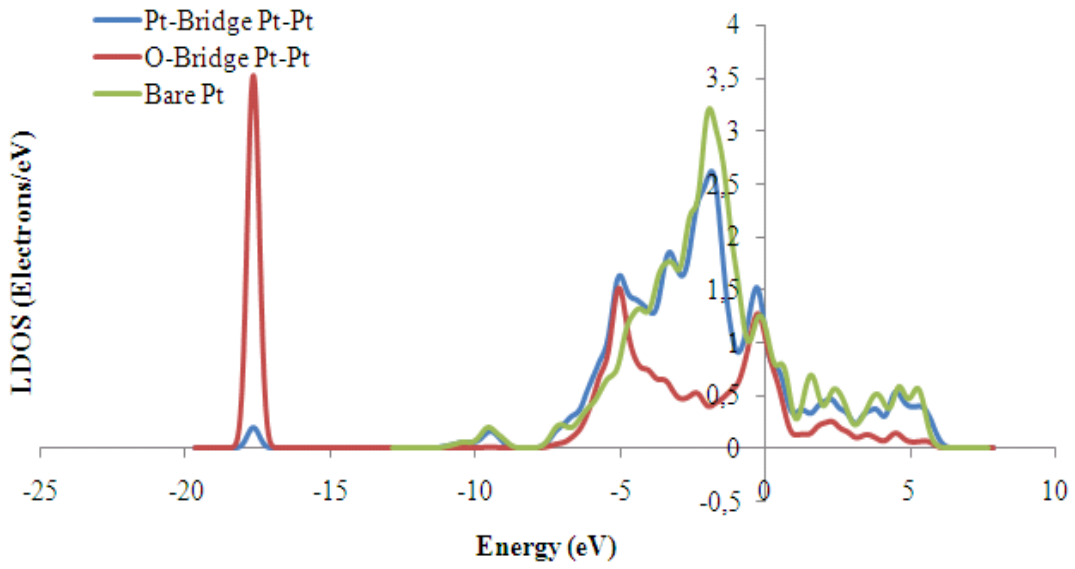

Figure 4.27. LDOS profiles of Pt atom at bridge site and adsorbed O atom for O adsorption on Pt-Pt bridge site on Sn atom, site H, on pure Pt atom ending termination of $Pt_3Sn(110)$. LDOS profile of bare Pt is given as comparison basis.

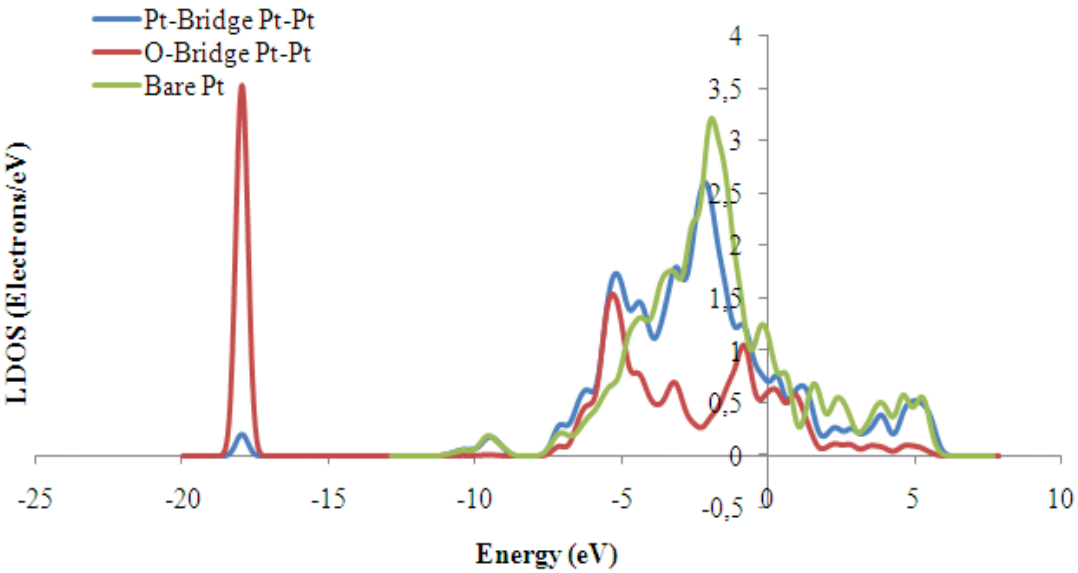

Figure 4.28. LDOS profiles of Pt atom at bridge site and adsorbed O atom for O adsorption on Pt-Pt bridge site on Pt atom on pure Pt atom ending termination of $Pt_3Sn(110)$ surface. LDOS profile of bare Pt is given as comparison basis.

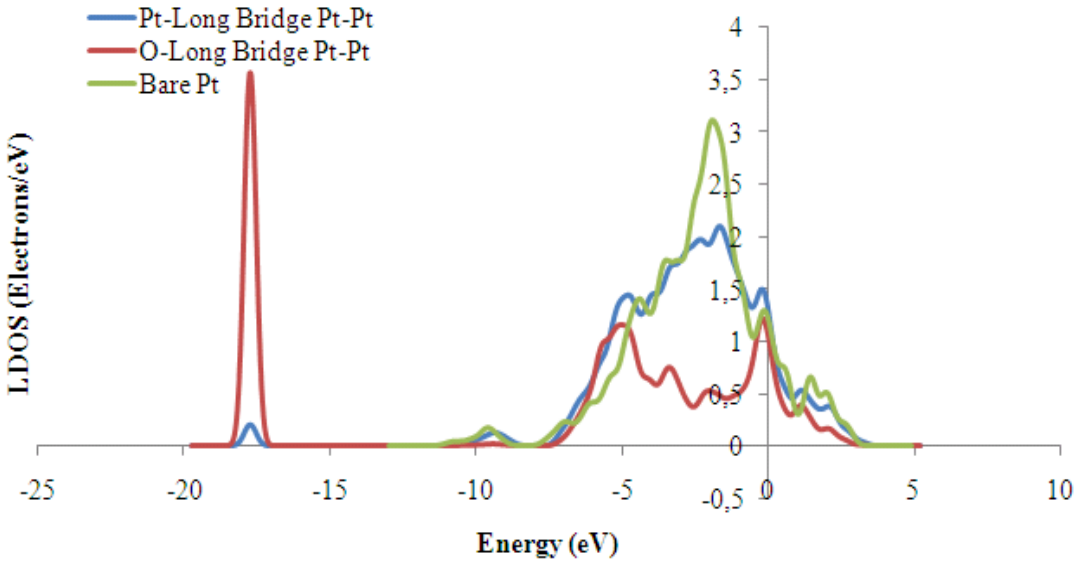

Figure 4.29. LDOS profiles of adsorbed O atom and Pt for Pt-Pt long bridge type O adsorption on pure Pt ending termination of $Pt_3Sn(110)$ surface. LDOS profile of bare Pt is given as comparison basis.

Stable oxygen adsorption was observed on Pt-Sn bridge site B of $Pt_3Sn(110)$ surface with mixed atom ending termination. The LDOS profiles of Pt and of O are given in Figure 4.30(a), and LDOS profile of Sn atom for its bare and oxygen adsorbed states are given in Figure 4.30(b). The peak at -8.5 eV at Sn LDOS did not changed after chemisorption; thus, it can be clearly said that 5s orbitals of Sn atom did not involved in oxygen adsorption. Above-7.5 eV, the metallic orbitals of both Pt and Sn atoms mixed with 2p orbitals of oxygen atom. The peak at -6 eV in LDOS of O indicates contribution of O 2p orbitals to adsorption. The decrease in intensity at -1.7 eV and -1 eV around Pt atom suggests electron transfer from Pt to O atom. However, around Fermi level the decrease in electron density around Sn atom is more remarkable compared to that around Pt. The bond lenghts have also suggested stronger Sn-O interaction than Pt-O interaction. (Table 4.5)

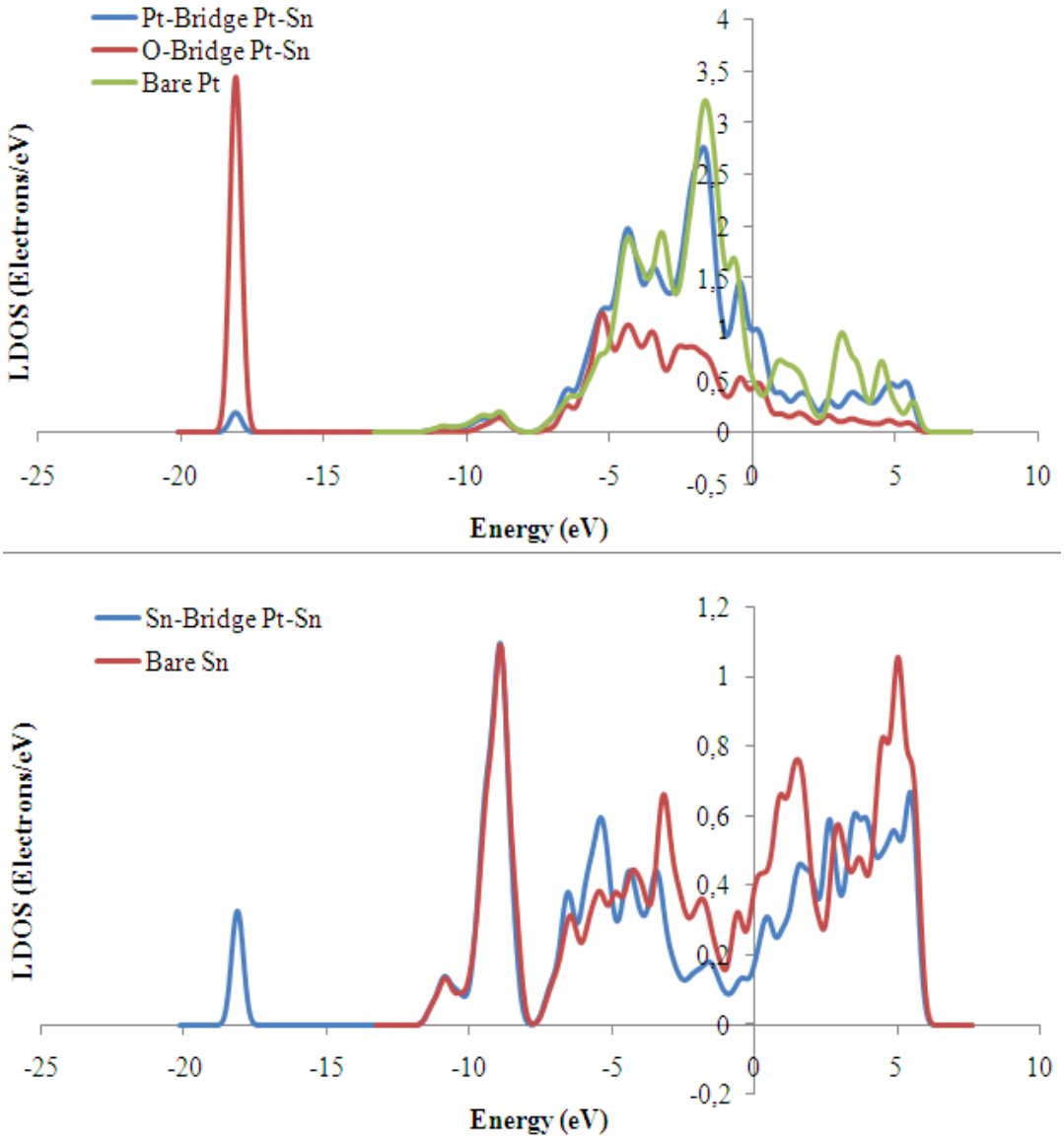

Figure 4.30. LDOS profiles for Pt-Sn bridge type O adsorption on mixed atom ending termination of $Pt_3Sn(110)$ surface (a) for adsorbed states of Pt and of O (b) for adsorbed states of Sn. LDOS of bare Pt in Figure 4.30(a) and LDOS of bare Sn in Figure 4.30(b) are given as comparion basis.

The Sn-Sn bridge site E was found adsorbing O stably. LDOS profiles of Sn for its bare and oxygen adsorbed states and of adsorbed O are given in Figure 4.31 for this site. The positive shift of the peak at -9.1 eV in LDOS profile of Sn upon O adsorption indicates

weak Sn-O interaction; whereas the mixing of 5p Sn states with 2p O orbitals established strong Sn-O bond after adsorption.

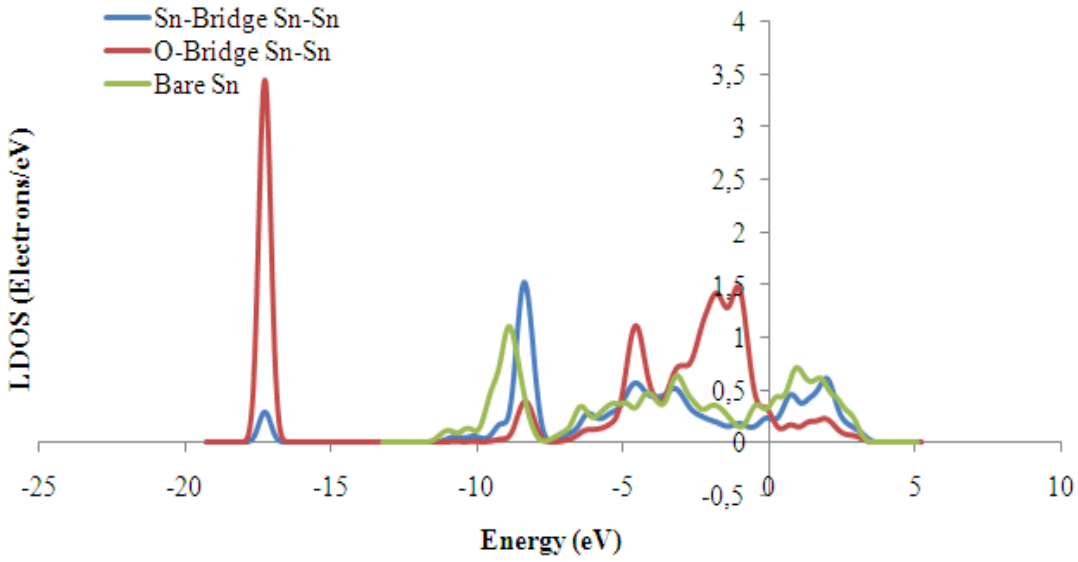

Figure 4.31. LDOS profiles of adsorbed O atom and Sn for Sn-Sn bridge type O adsorption on mixed atom ending termination of $Pt_3Sn(110)$ surface. LDOS profile of bare Sn is given as comparison basis.

Pt-Pt long bridge site D on mixed atom ending termination of $Pt_3Sn(110)$ surface was also found adsorbing oxygen stably. The LDOS profiles of Pt for its bare and oxygen adsorbed states and of O for its adsorbed state are given in Figure 4.32. The remarkable shift of peak at -1.7 eV to -2.1 eV and broadening of the peak in LDOS profile of Pt upon adsorption implies strong Pt-O interaction. The mixing of 2p O orbitals and Pt d states was reflected on the figure at -5 eV and -0.5 eV clearly.

On Pt(110) surface, atop Pt site A was found adsorbing O stably. The LDOS of Pt for its bare and oxygen adsorbed states and O for its adsorbed states are given in Figure 4.33. The electronic background of strong O adsorption on the site can be clearly observed from the LDOS profile. The peaks present in LDOS of Pt between -4 eV and 1 eV significantly shifted upon O adsorption to lower energy values, suggesting strong Pt-O interaction. Symmetrically, between -7 eV and -2 eV, the contribution of O 2p orbitals to adsorption were observed.

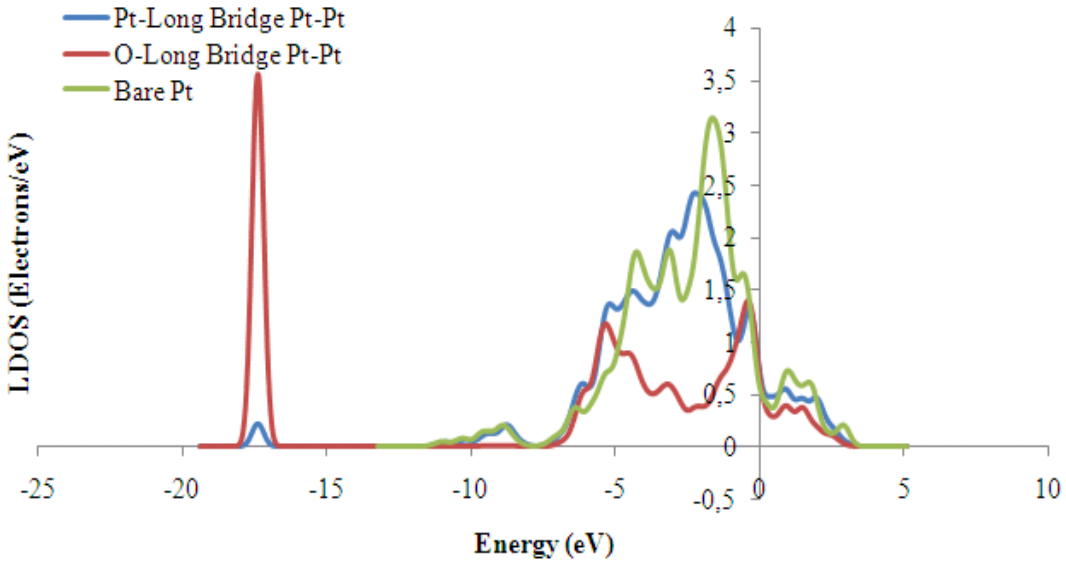

Figure 4.32. LDOS profiles of adsorbed O atom and Pt for Pt-Pt long bridge type O adsorption on mixed atom ending termination of $Pt_3Sn(110)$ surface. LDOS profile of bare Pt is given as comparison basis.

The short bridge site B on Pt(110) adsorbed O stably. The LDOS profiles of the atoms involved in O adsorption on the site are given Figure 4.34. The decrease in electron density below Fermi level, between -3 eV and 0 eV suggests mixing of metal d states with O 2p orbitals. At -5.7 eV, electron shift from adsorbed O to metallic states is clearly observed from comparison of LDOS of Pt for its bare and O-adsorbed states.

The LDOS profiles of atoms involved in O adsorption on Pt-Pt long bridge site C on Pt(110) surface are given in Figure 4.35 as the reference basis. At -5.7 eV, the electron density around Pt atom increased, indicating O contribution to adsorption. Above -3 eV to Fermi level, the electron transfer from metal d states to O atom was observed. The decrease in intensity of the peaks in LDOS of Pt upon adsorption in the region from -3 eV to Fermi level, indicates electron transfer from Pt d states to O atom.

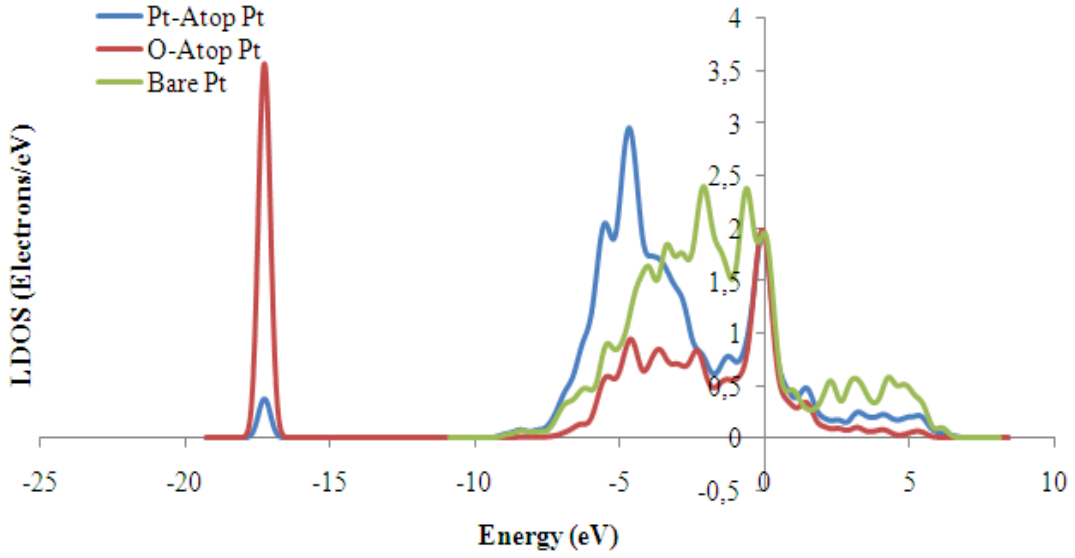

Figure 4.33. LDOS profiles of adsorbed O atom and Pt for atop type O adsorption on Pt(110) surface. LDOS profile of bare Pt is given as comparison basis.

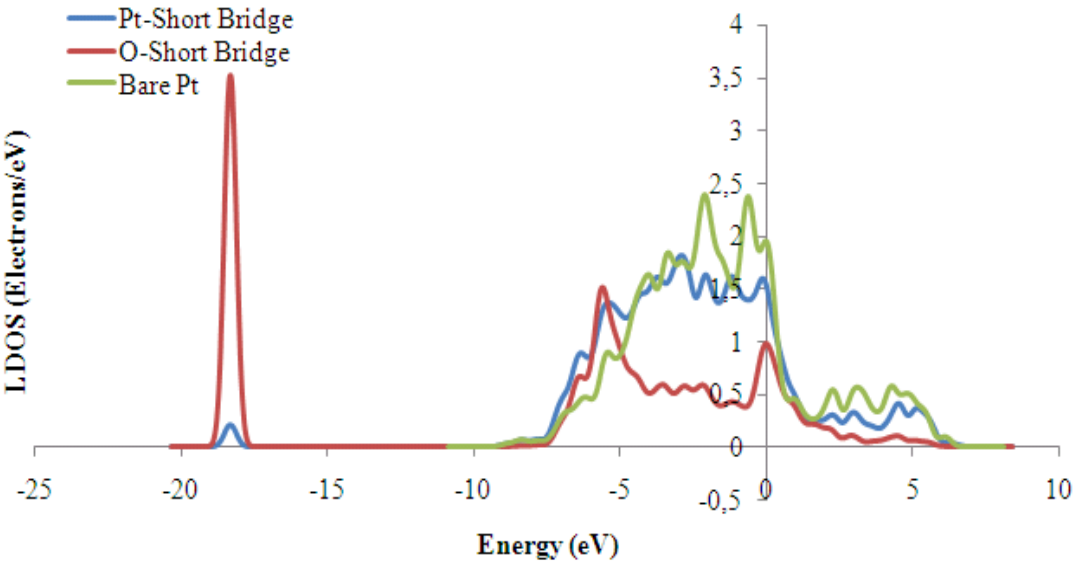

Figure 4.34. LDOS profiles of adsorbed O atom and Pt for short bridge type O adsorption on Pt(110) surface. LDOS profile of bare Pt is given as comparison basis.

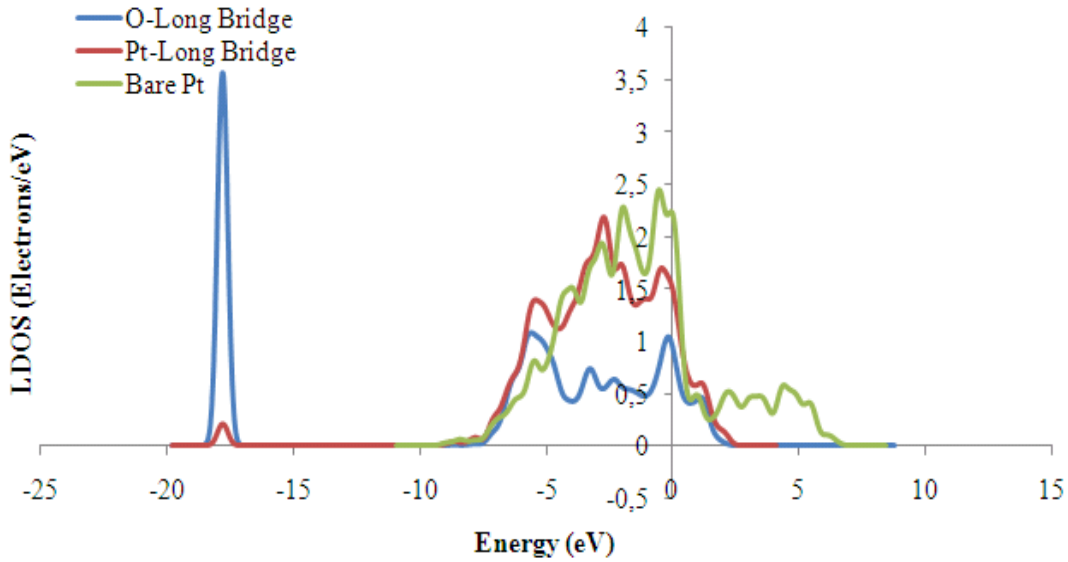

Figure 4.35. LDOS profiles of adsorbed O atom and Pt for long bridge type O adsorption on Pt(110) surface. LDOS profile of bare Pt is given as comparison basis.

The Pt-Pt bridge sites of the PtSn(110), Pt(110) and Pt_3Sn(110) surfaces are compared in Figure 4.36 and Figure 4.37. In Figure 4.36, the LDOS of Pt atom in Pt-Pt bridge site present on Pt, site G, of pure Pt ending termination of Pt_3Sn(110) is compared with those on Pt_3Sn and Pt. Figure 4.36(b) indicates that the participation of O 2p orbital in adsorption was almost same for all surfaces around -5.4 eV; whereas the contribution of O to the adsorption process increases with increasing Sn content around Fermi level. As Sn concentration of the alloy increased, the mixing of orbitals of O and Sn occured at slightly lower energies, as shown in Figure 4.36(b) Figure 4.37 illustrates the comparison of LDOS of Pt atom present in Pt-Pt bridge site on mixed atom ending configuration of Pt_3Sn(110) surface with those on Pt-Pt bridge on Pt(110) and Pt_3Sn(110) surfaces. The remarkable difference between LDOS of Pt at bridge sites of pure Pt ending and mixed atom ending terminations of Pt_3Sn(110) surface is the intensities of the peaks at -0.8 eV. For the site on mixed atom ending surface, presence of Sn is as effective as on PtSn surface, since the mixed atom ending surface has Sn atom on top layer.

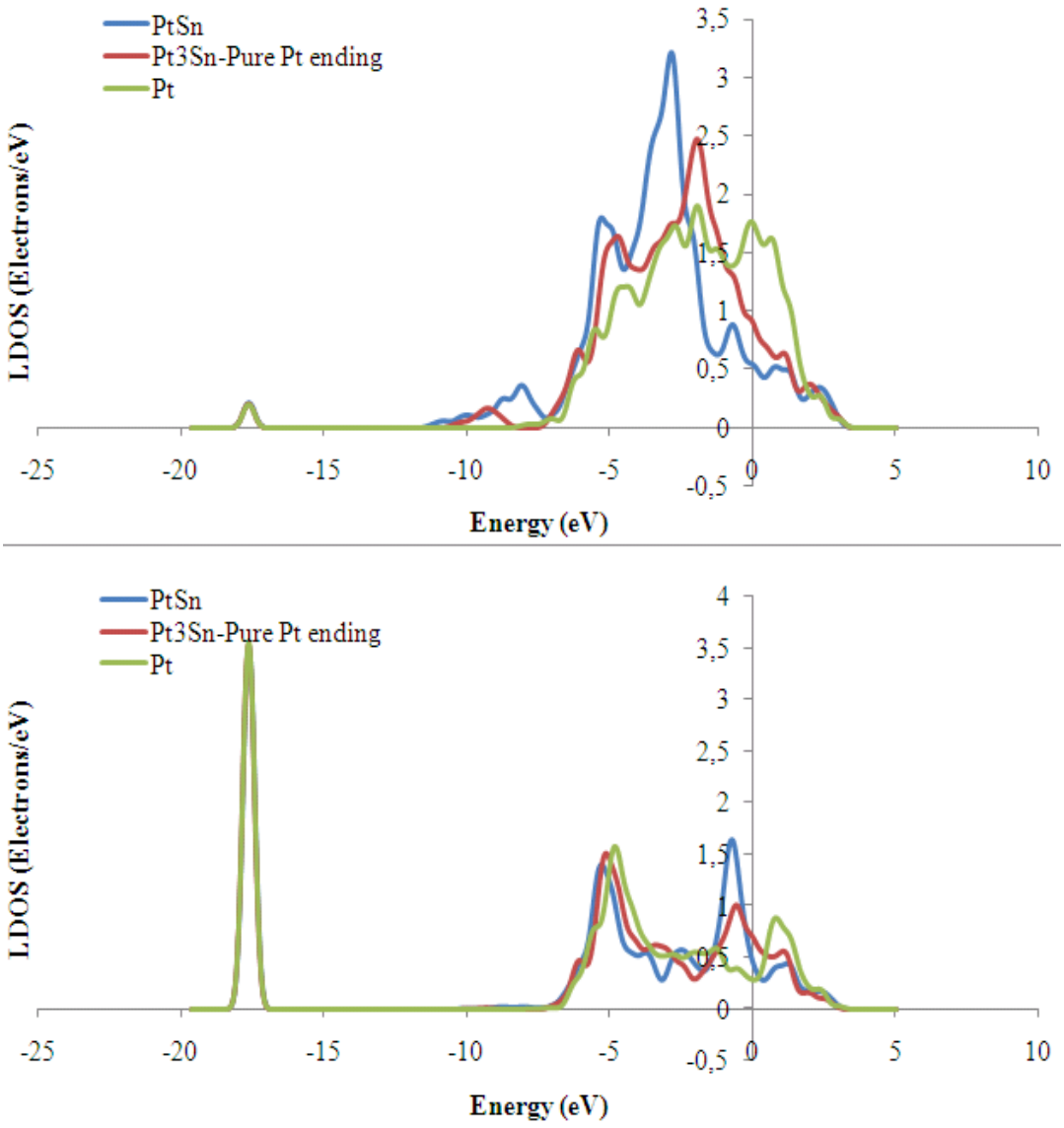

Figure 4.36. Comparison of LDOS profiles for Pt-Pt bridge type O adsorption on Pt(110), pure Pt atom ending termination of $Pt_3Sn(110)$ and Pt(110) surfaces (a) for adsorbed state of Pt and (b) for adsorbed O atom.

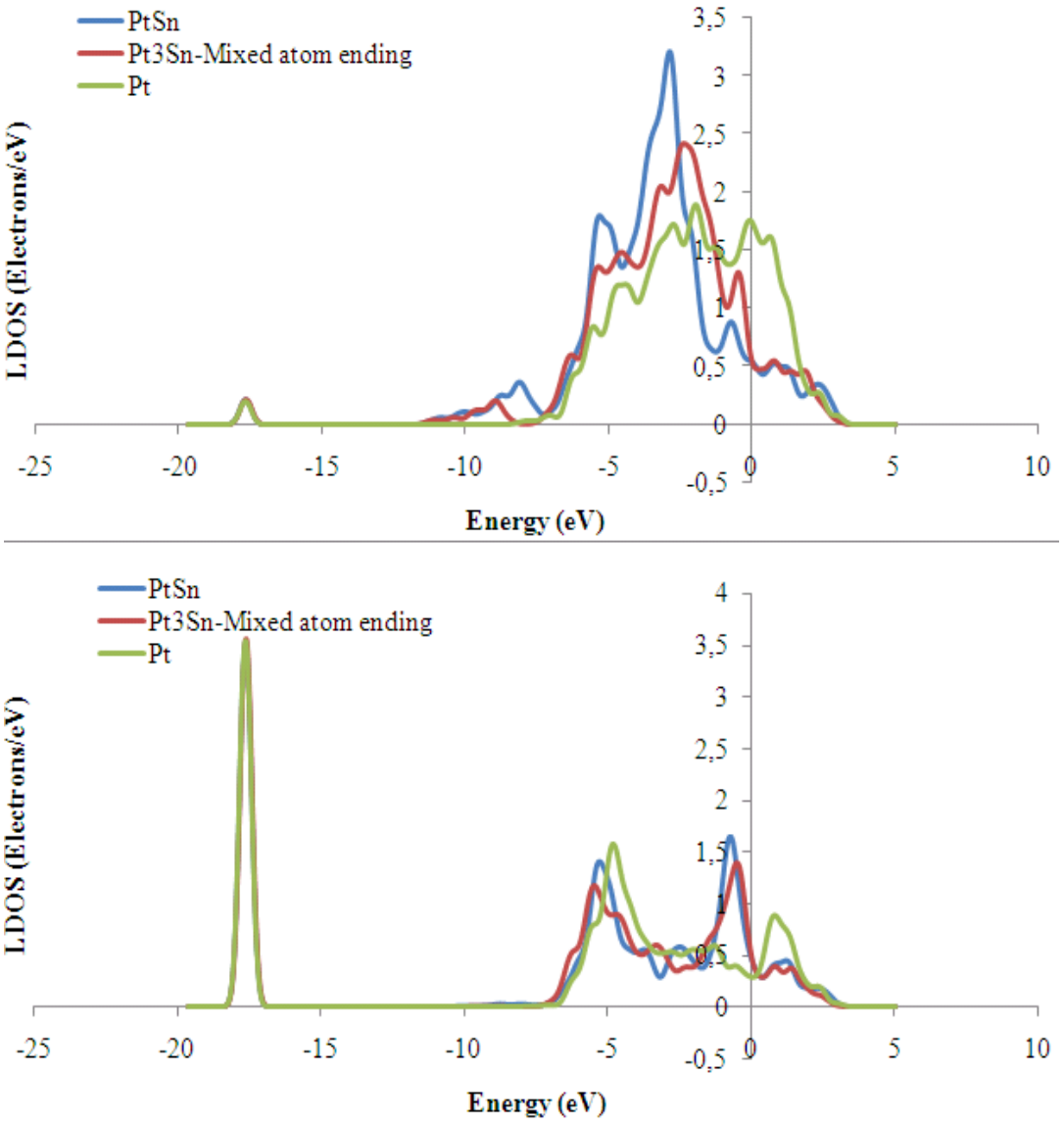

Figure 4.37. Comparison of LDOS profiles for Pt-Pt bridge type O adsorption on Pt(110), mixed atom ending termination of $Pt_3Sn(110)$ and Pt(110) surfaces (a) for adsorbed state of Pt and (b) for adsorbed O atom.

5. CONCLUSIONS

- For PtSn(110) surface, the most energetically preferred site for CO adsorption was found as Pt-Pt bridge site B. The comparison of bridge sites of there surfaces, namely PtSn, Pt_3Sn, and Pt, revealed that the adsorption strength decreases with increasing Sn content.

- Hydrogen was adsorbed stably only on Pt-Pt bridge site B on PtSn(110) surface. The comparison of adsorption properties of hydrogen on PtSn with the other two surfaces suggested that hydrogen was adsorbed less energetically on $Pt_3Sn(110)$ surface.

- CO_2 adsorption was found stable only on Pt-Sn bridge site C on PtSn(110) surface. When CO_2 adsorption properties of three surfaces were compared; it was found that the stability of CO_2 adsorption differs according to the characteristic of the surface. If the surface has Sn atoms on top layer, CO_2 was adsorbed stably on Pt-Sn bridge sites; whereas if surface does not contain Sn, Pt-Pt bridge sites were the most favoured sites for stable CO_2 adsorption.

- On PtSn(110) surface, Sn-Sn bridge site F was the most energetically favourable site for stable O adsorption. The comparison of oxygen adsorption on PtSn, Pt_3Sn and Pt surfaces suggested that the O adsorption strength decreases with increasing Sn content on the top layer of the surface for sites adsorb oxygen stably.

- Co-adsorption of O and CO on PtSn(110) surface revealed that at surface coverage of 0.125 ML CO, the second pre-adsorbed O atom had no significant effect on CO adsorption strength. However, for higher surface coverage of CO, i.e. 0.5 ML, an increase in O surface concentration enhanced the adsorption energy of CO on PtSn(110) surface.

6. RECOMMENDATIONS

- CO, H_2, CO_2, and O_2 adsorption properties of other low index surfaces of PtSn surfaces PtSn(100) and PtSn(001) should be investigated.

- Co-adsorption of CO with H and CO_2 should be studied to understand the complete behaviour of CO oxidation reactants on Pt-Sn alloy surfaces.

- To understand the co-adsorption properties of CO and O_2 with H_2 and CO_2 presence, a more detailed co-adsorption study can be carried out.

- Adsorption of H_2, CO_2, and O_2 can be carried out on stepped, kinked and reconstructed surfaces of Pt_3Sn alloy for understanding the adsorbate-adsorbent interaction under more realistic conditions.

REFERENCES

1. Trimm, D. L. and Z. İ. Önsan, "Onboard Fuel Conversion for Hydrogen-Fuel-Cell-Driven Vehicles", *Catalysis Reviews*, Vol. 43, No. 1-2, pp. 31-84, 2001.

2. Jhalani, A. and L. D. Schmidt, "Preferential CO Oxidation in the Presence of H_2, H_2O, and CO_2 at Short Contact-Times", *Catalysis Letters*, Vol. 104, No. 3-4, pp. 103-110, 2005.

3. Özkara, Ş. and A. E. Aksoylu, "Selective Low Temperature Carbon Monoxide Oxidation in H_2-Rich Streams over Activated Carbon Supported Catalysts", *Applied Catalysis A: General,* Vol. 251, pp. 75-83, 2003.

4. Young, J. and J. Canin, *Overview of Fuel Reformation and Processing Technologies for Hydrogen Fuel Cells*, Spokane Intercollegiate Research and Technology Institute, January 2004.

5. NASA Glenn Research Center, "Fuel Cell", http://www.grc.nasa.gov/WWW/Electro-chemistry/doc/fuelcell.html, February 2008.

6. Dudfield C. D., R. Chen, and P. L. Adcock, "A carbon monoxide PROX reactor for PEM fuel cell automotive application", *International Journal of Hydrogen Energy*, Vol. 26, pp. 763-775, 2001.

7. Cho S.H., J. S. Park, S. H. Choi and S. H. Kim, "Effect of magnesium on preferential oxidation of carbon monoxide on platinum catalyst in hydrogen-rich stream", *Journal of Power Resources*, pp. 260-266, 2006.

8. Pan L. and S. Wang, "A compact integrated fuel-processing system for proton exchange membrane fuel cells", *International Journal of Hydrogen Energy*, Vol. 31, No. 4, pp. 447-454, 2006.

9. Recupero V., L. Pino, A. Vita, F. Cipiti, M. Cordaro and M. Lagana, "Development of a LPG fuel processor for PEFC systems : Laboratory scale evaluation of autothermal reforming and preferential oxidation subunits", *International Journal of Hydrogen Energy*, Vol. 30, No. 9, pp. 963-971, 2005.

10. Wootsch A., C. Descorme and D. Duprez, "Preferential oxidation of carbon monoxide in the presence of hydrogen (PROX) over ceria-zirconia and alumina-supported Pt catalysts", *Journal of catalysis*, Vol. 225 No. 2, pp. 259-266, 2004.

11. Kahlich, M. J., H. A. Gasteiger and Behm, R. J., "Kinetics of the Selective Low-Temperature Oxidation of CO in H_2-Rich Gas over Au/α-Fe_2O_3", *Journal of Catalysis*, Vol. 182, No. 2, pp. 430-440, 1999.

12. Son, I. H., M. Shamsuzzoha and A. M. Lane, "Promotion of Pt/γ-Al_2O_3 by New Pretreatment for Low-Temperature Preferential Oxidation of CO in H_2 for PEM Fuel Cells", *Journal of Catalysis*, Vol. 210, No. 2, pp. 460-465, 2002.

13. Oh, S.H. and R. M. Sinkevitch, "Carbon Monoxide Removal from Hydrogen-Rich Fuel Cell Feedstreams by Selective Catalytic Oxidation", *Journal of Catalysis*, Vol. 142, No. 1, pp. 254-262, 1993.

14. Schubert, M. M., H. A. Gasteiger and R. J. Behm, "Surface Formates as Side Products in the Selective CO Oxidation on Pt/γ-Al_2O_3", *Journal of Catalysis*, Vol. 172, pp. 256-258, 1997.

15. Xinsheng, L., O. Korotkikh, and R. Farrauto, "Selective catalytic oxidation of CO in H_2: structural study of Fe oxide-promoted Pt/alumina catalyst", *Applied catalysis A: General*, Vol. 226, No. 1-2, pp. 293-303, 2002.

16. Watanabe, M., Igarashi, H., Suzuki, M., Sasaki, Y., and Uchida, H., "Removal of carbon monoxide from hydrogen-rich fuels by selective oxidation over platinum

catalyst supported on zeolite", *Applied catalysis A: General*, Vol. 159, No. 1-2, pp. 159-169, 1997.

17. Suh D.J., C. K. Kwak, J. H. Kim, S. M. Kwon and T. J. Park, "Removal of carbon monoxide from hydrogen-rich fuels by selective low-temperature oxidation over base metal added platinum catalysts", *Journal of Power Resources*, Vol. 142, No. 1-2, pp. 70-74, 2005.

18. Chin P., X. Sun, G. W. Roberts, J. J. Spivey, "Preferential oxidation of carbon monoxide with iron-promoted platinum catalysts supported on metal foams", *Applied catalysis A: General*, Vol. 302, No. 1, pp. 22-31, 2006.

19. Mirkelamoğlu B. and G. Karakaş, "The role of alkali-metal promotion on CO oxidation over PdO/SnO_2 catalysts", *Applied catalysis A: General*, Vol. 299, pp. 84-94, 2006.

20. Jung, C. R., A. Kundu, S. W. Nam and H. I. Lee, *Applied catalysis A: General*, doi:10.1016/ j.apcata.2007.07.034, 2007.

21. Chin S. Y., O. S. Alexeev and M. D. Amidiris, "Structure and reactivity of $Pt-Ru/SiO_2$ catalysts for the preferential oxidation of CO under excess H_2", *Journal of Catalysis*, Vol. 243, No. 2, pp. 329-339, 2006.

22. Haruta, M., S. Tsubota, T. Kobayashi, H. Kageyama, M. J. Genet and B. Delmon, "Low-Temperature Oxidation of CO over Gold Supported on TiO_2, α-Fe_2O_3, and Co_3O_4", *Journal of Catalysis*, Vol. 144, No. 1, pp.175-192, 1993.

23. Bollinger, M. A. and M. A. Vannice, "A kinetic and DRIFTS study of low-temperature carbon monoxide oxidation over $Au-TiO_2$ catalysts", *Applied Catalysis B: Environmental*, Vol. 8, pp. 417-443, 1996.

24. Ruth, K., M. Hayes, R. Burch, S. Tsubota and M. Haruta, "The effects of SO_2 on the oxidation of CO and propane on supported Pt and Au catalysts", *Applied Catalysis B: Environmental*, Vol. 24, No. 3-4, pp. L133-L138, 2000.

25. Deng W., J. D. Jesus, H. Saltsburg and M. F. Stephanopoulos, "Low-content gold-ceria catalysts for the water–gas shift and preferential CO oxidation reactions", *Applied Catalysis A: General*, Vol. 291, No. 1-2, pp. 126-135, 2005.

26. Chen, Y. J., D. Wu, C. Yeh, "Oxidation of Carbon Monoxide over Nanoparticles of Cobalt Oxides, *Reviews on Advanced Materials Science*, Vol. 5, No. 1, pp. 41-47, 2003.

27. Avgouropoulos, R., T. Ioannides, C. Papadopoulou, J. Batista, S. Hocevar and H. K. Matralis, "A Comparative Study of Pt/γ-Al2O3, Au/α-Fe2O3 and CuO-CeO2 Catalysts for Seletive Oxidation of Carbon Monoxide in Excess Hydrogen", Catalysis Today, Vol. 75, pp. 157-167, 2002.

28. Wang, A., Y. Hsieh, Y. Chen and C. Mou, "Au–Ag alloy nanoparticle as catalyst for CO oxidation: Effect of Si/Al ratio of mesoporous support", *Journal of Catalysis*, Vol. 237, No. 1, pp.197-206, 2006.

29. Driebergen, A.G., M. N. H. Kieboom, A. V. Dreumel and R. M. Wolf, "CO oxidation over silica supported Pt-Rh alloy catalysts", *Catalysis Letters*, Vol. 2, No. 2, pp.73-39, 1989.

30. Kalinkin, A. V., A. V. Pashis and V. I. Bukhtiyarov, "CO oxidation over the Pt-Rh system. 2. Reaction on an alloy", *Reaction Kinetics and Catalysis Letters*, Vol.78, No. 1, pp. 107-112, 2003.

31. Watanabe M., H. Uchida, K. Ohkubo and H. Igarashi, "Hydrogen purification for fuel cells: selective oxidation of carbon monoxide on Pt–Fe/zeolite catalysts", *Applied Catalysis B: Environmental*, Vol. 46, No. 3, pp. 595-600, 2003.

32. Monyanon, S., S. Pongstabodee and A. Luengnaruemitchai, "Catalytic activity of Pt–Au/CeO2 catalyst for the preferential oxidation of CO in H_2-rich stream", *Journal of Power Sources*, Vol. 163, No. 1, pp. 547-554, 2006.

33. Aksoylu, A.E., M. M. A. Freitas and J. L. Figueiredo, "Bimetallic Pt–Sn catalysts supported on activated carbon. II. CO oxidation", *Catalysis Today*, Vol. 62, No. 4, pp.337-346, 2000.

34. Aksoylu, A.E., M. M. A. Freitas and J. L. Figueiredo, "Bimetallic Pt–Sn catalysts supported on activated carbon: I. The effects of support modification and impregnation strategy", *Applied Catalysis A: General*, Vol. 192, No. 1, pp.29-42, 2000.

35. Landon P., J. Ferguson and B. E. Solsana, "Selective oxidation of CO in the presence H_2, H_2O and CO_2 via gold for use in fuel cells", *Chemical Communications*, Vol. 27, pp. 3385-3387, 2005.

36. Sirichaiprasert, K., A. Luengnaruemitchai and S. Pongstabodee, "Selective oxidation of CO to CO_2 over Cu–Ce–Fe–O composite-oxide catalyst in hydrogen feed stream", *International Journal of Hydrogen Energy*, Vol. 32, No.1, pp.915-926, 2007.

37. Şimşek, E., Ş. Özkara, A. E. Aksoylu and Z. İ. Önsan, "Preferential CO oxidation over activated carbon supported catalysts in H_2-rich gas streams containing CO_2 and H_2O" *Applied Catalysis A: General*, Vol. 316, No. 2, pp. 169-174, 2007.

38. Speller, S. and U. Bardi, *The Chemical Physics of Solid Surfaces*, Elsevier, 2002.

39. Kappenstein, C., M. Guerin, K. Lazar, K. Matusek and Z. Paal, "Characterisation and activity in n-hexane rearrangement reactions of metallic phases on catalysts of Pt-Sn/Al_2O_3 different preparations", *Faraday Transactions,* Vol. 94., No. 16, pp. 2463-2473, 1998.

40. Orita, H., N. Itoh and Y. Inada, "All electron scalar relativistic calculations on adsorption of CO on Pt(1 1 1) with full-geometry optimization: a correct estimation for CO site-preference", *Chemical Physics Letters*, Vol. 384, No. 4-6, pp. 271-276, 2004.

41. Lynch, M. and P. Hu, "A density functional theory study of CO and atomic oxygen chemisorption on Pt(111)", *Surface Science,* Vol. 458, No. 1-3, pp. 1-14, 2000.

42. Ge, Q. and D. A. King, "Surface diffusion potential energy surfaces from first principles: CO chemisorbed on Pt{110}" *Journal of Chemical Physics*, Vol. 111, No. 21, pp. 9461-9464, 1999.

43. Hammer B., O. H. Nielsen and J. K. Norskov, "Structure sensitivity in adsorption: CO interaction with stepped and reconstructed Pt surfaces", *Catalysis Letters*, Vol. 46, No. 1, pp. 31-35, 1997.

44. Hopster, H. and H. Ibach, "Adsorption of CO on Pt(111) and Pt 6(111) × (111) studied by high resolution electron energy loss spectroscopy and thermal desorption spectroscopy", *Surface Science*, Vol. 77, No. 1, pp.109-117, 1978.

45. McClellan, M. R., J. L. Gland and F. R. McFreeley, "Carbon monoxide adsorption on the kinked Pt(321) surface", *Surface Science*, Vol. 112, No. 1-2, pp. 63-77, 1981.

46. Hayden, B. E., K. Kretzschmar, A. M. Bradshaw and R. G. Greenler, "An infrared study of the adsorption of CO on a stepped platinum surface", *Surface Science*, Vol. 149, No. 2-3, pp. 394-406, 1985.

47. Yates, J. T., "Surface chemistry at metallic step defect sites", *Journal of Vacuum Science and Technology A*, Vol. 13, No. 3, pp. 1359-1367, 1995.

48. Feibelman, P. J., B. Hammer, J. K. Norskov, F. Wagner, M. Scheffler, R. Stumpf, R. Watwe and J. Dumesic, "The CO/Pt(111) Puzzle", *Journal of Physical Chemistry B*, Vol. 105, No. 18, pp. 4018-4025, 2001.

49. Gong, X., Z. Lui, R. Raval, P. Hu, "A Systematic Study of CO Oxidation on Metals and Metal Oxides: Density Functional Theory Calculations", *Journal of the American Chemical Society*, Vol. 126, No. 1, pp. 8-9, 2004.

50. Zhang, C.J., R. J Baxter, P. Hu, A. Alavi, M. H. Lee, "A density functional theory study of carbon monoxide oxidation on the Cu3Pt(111) alloy surface: Comparison with the reactions on Pt(111) and Cu(111)", *Journal of Chemical Physics*, Vol. 115, No. 11, pp. 5272-, 2001.

51. Shubina, T.E. and M. T. M. Koper, "Quantum-chemical calculations of CO and OH interacting with bimetallic surfaces", *Electrochimica Acta*, Vol. 47, No. 22-23, pp. 3621-3628, 2002.

52. Gülmen, M. A., A. Sümer and A. E. Aksoylu, "Adsorption properties of CO on low-index Pt_3Sn surfaces" *Surface Science*, Vol. 600, No. 21, pp. 4909-4921, 2006.

53. Sümer, A., M. A. Gülmen, A. E. Aksoylu, "A theoretical investigation on Pt_3Sn(1 0 2) surface alloy and CO–Pt_3Sn(1 0 2) system", *Surface Science*, Vol. 600, No. 10, pp. 2026-2039, 2006.

54. Kohn, W. and L. J. Sham, "Self-Consistent Equations Including Exchange and Correlation Effects", *Physical Review*, Vol. 140. No. 4A, pp. A1133-A1138, November 1965.

55. Accelrys Inc., Materials Studio CASTEP, San Diego: Accelrys Inc., 2001

56. Ge, Q. and D. A. King., "Surface Diffusion Potential Energy Surfaces From First Principles: CO Chemisorbed on Pt(110)", *Journal of Chemical Physics,* Vol. 111, No. 21, pp. 9461-9464, 1999.

57. Hu, P., D. A. King, S. Crampin, M. H. Lee and M. C. Payne, "Ab inito Diffusional Potential Energy Surface for CO Chemisorption on Pd(110) at High Coverage: Coupled Translation and Rotation", *Journal of Chemical Physics*, Vol. 107, No. 19, pp. 8103-8109, 1997.

58. Hoheisel, M., S. Speller, J. Kuntze, A. Atrei, U. Bardi and W. Heiland, "Structure of $Pt_3Sn(110)$ Studied by Scanning Tunneling Microscopy", *Physical Review B*, Vol. 63, pp. 1-7, 2001.

59. Kuntze, J., S. Speller, W. Heiland, A. Atrei, I. Spoveri and U. Bardi, "Reconstruction and Dislocation Network Formation of the (111) Surface of the Ordered Alloy Pt_3Sn", *Physical Review B*, Vol. 58, pp. 16005-16008, 1998.

60. Hammer, B., O. H. Nielsen, J. K. Norskov, "Structure Sensitivity in Adsorption: CO Interaction with Stepped and Reconstucted Pt Surfaces", *Catalysis Letters*, Vol. 46, pp. 31-35, 1997.

61. Legare, P., "A theoretical Study of H Surface and Subsurface Species on Pt(111)", *Surface Science*, Vol. 559, No. 1, pp.169-178, 2004.

62. Zhang, Z., M. Minca, C. Deisl, T. Loerting, A. Menzel and E. Bertel, "H on Pt(110): An atypical chemisorption site at low coverages", *Physical Review B*, Vol. 70, pp. 121401R, 2004.

63. Downs, R. T. and M. S. Somayazulu, " Carbon Dioxide at 1.0 GPa", *Acta Crystallographia: Section C, Crystal Structure Communications*, Vol. C54, pp. 897-898, 1998.

64. Wang, S. G., D. B. Cao, Y. W. Li, J. G. Wang and H. J. Jiao, "Chemisorption of CO_2 on Nickel Surfaces", *Journal of Physical Chemistry B*, Vol. 109, No. 40, pp. 18956-18963, 2005.

65. Janin, E, H. V. Schenck, M. Göthelid and U. O. Karlsson, "Bridge-bonded Atomic Oxygen on Pt(110)", *Physical Review B*, Vol. 61, No. 19, pp. 13144-13149, 2000.

66. Burnett, D. J, A. T. Capitano, A. M. Gabelnick, A. L. Marsh, D. A. Fischer and J. L. Gland, "In-situ soft X-ray studies of CO oxidation on the Pt(1 1 1) surface", *Surface Science*, Vol. 564, No. 1-3, pp. 29-37, 2004.